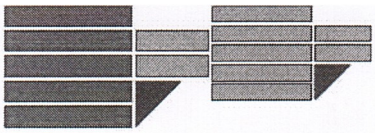

UNIVERSITA' DELLA CALABRIA

UNIVERSITA' DEGLI STUDI DELLA CALABRIA

DIPARTIMENTO DI FISICA

BERNARDINO TELESIO - DOCTORATE SCHOOL OF SCIENCE AND TECHNIQUE

TESI DI DOTTORATO DI RICERCA IN FISICA DEI SISTEMI COMPLESSI

CICLO XXIV

SETTORE DISCIPLINARE

02/B1

Methane Physisorption Processes on Porous Nanostructured Materials

DIRETTORE

Prof. Roberto Bartolino

COORDINATORE

Prof. Vincenzo Carbone

SUPERVISORE

Prof. Raffaele Giuseppe Agostino

DOTTORANDA

Myrsini Kyriaki Antoniou

ANNO ACCADEMICO 2010/2011

Dedicated to

my beloved grandmother ***Georgia***

Contents

1.Introduction

1.1 Methane

Nowadays, the increasing air pollution from automobile exhaust gas affects every day the environment and our health. Therefore, there is a great need of using vehicles of which emissions will not worsen the atmosphere. In order to obtain a clean and healthy environment, many researchers focus their efforts on the development of alternative energy sources that are plentiful globally, low-priced and can offer low toxic gas emissions. Natural gas fulfil these characteristics since it is the cleanest of all the fossil fuels (gasoline, diesel etc): its combustion produces less carbon dioxide emissions providing energy security and enviromental benefits [1]. Accordingly, the last twenty years the interest in natural gas as a vehicular fuel has grown remarkably. However, the important disadvantage of natural gas is its low energy density (heat of combustion/volume) [1]. In order to solve this problem, natural gas could be stored as liquifided [2] or compressed [3,4] but in both cases many safety problems arise. Compressed natural gas requires not only costly multi-stage compression but also large, heavy and pressure-resistance tanks, for its storage, which cannot provide safety. On the other hand, the liquefied natural gas shows multiple inconveniences, mainly because increases inevitably the temperature within the tank. Thus, the pressure rises and could result in a dangerous situation.

An interesting alternative, is to store natural gas as an adsorbed phase [5-7] in porous materials which require low pressures resulting in safety advantages and overcomes the above mentioned problems. This technology is yet in scientifc level and the studies on storage by adsorbed natural gas method are

carried out by using methane (CH_4), which is the major component of natural gas.

1.2 Methane molecules adsorption: Chemisorption and Physisorption mechanisms

The surface of a solid has a tendency to attract and to retain molecules of other species (gas or liquid) with which such surface come in contact. This phenomenon of surfaces is termed as adsorption. It denotes the taking up of gases or liquids by a surface. It is a property of a solid to retain on, or concentrate at its surface, one or more components (atoms, molecules, or ions) from another liquid or gas in contact with the surface.

Gases, and therefore in our case methane, can be stored in porous materials through two mechanisms, the chemisorption and the physisorption. In the case of chemisorption, the interaction between methane and the sample can occur either in the bulk or on the surface. High barrier dissociation energy is required, which shifts the desorption temperature to higher temperatures [8] while the enthalpy of formation (ΔH) is particularly high and lies in the range of (10 – 100) kJ/mol. Finally, in several cases, the chemisorption mechanism results in an irreversible process [9].

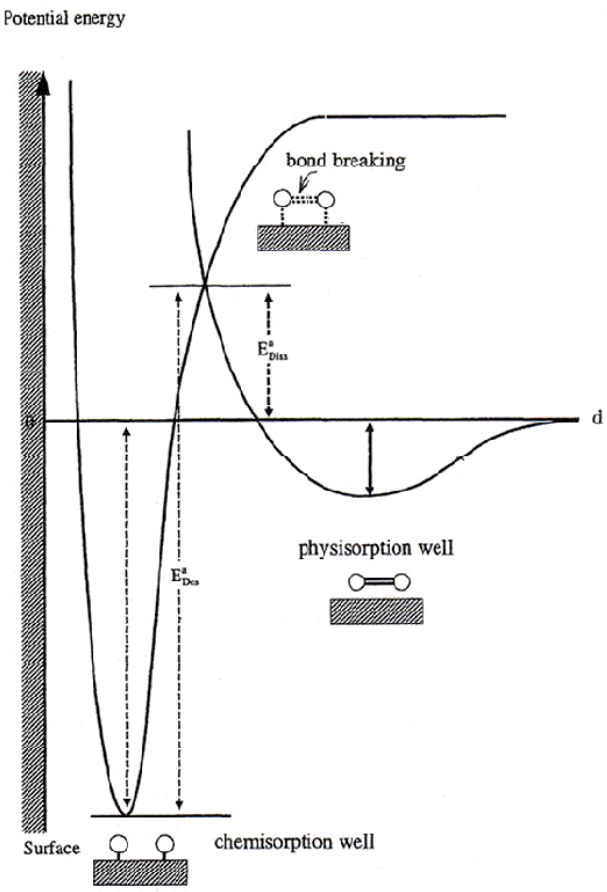

Figure 1.1. Potential energy curve as a function of gas-surface distance

On the other hand, in the case of physisorption, the interaction between the solid surface and the adsorbed methane molecules takes place on the surface of the sample [10] and the forces occurring are weak Van der Waals type [1]. With physisorption the whole adsorption/desorption cycle could occur in a small range of temperatures [8] while the isosteric heats of adsorption generally range from 10–20 kJ mol^{-1} [11]**.** Finally, storage by physisorption is a promising solution to the reversible high methane uptake [9].

1.3 Important characteristics for suitable porous materials for methane physisorption

Adsorbent is a substance that has a molecular structure that allows smaller molecules to penetrate its surface area and be kept inside its pores.

Before to consider a material suitable for methane uptake, some of the main parameters that can affect its storage capacity have also to be considered. These parameters can be: sample's temperature, specific surface area (SSA), pore size distribution, curvature of the pores, surface's heterogeneity and finally the a possible functionalization of the samples.

The SSA is the adsorbent's surface accessible to the adsorbate per mass unit of the adsorbent. A large specific surface area is preferable for providing large adsorption capacity. Larger surface area will allow more contact between methane molecules and adsorbent surface area to give way to more adsorption to take place. In fact, it has been demonstrated that by increasing the SSA of a material is increased also linearly its storage capacity [12,13].

On the other hand, the pore size is important and must be of a suitable size to admit, hold, and discharge individual methane molecules. For example, if the pores are too small, the methane molecules cannot enter. Therefore by tuning the pore size of a material, different adsorption capacity can be obtained [13-15]. According to the calculation of Bathia et al. [13] the optimum conditions for methane storage is obtained into the samples with pore size equal or even higher than 1.76 nm. While the optimal pore size that Gubbins and Jiang discovered is the width between two methane molecules. [16]. In this work will be shown that the definition "optimum" pore size might change depending the different materials used as adsorbents (see chapter 4).

Additionaly, the variation of the surface chemical constituent into the porous materials could enhance the physical interaction between adsorbent surface – adsorbate by introducing light metals (Li+, Mg+) or by inserting aromatic rings in the structure of the porous material [17-19].

Furthermore, surface heterogeneity and adsorption strength are two factors that are never independent (in real systems) [20].

Finally, the sample's temperature must also be considered as a factor that modifies the storage capacity. As a fact, an increase of the temperature will decrease the amount adsorbed at a given pressure due to the greater energy acquired by the adsorbed molecule to evaporate [20].

Decrease of adsorption capacity with temperature rise can be explained by the Chateleir's principle. Adsorption reaction can be written as follows:

$$\textit{Adsorbate} + \textit{Adsorbent} \rightleftharpoons \textit{Adsorption} + \textit{heat} \qquad \textbf{(1.1)}$$

When natural gas is adsorbed, heat of adsorption is released. When heat increases, reaction system will transfer the equilibrium to the left side and causing more gas molecules not to be adsorbed and subsequently reduces adsorption capacity.

Consequently, in order a material to be considerd suitable for adsorbed natural gas (and furthermore be used in mobile applications) has to fulfil some requirements: to have high adsorption capacity, high specific surface area (SSA), appropriate pore size distribution, well ordered posority, structular stability (therefore long lifetime), small weight and low cost.

The growth attention on the synthesis of suitable materials for methane storage is the main aim of many researchers and in particular the US Department of Energy (DOE) has set a storage target of 150 v/v, which has been recently revised to 180 v/v [13,21,22] (the volume of gas adsorbed at standard temperature and pressure: 298 K, 0.1 MPa, per volume of the storage vessel) or equivalently 35wt% [11] at 3.5 MPa, in order to have methane adsorbent materials of applicative interest.

1.4Types of adsorption isotherms

The typical curves utilized to investigate the samples' storage capacity are the isotherm plots. These adsorption isotherms provide information for adsorption capacity in increasing pressures and fixed temperature.

Generally, the surface coverage of adsorbate is determined from the coefficient $\boldsymbol{\theta}$:

$$\theta = \frac{number\ of\ sites\ occupied\ by\ the\ adsorbate\ (N_s)}{total\ number\ of\ sites\ available\ on\ the\ adsorbent\ (N)} \quad (1.2)$$

when $\boldsymbol{\theta}$ is equal to 1, then the adsorbate esemble is called a monolayer [23].

All types of adsorption isotherms by physisorption ever recordered in literature can be grouped in six categories as IUPAC recommends [10] (figure 1.2). The different shape of the isotherms can reveal the diverse processes that might occur as the pressure increases.

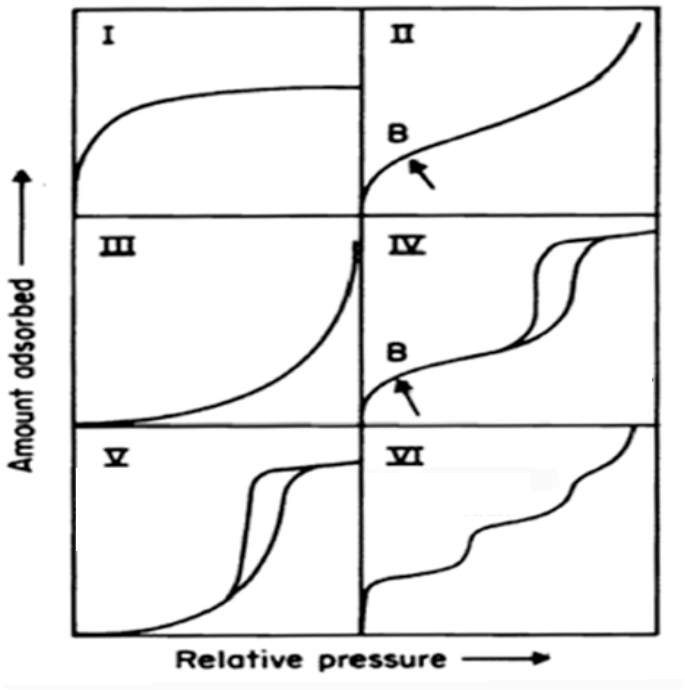

Figure 1.2 Classification of adsorption isotherms in porous materials by IUPAC [10].

For methane storage (and generally gas storage), the materials of interest must have micropores that show Type I isotherms at the low-pressures region. However, at high pressures, these materials can have a mono-multilayer filling, typical of mesopores, and hysteresis loops, related to the pore geometry. Type I may be characterized as closely resembling "Langmuir" behavior but it mostly corresponds to the uptake by the accessible micropore volume rather than by the internal surface area.

A typical Type I methane adsorption isotherm is presented in figure 1.3 (see also chapter 4) for silicalite-1 MFI topology [24-26], a well-studied material in the literature. This material shows a methane storage capacity of about 3.6 wt% at 3.5 MPa and 298 K.

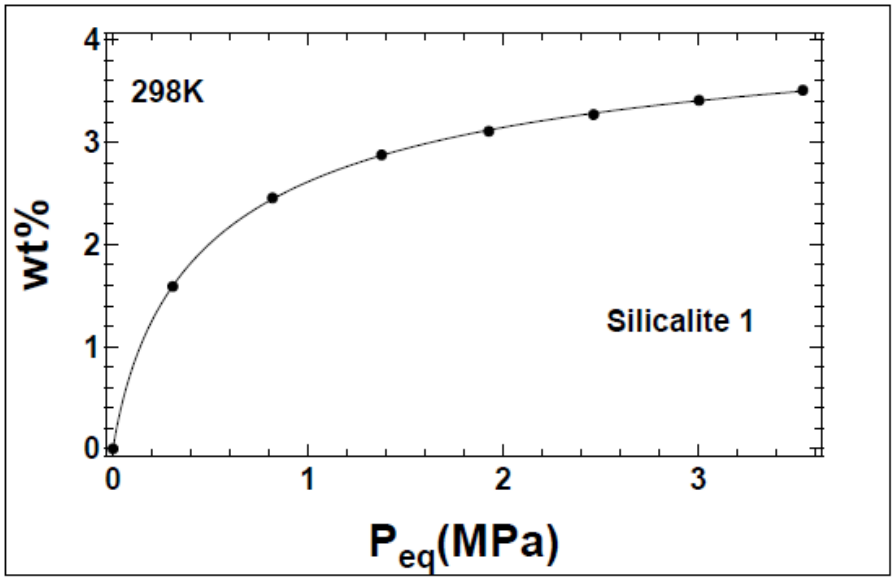

Figure 1.3. Typical isotherm curve for Silicalite-1 by volumetric apparatus.

The adsorption isotherms play a crucial functional role on predictive modelling procedures for analysis and design of adsorption systems. The Langmuir [27] and Toth [28] models are useful to describe the adsorption isotherms of gases. The Langmuir model can be considered the base of all theories of adsorption while the three-parameter Toth model can help to obtain knowledge about the enthalpy of adsorption and heterogeneity of the surface of the investigated samples.

1.5 Theoretical Model Approaches

1.5.1 Langmuir model

The adsorption isotherms of porous solids with high SSA can be interpreted, at first approach, by making use of the Langmuir model [20,27,29] which considers the following approximations:.

1. The surface containing the adsorbing sites is perfectly flat plane andhomogeneous therefore all sites are energetically equivalent and the adsorbent's surface is considered uniform.

2. Each site can hold at most one molecule therefore is possible a mono-layer coverage only.

3. The adsorbate molecules interact and create either physical or chemical bond with the adsorbent surface, while interactions between adsorbate molecules are neglected, avoiding the formation of second monolayer.

4. At constant temperature there is a dynamic equilibrium during adsorption and desorption processes.

5. The heat of adsorption is independent of the surface coverage.

The Langmuir equation can be derived in various ways based on different physical pictures (statistical mechanics, thermodynamics, kinetics etc.) [28]. The most simple method for derivation is the kinetic description of the adsorptive equilibrium. As it is known the rate of adsorption (v_a) is proportional to the equilibrium pressure and to the uncovered part of the surface

$$v_a = k_a(1-\Theta)p \qquad (1.3)$$

where **θ** is the surface coverage and $\mathbf{k_a}$ is the kinetic constant of the adsorption. The rate of desorption ($\mathbf{v_d}$) can similarly be defined by the following equation:

$$\mathbf{vd=kd\Theta} \tag{1.4}$$

where $\mathbf{k_d}$ is the kinetic constant of the adsorption.

Taking into account equation (1.2) is possible to determine the grade of adsorption like:

$$\theta = \frac{N_S}{N} = \frac{(KP)^{1/c}}{1+(KP)^{1/c}} \tag{1.5}$$

where **c** is equal to either 1 or 2 in the case of physisorption and chemisorption respectively, **θ** is the surface coverage **P** the pressure and **K** the equilibrium constant.

The concentration in weight of the adsorbed molecules per percentage of mass unit (wt%) is expressed:

$$wt\% = A\frac{(KP)^{1/c}}{1+(KP)^{1/c}} \tag{1.6}$$

A is the maximum storage capacity of the adsorbent, while **K** as mentioned before represents the ratio between adsorption and desorption constants giving us information about the interaction between the adsorbed gas molecules and the surface. Values of K higher than 1 indicate that this interaction is strong.

The Langmuir isotherm equation reduces to the Henry law isotherm when the pressure is very low. The typology of the Langmuir isotherm demonstrates a quick increase in adsorption at low pressures and then an asymptotic behavior indicating the saturation of the adsobate's surface.

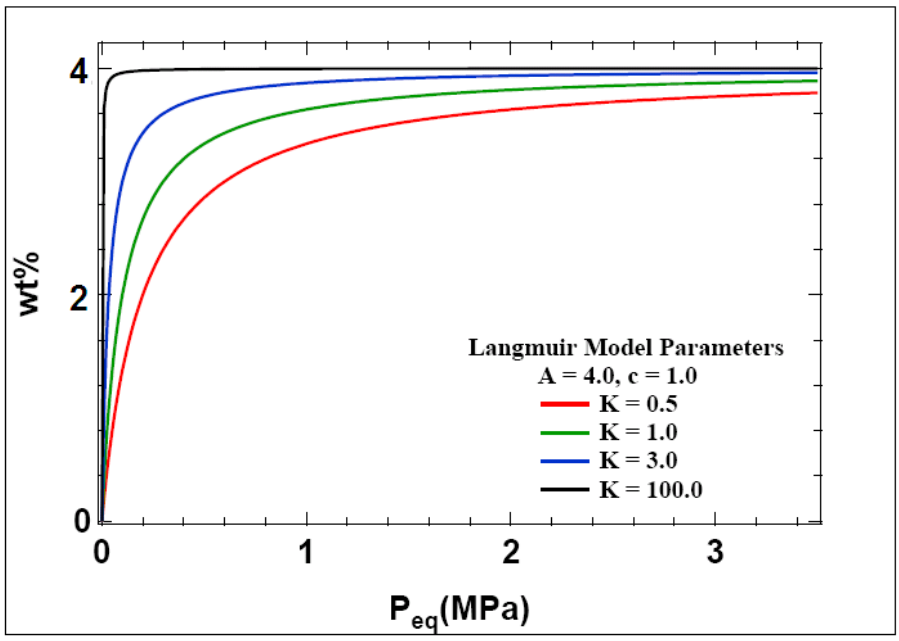

Figure 1.4. Langmuir Equation shape different K-values in physisorption mechanism.

The enhancement of the *K*-value increases the adsorption in lower pressure values (figure 1.4) therefore indicating a stronger interaction between surface

and adsorbent. Following this, maximum storage capacity (*A*-value) is reached in higher pressure values.

1.5.2 Toth model

Langmuir model's approximations are not applicable if we consider real experimental conditions. As mentioned before, this model considers mainly equivalent energetically sites therefore homogeneous surfaces and can be applicable for low pressures (0-1 bar), as over this limit Henry's law is applied.

An isotherm equation with a good applicability in practice has to meet a very simple but important requirement: to be applicable for heterogeneous adsorbent surfaces where the adsorptive potential changes as a function of the coverage.

Tóth [28,30-34] was the first author who derived a new equation in 1961 describing adsorption in relatively high pressures and heterogeneous surfaces. The starting point of his theory is the fact that a heterogeneous surface uptakes more gas molecules, at the same relative equilibrium pressure, than a homogeneous adsorbent with constant adsorptive potential and with the specific surface area identical to that of the heterogeneous adsorbent. However, there must not be any difference in monolayer capacities of the homogeneous and the heterogeneous surface owning the same specific surface area. In order to have higher grade of adsorption θ, Tóth introduced the relation

$$\theta t > \theta \text{ with } 0 < t < 1 \qquad (1.7)$$

and the equation that Tóth has proposed is

$$wt\% = A\frac{KP}{(1+(KP)^t)^{1/t}} \tag{1.8}$$

where **A** is the maximum theoretical storage capacity and **K** the equilibrium constant as described in the Langmuir model

$$K = \frac{Kads}{Kdes}\ ,\ \ Kdes = e^{(\frac{-\Delta H}{KT})} \tag{1.9}$$

The parameter **t** is said to characterize the system heterogeneity. When t = 1, the Toth isotherm reduces to the famous Langmuir equation while the more the parameter **t** deviates from unity, the more heterogeneous is the system.

In this work heterogeneity will be used to describe differences in samples porosity and morphology. In order to comprehend the Tóth model, its relation (1.7) has been plotted for a fixed theoretical maximum storage capacity A and K- and t-values as the varying parameters (figures 1.5(a,b) and 1.6(a,b)).

Due to a low K-value, therefore low interaction between the gas molecules and the surface, the adsorption sites are occupied by increase in the pressure as shown in figure 1.5a. Increasing homogeneity drives the isotherms to saturation faster. On the other hand a high K-value, which indicates a strong interaction between the adsorbate and the surface, enhances adsorption in

low pressures (figure 1.5b). Again, in this case by increasing the homogeneity the saturation is reached quicker.

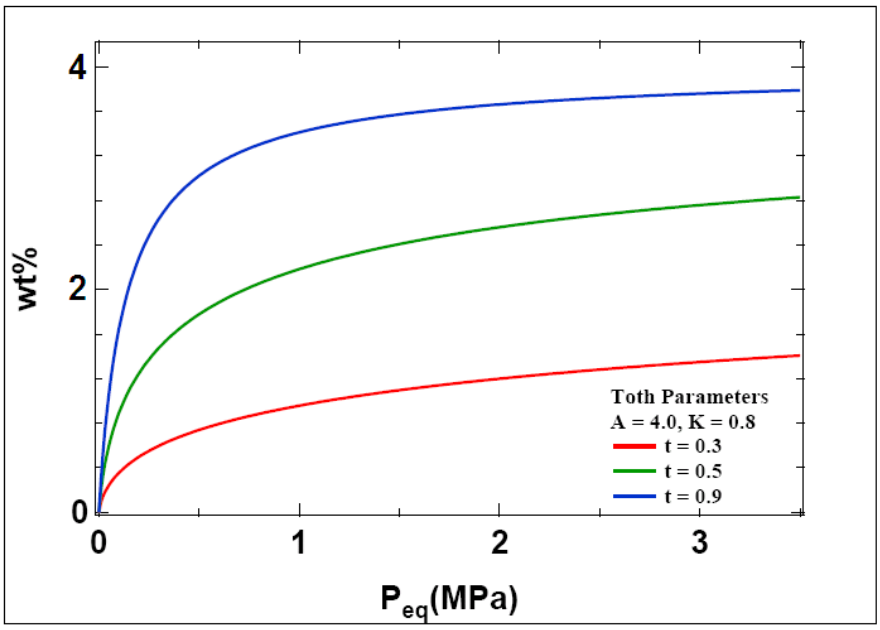

(a)

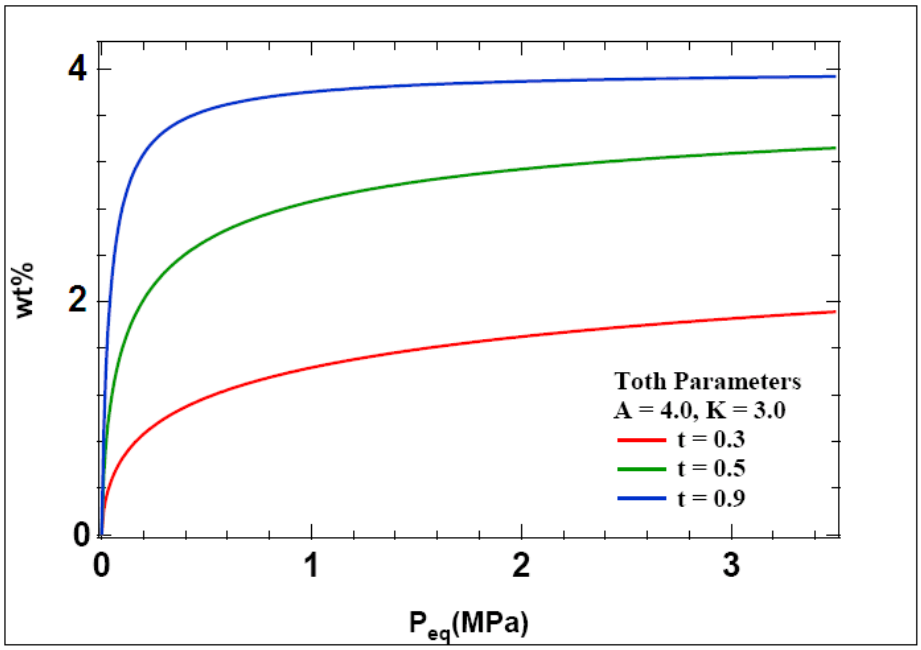

(b)

Figure 1.5. Tóth Equation shape for different values of t for a low K-value ***(a)*** and high Kvalue ***(b)***.

A low *t*-value (strong degree of heterogeneity) describes a surface with non-equivalent adsorption sites and in order to reach the fixed maximum storage capacity, it requires higher pressure values because of the less favorable adsorption sites (figure 1.6a). On the other hand, a high t-value describes a surface of several equivalent adsorption sites which results in a quicker saturation of adsorption sites (figure 1.6b). In this case, the Tóth model is similar to the Langmuir model, because of the high value of *t* which is close to unity. In both the above cases, high K-value means high ΔH, therefore higher bonding energy between the adsorbent and the adsorbate.

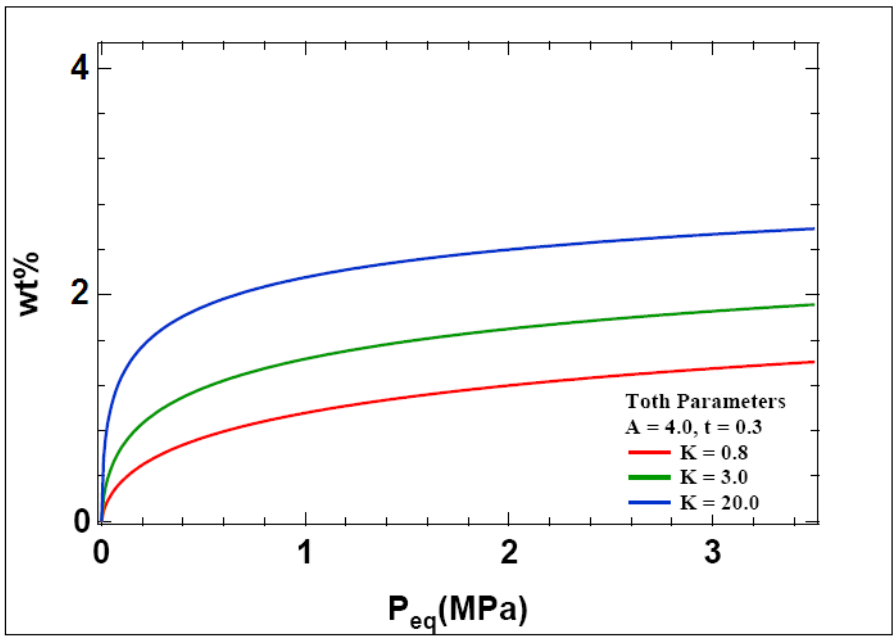

(a)

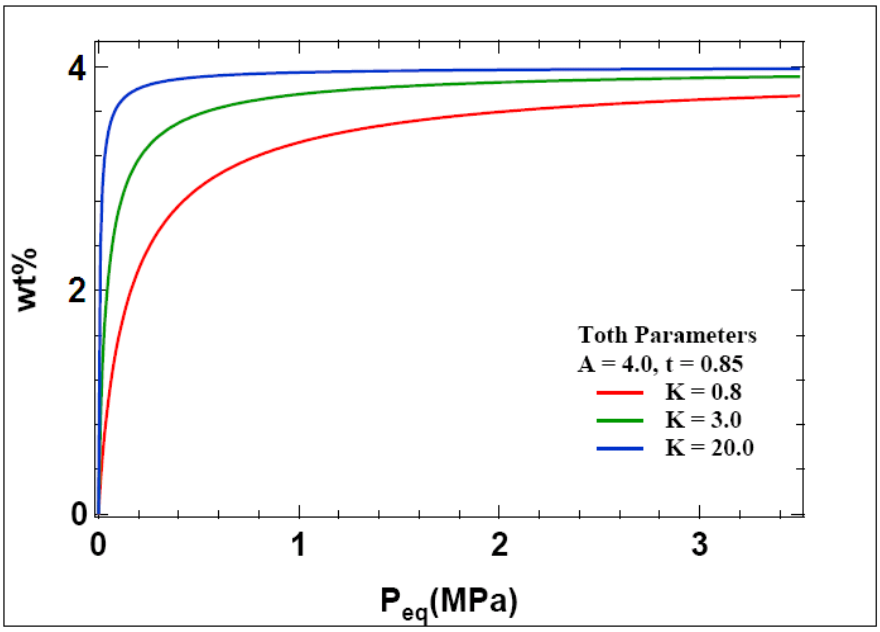

(b)

Figure 1.6. Tóth Equation shape for low t-value ***(a)*** and high t-value ***(b)***. Three different values are assigned to K-value in each case.

1.6 Adsorbed molecules per nm^2

One of the most important properties of a material for methane storage is its specific surface area (SSA) as mentioned above. The SSA takes into account the active sites which are involved in methane adsorption therefore material with higher SSA are expected to give a higher storage capacity in methane adsorption experiments. In fact, as mentioned before (see chapter 1.3), it has been demonstrated that by increasing the SSA of a material is increased also linearly its storage capacity [12,13].

However, the ability of a material to store methane molecular species does not depend only on the SSA but can also be due to the possibility to form more

than one monolayer. Therefore, after the first layer of methane molecules along the pore's sides is formed (where the interaction between the molecules and the surface dominates), the formation of a second layer begins and in this case the forces between the adsorbate molecules have to be considered as well. Therefore, the evaluation of the adsorbed molecules per nm^2 (molec/nm^2) could indicate the efficacy of the sample to create more than one mono layer and can be evaluated by using the following formula:

$$\mathbf{N_{molec}/nm^2 = N_A * wt\% / (10^{20} * MW_{GAS} * SSA)} \quad (1.10)$$

where $\mathbf{N_A}$ is the Avogadro's number, $\mathbf{MW_{GAS}}$ the molecular weight of the adsorbed gas and **SSA** the spesific surface area obtained by the BET method.

For methane storage, the formation of one monolayer is reached when about 3 molecules per nm^2 are adsorbed (as the area occupied by a CH_4 molecule is about 0.3 nm^2).

As an example, the evaluation of adsorbed molecules per nm^2 is presented for silicalite-1. As it is shown in figure 1.7 silicalite-1 forms one monolayer of adsobed methane molecules at 3.5 MPa and 298K.

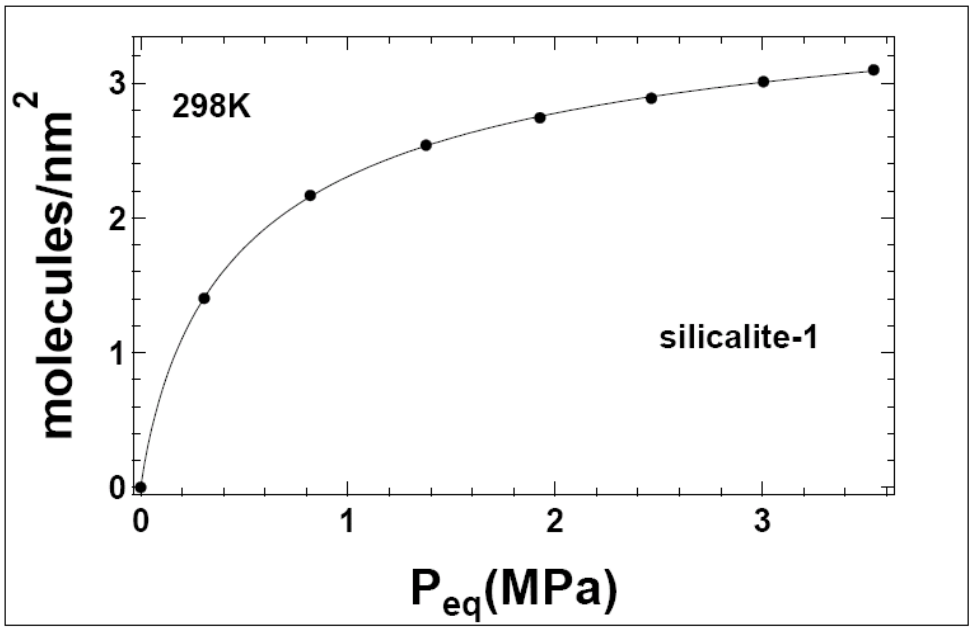

Figure 1.7. Number of molecules per surface's nm^2.

1.7 Isosteric heat of adsorption

One of the basic quantities in adsorption studies is the isosteric heat of adsorption (the enthalpy change on adsorption is commonly referred to as the isosteric heat of adsorption). The adsorption process involves the loss of degree of freedom of the adsorbate, as it pass into the adsorbed film, there is a decrease in the entropy of the system. As the entropy and free energy decrease in adsorption, the enthalpy of the system decreases. This decrease in enthalpy appears as heat. Hence, the adsorption process must always be exothermic or heat releasing. Therefore, the adsorption of gas molecules into pores on adsorbent surface will release some amount of heat called heat of adsorption which gives us information about the binding energy between the gas molecules and the surface.

In this work, the isosteric heat of adsorption for the investigated materials is evaluated according to the Clausius–Clapeyron equation:

$$\mathbf{lnP = -(\Delta H/RT) + C} \qquad (1.11)$$

As long as the pressure (**P**) and temperature (**T**) values are known for a series of data points, then the enthalpy may be determined from a plot of *lnP* against *1/T* (see chapter 4). The plot is linear for some constant amount adsorbed while the isosteric heats of adsorption for different amounts adsorbed can be evaluated from the slope of these linear plots [28].

The above formula has been utilized to the isotherm curves obtained on the investigated samples at 286 K, 298 K and 313 K and low pressures (500mb-1bar). The reason for which low pressures are used for the evaluation of the isosteric heat of adsorption is because in this range of pressures (and therefore coverages) the interaction between the surface and the methane molecules is stronger compared to higher pressures where the interaction between the methane molecules has to be considered as well.

The negativity of the enthalpy change indicates that the adsorption process is exothermic. The isosteric heat of adsorption will remain constant during the process of surface covering if the surface is energetically uniform; however, it will vary with the increasing amount adsorbed for an energetically heterogeneous surface. Molecules, firstly, prefer to be adsorbed onto sites which posses higher energy of adsorption and as adsorption proceeds molecules then are being adsorbed onto sites of progressingly lower energy of adsorption, resulting in a decrease of heat of adsorption with loading [20].

1.8 Investigated materials

In this work, three principal groups of porous materials will be presented: Periodic Nanoporous Organosilicas (PNOs) [35,36], Carbon nanostructured materials [37,38] and Zeolites [39].

These materials can be synthesized with tailored adsorption properties by tuning either the pore size, or the SSA, or introducing appropriate functionalization.

1.8.1 Periodic Nanoporous Organisilicas (PNOs)

Among many materials that have been studied for physical adsorbed methane, are the MCM-41 [40] which are silica-based materials with an hexagonal array of cylindrical pores. For these materials, Seaton et al. [41] reported a methane storage capacity of about 3.7 wt% at 303.15 K and 3.2 MPa.

The high specific surface areas of this kind of materials settle them as ideal absorbents. However, these materials lack of active sites that would expand their applicability. For this reason the research was directed toward the synthesis of periodic mesoporous organosilicas (PMOs).

These suitably functionalized porous solids based on the organosilicate family of compounds, are targeted for the development of materials with high and reversible methane adsorption capacity. PMOs, are a special class of templated porous materials in which organic groups are located within the channel walls as bridges between Si centers [42-46].

They can be easily obtained by using simple hydrolysis-condensation reactions of a suitable organosilane precursor in the presence of templating molecules, acting as structure directing agents to provide the necessary

porosity (shape, size and topology). The use of different organosilane precursors and varying surfactant's chain lengths can tune the chemical and physical properties of the final PMOs samples. The procedure of synthesis of these materials depends very much on the interaction between the precursor and the surfactant (see chapter 3).

These materials combine the high surface area and the narrow and tunable pore size distributions of the traditional templated pure silicate materials (e.g. MCM, SBA family of solids) with the enormous functional variation of organic chemistry [35,47]. In the literature, a lot of work can be found and results are already reported on the hydrogen adsorption for this type of materials.

On the contrary, for methane adsorption, only theoritical studies have been done using density functional theory (DFT) calculations on the interaction of methane, with the internal walls of p-phenylenesilica, an hybrid mesoporous material derived from 1,4-bis(triethoxysilyl)benzene [48].

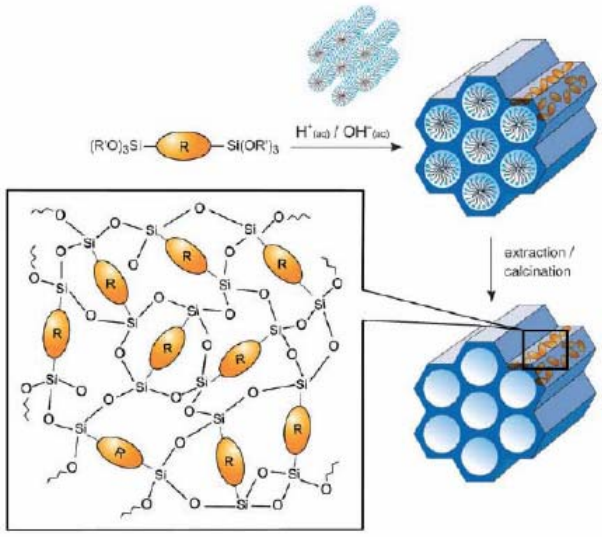

Figure 1.8. Periodic Mesoporous Organoslicas [35].

1.8.1.1 Phenylene Bridged PNOs

In this work will be presented the methane adsorption properties and the morphological and structural characterization of ordered and disordered Periodic Nanoporous Organosilicas (PNOs) which combine high surface area and tunable pore size distributions.

Some main characteristics of the PMOs materials are:

- the high percentage of organic material;

- their sites are chemically reactive;

- the functionalization groups get distributed in an homogeneous way;

- the material's surface can be completely functionalised;

- the porosity is determined from the surfactant.

In figure 1.9 is shown a SEM image obtained in our laboratory, demonstrating a high exagonal degree of one of the investigated PNOs samples in this work.

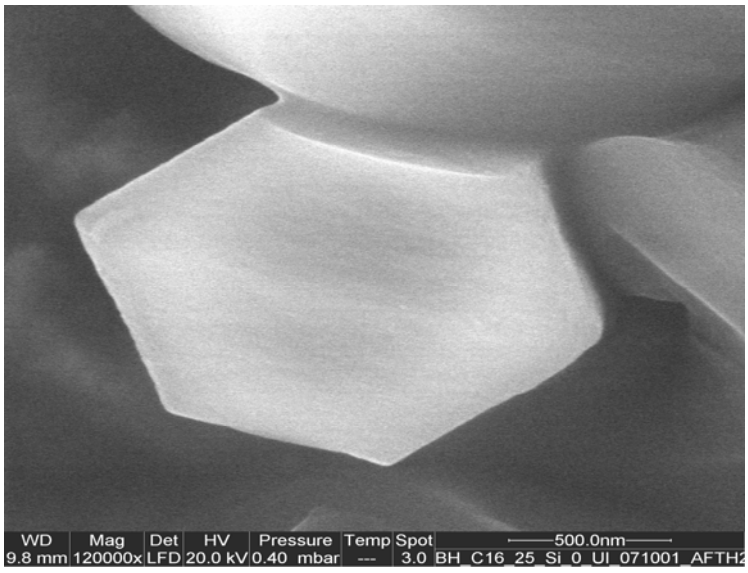

Figure 1.9. SEM image of hexagonal PNO sample studied in this work.

The varied synthesis parameters of the PNOs are:

1. surfactant used and its chain length, in order to change the pores size distribution and the specific pore volumes;

2. the sample aromaticity, in order to change the physical interaction between the adsorbent and the adsorbate;

3. insertion of polar atoms (e.g. Li+) in order to attract more methane molecules;

4. substitution of the starting material with phenyl triethoxy silane. Phenyl rings can create point charge in the surface.

This strategy will be applied either on the samples synthesized making use of 1,4- Bis(triethoxysilyl)-benzene (BTB) as the starting material [44] or on the samples obtained making use of 4,4-Bis-triethoxy-biphenyl (DBTB) as the starting material [49].

The samples will be named according to different labels which correspond to the previous synthesis parameter (see detailed description below):

1H_C2_3_4

1) The starting material (BTB≡B and DBTB≡D)

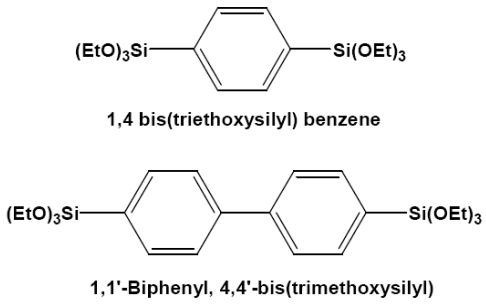

Figure 1.10. Organosilane groups 1,4 bis(triethoxysilyl)benzene (BTB) & 4,4 bis(triethoxysilyl)-biphenyl (DBTB) used as precursors for PNO synthesis.

2) This label corresponds to the surfactant utilized of the type $R(CH_3)_3N+Br-$

On this label the numerical value represents the carbon atoms present in the main chain of the surfactant. This value changes in the range (10 – 18) carbon atoms.

3) This label indicates the percentage of the BTB or DBTB in the starting material. When no supplementary starting material (tetraethoxysilane (TEOS)) is used the percentage is 100%. When the BTB or DBTB is not used and only the supplementary material is present, the label is 0.

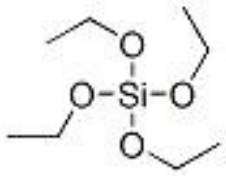

Figure 1.11. Tetraethoxysilane (TEOS).

4) The last label indicates eventually, added doping atoms. Here doping took place with Li+ cations.

For instance, BH_C18_100 means sample synthesized by using BTB as precursor, 18 carbon atoms in the surfactant chain and no supplementary material was used since 100% of BTB starting material is indicated. While DH_C10_100_Li means sample synthesized by using DBTB as precursor, 10 carbon atoms in the surfactant chain 100% percentage of the starting material (no supplementary material) and the sample was doped with Li+. Finally, BH_C16_50 means sample synthesized by using BTB as precursor, 16 carbon

atoms in the surfactant chain, and 50% of BTB (therefore 50% of TEOS was used too as starting material).

The phenylene bridged PNO samples were provided by Prof. Dimitrios Gournis and Dr. Apostolos Enotiadis from the Department Materials Science and Engineering (University of Ioannina, Greece).

1.8.1.2 Naphthalene PNOs

Regarding our work [50], it has been demonstrated that PNO materials may be obtained not only by the use of bissilylated organic precursors, as their strict definition reports, but also by the use of analogous monosilylated organic precursors. Therefore, it has been shown [50] that PMOs may also be produced even if we substitute the bissilylated with a monosilylated organic precursor, since the final hybrid organic-inorganic products exhibit same properties.

The samples were synthesized by direct co-condensation of tetraethylorthosilicate (TEOS) and the prior composed chemical substance triethoxy(naphthalen-1-yl)silane. The carbon atoms present in the main chain of the surfactant are 16 while the evacuation of the pores from the surfactant was achieved either by treatment with HCl 37 wt% (sample: Naph-PNO-H^+) or by heat treatment at 350 ^oC (sample: Naph-PNO-350).

The naphthalene containing PNOs were obtained by Prof. Dimitrios Gournis and Dr. Konstantinos Dimos from the Department Materials Science and Engineering (University of Ioannina, Greece).

1.8.2 Zeolite-like carbon materials

Among the various adsorber materials, zeolites and carbon materials have been considered as good candidates for methane storage [51]. Both these groups of materials are of interest because of their low cost, light weight, high surface area, high thermal stability, high bulk density and adjustable composition.

Various types of zeolites have been investigated for methane adsorption [25,26,52-54]. For example, Zhang et al. [55] reported a high methane storage capacity of about 8.2 wt% at 3.0 MPa and 298 K for zeolite CaX while Rolniak et al. [56] obtained a methane capacity of about 6.8 wt% at 3.0 MPa and near ambient temperature for zeolite 13X.

On the other hand, the development of carbonaceous porous materials with pre-determined accurately tuned nano-sized reactive channels (which can have application-tailored surface properties) is of primary importance. Such materials have strong potential to achieve among else high and reversible methane adsorption. [1,57-61] D. Lozano-Castelό et al. [14] reported a high methane storage capacity of about 19.2 wt% at 4.0 MPa and 298 K for activated carbon materials.

Among many methods that have been applied in order to obtain mesoporous carbon materials, is the hard template method combined with the Chemical Vapor Deposition (CVD) that allows to control the porosity and the structure of the final material by using the appropriate template [62,63]. Thus, by changing the diameter of the channels, is enabled the effective trapping of differently sized gas molecules.

Among many materials, zeolites have been widely explored as hard templates because of their advantages such as high porosity and large accessible surface

area. Zeolites Y [64], 13X [65], L [66], ZSM-5 [66] and beta [66,67] have been used as templates to prepare carbon materials, mainly by using acetonitrile as carbon precursor and nitrogen as gas carrier resulting in N-doped carbons. These materials have been tested for hydrogen uptake capacity [65,68,69] while limited literature can be found for methane storage. Guan et al. [70] reported that pyrolysis of carbonaceous precursors resulted to carbon-templated materials, by using as template an ammonium-form zeolite Y, which possess about 12.8 wt% methane storage capacity at 4.0 MPa and 300 K.

In this work, zeolite-like carbon materials, with high specific surface area (SSA), were prepared by CVD using acetylene as carbon precursor and zeolite beta as template. Acetylene was used as a carbon source since it is more reactive than other hydrocarbons at the same reaction temperature leading to carbon materials of better quality [71-73]. The aim was to develop nitrogen-free zeolite-like carbon materials that will combine the numerous advantages of zeolites and carbons, in order to pave the way for the production of novel carbon based materials with high reversible methane adsorption capacity.

The choice of zeolite beta as hard template material is due to its peculiar structure: it consists of an intergrowth of two distinct structures termed polymorphs A and B, which both possess a three-dimensional network of 12-ring pores, and grow as randomly alternating two-dimensional sheets. The intergrowth of the polymorphs does not significantly affect the pores in two of the dimensions, but in the direction of the faulting [68,74].

The samples will be denoted according to the different CVD temperatures used during the synthesis: CZ1023 (1023 K), CZ1073 (1073 K) and CZ1123 (1123 K).

The synthesis of these samples has been done at the CCL laboratory of Prof. Dimitrios Gournis at the Department Materials Science and Engineering (University of Ioannina, Greece).

In figure 1.12 is briefly illustrated how we can obtain a carbon material by using a zeolite like hard template.

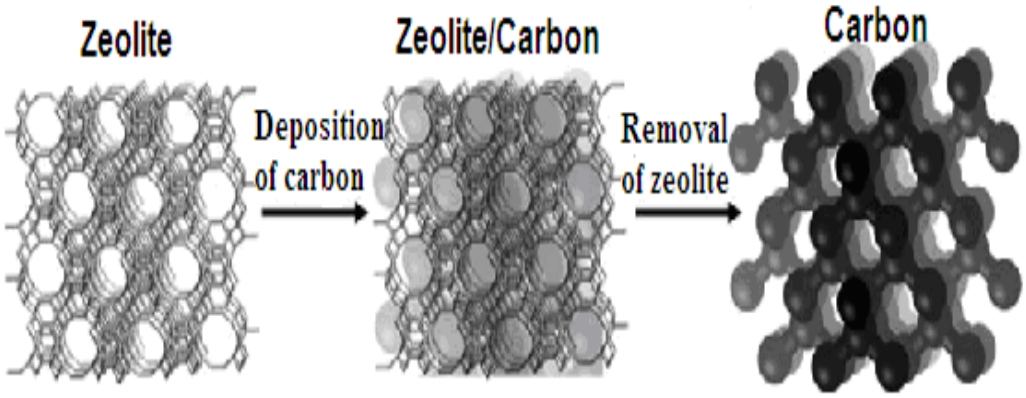

Figure 1.12. Schematic procedure for the synthesis of zeolite-like carbon material.

1.8.3 Zeolites

1.8.3.1 Sapo-34

The synthesis of new materials for gas separation is a big issue in the energy market and particularly the separation of CO_2 from CH_4 is important in natural gas processing because CO_2 reduces energy content of natural gas. The optimal material to separate the gas has to offer high gas flux and selectivity [75] at a reasonable cost. The technology most widely used for CO_2 removal is amine adsorption, but amine plants are complex and costly. Polymeric membranes have been also tested but the main problem that limits their use is their poor performance stability at high pressure and in the presence of highly

sorbing components [76]. However, organic-inorganic mixed matrix membranes (MMMs) have been proposed [77] in order to exploit the advantages of both polymers and inorganic compounds In fact, MMMs can combine the low cost and ease of preparation of polymeric membranes and the numerous properties of the inorganic porous materials like seperation, selectivity, permeability and resistance [78].

One of the most used inorganic materials for MMMs are zeolites[79].The zeolites structures contain (-Si-O-Al-) linkages that form surface pores of uniform diameter and enclose regular internal cavities and channels of discrete sizes and shapes, depending on the chemical composition and crystal structure of the specific zeolites involved. Zeolites possess many important characteristics as mentioned above (see chapter 1.8.2) and are used for gas separation and catalysis [80-82].

MMMs containing SAPO-34 crystals dispersed in a polymeric matrix are believed to represent a viable and non expensive option to improve the gas performance of today's commercial membranes for the removal of CO_2 from natural gas [76,83-85]. In particular, the selectivity of these membranes is high, if the fillers are platelet and aligned.

The SAPO-34 is a silicoaluminophosphate having the composition $Si_xAl_yP_zO_2$, where x = 0.01–0.98, y = 0.01–0.60, and z = 0.01–0.52 [75]. Its structure is generally considered to be formed by substituting silicon for phosphorous in $AlPO_4$, which has a neutral framework and exhibits no ion exchange capacity.

In this work, methane and carbon dioxide adsorption results for SAPO-34 crystals with different morphologies and high aspect ratio will be presented. Particularly, the samples were prepared containing different N/Si ratios. Tetraethylammonium hydroxide and dipropylamine have been used as

primary and secondary structure-directing agents (SDAs), respectively, and methylene blue as a crystal growth inhibitor.

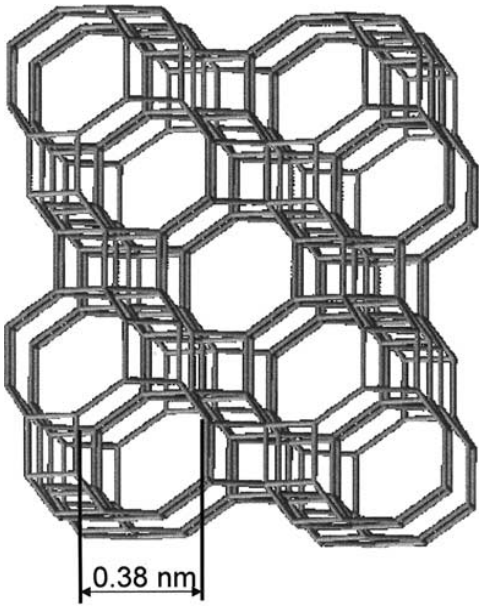

Figure 1.13. The structure of a SAPO -34 [75].

1.8.3.2 Silicalite-1

The modification of zeolite frameworks by covalently bound organic molecules either externally or internally to the micropores could convert these materials in organic-inorganic hybrid composites efficient to fulfil the requirement of several applications [86,87].

In the literature a lot of work on different type of modifications by organic molecules can be found [88-91]. One of the most important modifications of zeolites in the literature is this with organosilane molecules [90] which allows to the zeolite to be reactive and connected with different composites like polymers.

In this work, the zeolite chosen in order to be modified with different organosilane molecules is silicalite-1.

Silicalite-1 is a well defined MFI-type zeolite with a channel-like pore structure and a nearly energetically homogeneous surface. It consists essentially of pure silica. It has a medium-pore 10-member-ring structure which is described by two types of channels straight and zig-zag connected with intersections.

In the literature, results can be found on methane adsorption for silicalite-1 [25,26,92,93]. Nevertheless, in this work, methane adsorption results of the starting material, silicalite-1 MFI type and modified with different organosilane molecules: Cl_3SiCH_3, $Cl_2Si(CH_3)_2$ and $Cl_3Si(CH_2)_2(CF_2)_8F$ will be presented.

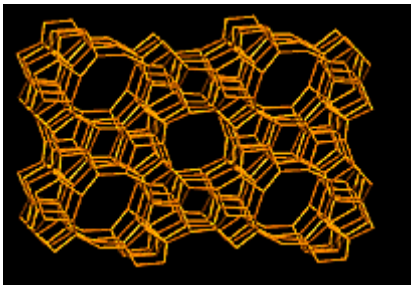

Figure 1.14. The structure of a Silicalite-1

The above samples were provided by Prof. Gianni Golemme and Dr. Maria Giovanna Buonomenna from the Department of Chemical Engineering (University of Calabria, Italy)

1.9 Characterization

The methane adsorption measurements of all the invastigated materials (PNOs, Zeolite-like Carbons, modified SAPO-34 and modified Silicalite-1) have been obtained up to 3.5 MPa and at different temperatures (287K, 298K and 313K) by a volumetric technique [94], using a novel volumetric Sievert-type [95] apparatus (*f*-PcT - DeltaE S.r.l) replacing and optimizing different part of a similar apparatus described in the literature (dotted lines in figure figure 1.15) [96]. Its function is based on the real gas law

$$PV = Z(P,T)nRT \tag{1.12}$$

where Z(P,T) is the compressibility of the gas. Moles n are what it is required in order to calculate the methane storage capacity.

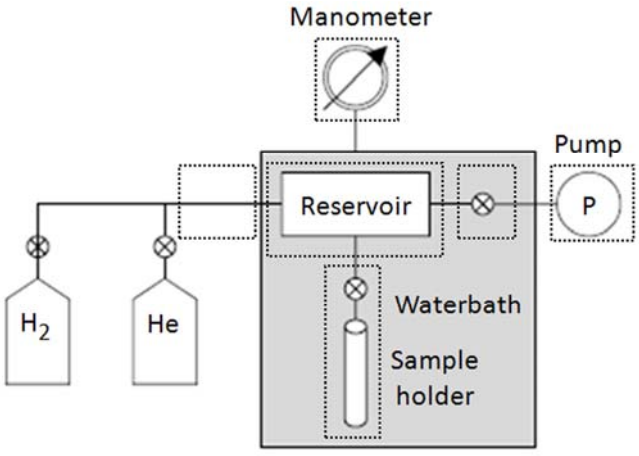

Figure 1.15. Schematic representation of the Sieverts' apparatus [97].

The development of this novel apparatus will be furthest described by considering and resolving issues like system calibration, temperature control

and monitoring in the system and on the sample, pressure reading, error propagation, gas purity and compressibility, sample's degassing, system to sample volume ratio and approach to the pressure gas equilibrium.

Furthermore, the number of adsorbed molecules per nm^2 and the isosteric heat of adsoprtion were evaluated for all the invastigated samples.

Finally, the porosity, structure and morphology of the samples have been characterized by Brunauer-Emmett-Teller (BET), X-ray diffraction (XRD) techniques and Scanning Electron Microscopy (SEM) respectively.

Bibliography Chapter 1

[1] C. Solar, A. G. Blanco, A. Vallone, K. Sapag, Natural Gas, Primoz Potocnik (Ed.), ISBN:978-953-307-112-1, InTech, (2010) Available from: http://www.intechopen.com/articles/show/title/adsorption-of-methane-in-porous-materials-as-the-basis-for-the-storage-of-natural-gas.

[2] R.F. Cracknell, P. Gordon, and K.E. Gubbins, J. Phys. Chem. 97, 494–499 (1993)

[3] R.J. Remick and A.J. Tiller, Proc. of Symposium on Nonpetroleum Vehicular Fuels V (CNG Fuel, Arlington, 1985), pp. 105–119

[4] D. Elliot and T. Topaloglu, Conf. Proc. of Gaseous Fuels for Transportation I (Vancouver, 1986), pp. 489–504

[5] L.J. Engel and J.W. Turko, , U.S. Patent 4,522,159, 1985

[6] L.J. Engel and J.W. Turko, U.S. Patent 4,523,548, 1985

[7] L.J. Engel and J.W. Turko, U.S. Patent 4,531,558, 1985

[8]Fariba Sadat Hashemi, Alireza Zolfaghari, Parisa Pourhossein, and Hossein Zolfghari Jooya, Fullerenes, Nanotubes, and Carbon Nanostructures, 16: 186–195, 2008

[9] Chang Liu, Feng Li, Lai-Peng Ma, and Hui-Ming Cheng*, Adv. Mater. 2010, 22, E28–E62

[10] K.S.W. Sing, D.H. Everett, R.A.W. Haul, L. Moscou, R.A. Pierotti, J. Rouquerol, Pure & Appl. Chem., 57 (1985) 603—619.

[11] Russell E. Morris Paul S. Wheatley, Angewandte Chemie International Edition Volume 47, Issue 27, pages 4966–4981, June 23, 2008

[12] Xiaohong, S.; Wenchuan, W.; Xuejun, Z. Carbon 2006, 45, 188-195.

[13] Panella, B.; Hones, K.; Muller, U.; Trukhan, N.; Schubert, M.; Putter, H.; Hirscher, M. Angew. Chem. Int. Ed. 2008, 47, 2138 –2142.

[13] Bhatia, S. K.; Myers, A. L. Langmuir 2006, 22, 1688-1700.

[14] Lozano-Castello, D.; Cazorla-Amoros, D.; Linares-Solano, A.; Quinn, D. F. Carbon 2002, 40, 989–1002.

[15] Z. Tan, K.E. Gubbins, J. Phys. Chem. 94 (1990) 6061, Adsorption in Carbon Micropores at Supercritlcal Temperatures

[16] Gubbins, K. E. and Jiang, S. (1997). "Adsorbing Work: Design of New Material". University of California.

[17] Klontzas, E., Mavrandonakis, A., Tylianakis, E. et al. Nano Lett., 2008, 8, 1572-1576

[18] Mavrandonakis, A., Tylianakis, E., Stubos, A. K. et al. J. Phys. Chem. C, 2008, 112, 7290-7294.

[19] Mpourmpakis, G., Tylianakis, E., Papanikolaou, D. et al. J. Nanosci. Nanotechnol., 2006,6, 3731-3735

[20] Duong, D., Do, ADSORPTION ANALYSIS: EQUILIBRIA AND KINETICS. 1998; Vol. 2

[21] Duren T., Sarkisov L., Yaghi O. M., Snurr R. Q. Langmuir 2004, 20, 2683-2689.

[22] Burchell T., Rogers M. SAE Tech. Pap. Ser 2000, 2000-01-2205

[23] Gary Attard, Colin Barnes, Surfaces, Oxford University Press, 1998

[24] van Koningsveld, H.; Jansen, J.C.; van Bekkum, H. Zeolite, 1990, 10, 235-242

[25] Eckhard Buss and Matthias Heuchel J. Chem. Soc., Faraday T rans., 1997; 93(8):1621-1628

[26] Otto K., Alternative energy sources IV, Ann Arbor, MI: Ann Arbor Science; 1981; 6:241–59

[27] Langmuir, I.; Physical Review, 1916, 8, 149

[28] Toth J. Adsorption Theory Modelling and Analysis. Dekker: New York, 2002

[29] Richard I. Masel Principles of adsorption and reaction on solid surfaces

[30] Toth, J. Journal of Acta Chimica Academiae Scientiarum Hungaricae, 1962, 32, 39

[31] Toth, J. Advances in Colloid and Interface Science, 1995, 55, 1-239

[32] Toth, J. Journal of Acta Chimica Academiae Scientiarum Hungaricae, 1971, 69, 311

[33] Toth, J. Journal of Colloid and Interface Science, 1994, 163, 299-302

[34] Toth, J. Journal of Colloid and Interface Science, 1997, 185, 228-235

[35] F.Hoffmann, M. Cornelius, J. Morell, M. Froba, Angew. Chem. Int. Ed. 2006, 45, 3216 – 3251

[36] Bbenjamin Hatton, Kai Landskron, Wesley Whitnall, Douglas Perovic, Geoffrey A. Ozin, Vol. 38, no. 4, 2005 / Accounts of Chemical Research

[37] H. Gleiter, acta mater. 48 (2000) 1-29

[38] Antonino Salvatore Aricò, Peter Bruce, Bruno Scrosati, Jean-Marie Tarascon and Walter van Schalkwijk, Nature Materials | vol 4 | may 2005

[39] Scott M. Auerbach, Kathleen A. Carrado, Prabir K. Dutta, Handbook of zeolite science and technology, Dekker 2003

[40] P. Selvam, S. K. Bhatia, C.G. Sonwane, Ind. Eng. Chem. Res., 40 (2001) 3237-3261

[41] J.H. Yun, T. Duren, F. J. Keil, N.A. Seaton, Langmuir, 18 (2002) 2693-2701

[42] S. Inagaki, S. Guan, T. Ohsuna, et al. Nature, 416 (2002) 304-307

[43] S. Inagaki, S. Guan, Fukushima, Y. T. Ohsuna, O. Terasaki, J. Am. Chem. Soc. 121 (1999) 9611-9614

[44] T. Asefa, M. J. MacLachan, N. Coombs, G. A. Ozin, Nature 402 (1999) 867-871

[45] B. J. Melde, B. T. Holland, C. F. Blanford, A. Stein, Chem. Mater. 11 (1999) 3302-3308

[46] Q.Yang, J.Liu, L. Zhang, C. Li, J. Mater. Chem., 19 (2009) 1945–1955

[47] W.J. Hunks, G.A. Ozin, J. Mater. Chem. 15 (2005) 3716-3724

[48] U. Martinez, G. Pacchioni, Microporous and Mesoporous Materials, 129 (2010) 62–67

[49] Kapoor, M. P.; Yang, Q. H.; Inagaki, S. Journal of the American Chemical Society, 2002, 124, 15176-15177

[50] K. Dimos, A. Meichanetzoglou, S. Lymperopoulou, M.-D. Ouzouni, I.B. Koutselas, M.K. Antoniou, D. Fokas, D. Gournis, M.A. Karakassides, R.G. Agostino, Micropor. Mesopor. Mater. XX (201X) XX

[51] V.C. Menon, S. Komarneni, Journal of Porous Materials 5, 43–58 (1998)

[52] Joseph L. Zuech, Anthony L. Hines, E. Dendy Sloan. Ind. Eng. Chem. Process Des. Dev., 1983; 22 (1) : 172–174

[53] Chkhaidze E.V., Fomkin A.A. Izv. Akad. Nauk. SSSR, Ser. Khim., 1985; 5: 974

[54] Remick RJ, Elkins RH, Camara EH, Bulicz T. Report, IGT project no. 61067; 1984

[55] Si-Yang Zhang, Orhan Talu, and David T. Hayhurst, J. Phys. Chem. 1991; 95:1722-1726

[56] Paul D. Rolniak, Riki Kobayashi,. AIChE Journal. 1980; 26 (4): 616–625

[57] Rasoolzadeh, M., et al. Study of Methane Storage and Adsorption Equilibria in Multi-Walled Carbon Nanotubes. Iran. J. Chem. Chem. Eng. 2008; 27(3):127-134

[58] Isabel A.A.C. Esteves, Marta S.S. Lopes, Pedro M.C. Nunes, Jos´e P.B. Mota I.A.A.C. Esteves et al. Adsorption of natural gas and biogas components on activated carbon. Separation and Purification Technology 2008; 62: 281–296

[59] D. Lozano-Castello´ et al. Advances in the study of methane storage in porous carbonaceous materials. Fuel 2002; 81: 1777–1803

[60] Cook TL, Komodromos C, Quinn DF, Ragan S. Carbon materials for advanced technologies In: Burchell TD, editor. New York: Pergamon; 1999; 269–302

[61] Parkyns ND, Quinn DF. Porosity in carbons. In: Patrick JW, editor. London: Edward Arnold; 1995; 293–325

[62] Billur Sakintuna and Yuda Yurum, Ind. Eng. Chem. Res. 2005; 44: 2893-2902

[63] Jinwoo Lee, Jaeyun Kim, and Taeghwan Hyeon. Adv. Mater. 2006; 18: 2073–2094

[64] Takashi Kyotani, Takayuki Nagai, Sanjuro Inoue, and Akira Tomita. Chem. Mater. 1997; 9: 609-615

[65] Yang Z., Xia Y., Sun X., Mokaya R. J. Phys. Chem. B 2006; 110: 18424-18431

[66] Takashi Kyotani, Zhixin Ma, Akira Tomita. Carbon 2003; 41:1451–1459

[67] P.M. Barata-Rodrigues, T.J. Mays, G.D. Moggridge . Carbon 2003; 41: 2231–2246

[68] Yang Z., Xia Y., Mokaya R. J. AM. CHEM. SOC. 2007; 129: 1673-1679

[69] Xia Y. et al. Carbon (2010), doi:10.1016/j.carbon.2010.10.028

[70] Cong Guan, Fabing Su, X.S Zhao, Kean Wang Separation and Purification Technology. 2008; 64: 124-126

[71] Tsoufis T., Xidas P., Jankovic L., Gournis D., Saranti A., Bakas T., Karakassides M. A. Diamond & Related Materials. 2007, 16, 155– 160

[72] Maccallini E. , Tsoufis T. , Policicchio A. , La Rosa S. , Caruso T. , Chiarello G. , Colavita E. , Formoso V. , Gournis D. , Agostino R. G. Carbon. 2010, 48, 3434-3445

[73] Policicchio A. , Caruso T. , Agostino R. G. , Chiarello G. , Formoso V. , Colavita E. , Tsoufis T. , Gournis D. , La Rosa S. Surface Science. 2007, 2823-2827

[74]International zeolite association: http://www.personal.utulsa.edu/~geoffrey price/zeolite/beta.htm

[75] Scholes, C.; Kentish, S.; Stevens, G. Separation and Purification Reviews, 2009, 38, DOI 10.1080/15422110802411442|PII 908455701

[76] Shiguang Li, John L. Falconer, Richard D. Noble, Journal of Membrane Science 241 (2004) 121–135

[77] Chung, T. S., Jiang, L. Y., Li, Y. et al. Progress in Polymer Science, 2007, 32, 483-507

[78] Joshua A. Sheffel, Michael Tsapatsis, Journal of Membrane Science 326 (2009) 595–607

[79] Mahajan, R.; Koros, W. J. Industrial & Engineering Chemistry Research, 2000, 39, 2692-2696

[80] Davis, M. E. Nature, 2002, 417, 813-821

[81] Diaz, U.; Vidal-Moya, J. A.; Corma, A. Microporous and Mesoporous Materials, 2006, 93, 180-189

[82] Jones, C. W.; Tsuji, K.; Davis, M. E. Nature, 1998, 393, 52-54

[83] J.C. Poshusta, V.A. Tuan, E.A. Pape, R.D. Noble, J.L. Falconer, AIChE J. 46 (2000) 779

[84] Li S., Alvarado G., Falconer J.L., Noble R.D, J. Membr. Sci. 2005, 251, 59-66

[85] J.C. Poshusta, V.A. Tuan, J.L. Falconer, R.D. Noble, Ind. Eng. Chem. Res. 37 (1998) 3924

[86] Gu, X. H.; Tang, Z.; Dong, J. H. Microporous and Mesoporous Materials, 2008, 111, 441-448

[87] Zimmerman, C. M.; Singh, A.; Koros, W. J. Journal of Membrane Science, 1997, 137,145-154

[88] Weber, R. W., Moller, K. P., Unger, M. et al. Microporous and Mesoporous Materials, 1998, 23, 179-187.

[89] Zhang, H. Y.; Kim, Y.; Dutta, P. K. Microporous and Mesoporous Materials, 2006, 88, 312-318.

[90] Kawai, T.; Tsutsumi, K. Colloid and Polymer Science, 1998, 276, 992-998

[91] Han, A. J., Guo, J. G., Yu, H. et al. Chemphyschem, 2006, 7, 607-613

[92] Klaus Otto,* Clifford N. Montreuil, Olimpia Todor,? Robert W. McCabe, and Haren S. Gandhi, Ind. Eng. Chem. Res., Vol. 30, No. 10, 1991

[93] W. Zhu, J.M. van de Graaf, L.J.P. van den Broeke, F. Kapteijn, J.A. Moulijn, Ind. Eng. Chem. Res. 1998, 37, 1934-1942

[94] Sieverts, A.Z. Physical Chemistry, 1907, 60, 129

[95] Maccallini, E., Policicchio, A., Kalantzopoulos, G. et al. in preparation, 2009

[96] Cento C. et al., How carbon affects hydrogen desorption in NaAlH4 and Ti-doped NaAlH4, Journal of Alloys and Compounds (2006), doi:10.1016/j.jallcom.2006.09.025

[97] Panella B., Hirscher M., Roth S. Carbon. 2005, 43, 2209-2214

2. Experimental apparatus

2.1 Sievert's type apparatus

The volumetric gas storage apparatus (also known as a Sieverts' apparatus) consists of a gas manifold with a series of tubes and valves connecting the sample holder void volume to the gas reservoirs void volume and pressure transducers (figure 2.1). The achievement of reliable results on the gas storage isotherms, (also known as *Pressure concentration Temperature (PcT) curves)*, with high accuracy up to 8.0 MPa, has been obtained by novel apparatus (*f*-PcT - DeltaE S.r.l) replacing and optimizing different part of similar apparatus described in the literature [1-6] and developing both an accurate calibration procedure and new data acquisition and treatment algorithms.

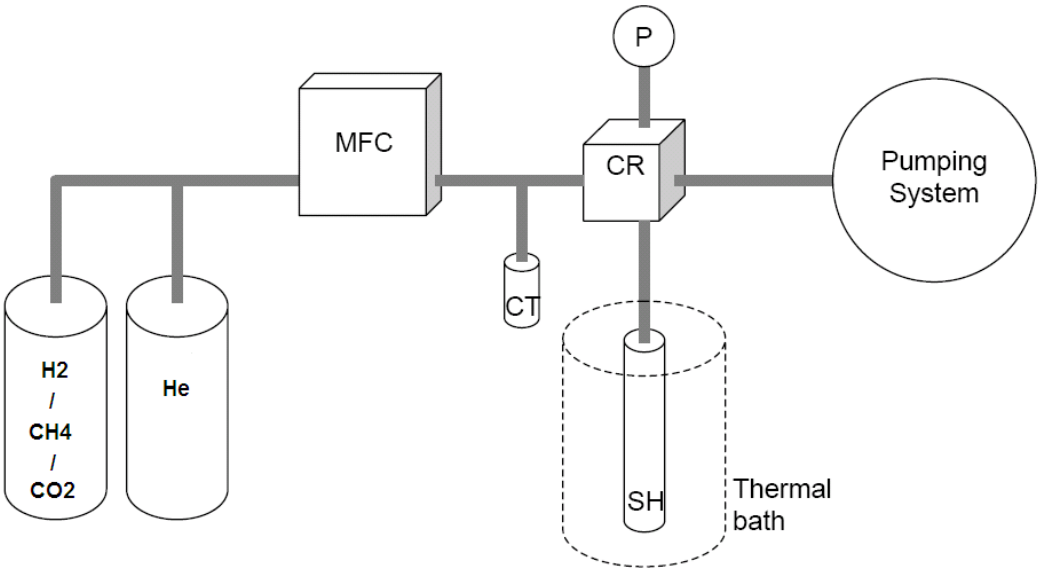

Figure 2.1. Schematic representation of the *f*-PcT Sieverts' apparatus. MFC Mass Flow Controller, CR Calibrated Reservoir, CT Cryogenic Trap, SH Sample Holder, P Pressure Transducer.

The apparatus allows the admittance of different species from a gas manifold into a calibrated reservoir (CR) and the subsequent expansion of that gas in the sample holder volume (SH) hold at a fixed temperature. The missing moles after the gas expansion, calculated considering the gas pressure and temperature, are adsorbed into the sample. The gas expansion is repeated at increasing pressures allowing the evaluation of the sorption isotherm in terms of sorbed moles versus equilibrium pressure. Desorption curve is measured by letting the gas contained in the SH volume expands into the previously evacuated CR. In this case, the desorbed moles contribute to the measured pressure as an excess value.

2.1.1 Apparatus brief description

A mass flow controller (MFC) is inserted to control the admittance gas in the reservoir. Two pressure transducers with end scale of 0.1 MPa (P1) and 10 MPa (P100) are mounted in the reservoir volume to measure the lower and higher pressures ranges respectively. Errors of 0.001 kPa and 0.001 MPa are made in the pressure measurements respectively. The principal system void volumes are divided by electrovalves.

The sample holder is thermalized with a specific bath at different temperatures (depending the gas used, hydrogen, methane, carbon dioxide etc). The temperature of the reservoir is measured by a probe (A) with a precision of ca. 0.015 K while the SH temperature is measured by k-type thermocouple which takes in account the A probe measurements as reference temperature. The temperatures of the reservoir and SH is monitored at different points checking his uniformity within the error of 0.1%.

The vacuum has been obtained by pumping system consisting of membrane and turbo molecular pump achieving pressures less than 1.3×10-3 mbar. The

system volumes have been chosen according to the evaluation of the volume/mass relationship of Wang and Suda [7].

All the equipment (pressure and temperature measurements, valves, pumping system, time settings and data acquisition and analysis) is controlled by homemade software which manages the apparatus by an acquisition card.

The system has been tested by measuring the PcT isotherms of Silicalite-1 (ZSM-like sample with MFI topology). The tests have been done mainly using hydrogen but the methane adsorption isotherm of silicalite-1 are as well presented in chapter 1, indicating the sufficient function of the PcT apparatus.

However, before the discussion of the experimental results, we present all the

experimental details underlying the PcT apparatus. As reference, the review-article of Broom is taken into account which exposes all the experimental problems concerning gas adsorption measurements [1]. Broom defines some simple but fundamental concepts: repeatability, reproducibility and accuracy of measurements. Repeatability is the closeness of the agreement between the results of successive measurements carried out under the same conditions. The reproducibility is the closeness of the agreement between the results of measurements carried out under changed conditions. To conclude the accuracy of the instruments and measurements is the ability to provide experimental data close to the expected results. To fulfill those requirements great care has to be taken into account on the measurements procedure, observer, experimental conditions and location.

Keeping in mind all the experimental considerations of Broom, we focused carefully on the PcT experimental setup showing all the solutions.

First of all, the PcT measurements require the knowledge of methane adsorbed moles into the sample which are obtained taking into account the real gas law (see formula 1.12).

Therefore great care has to be considered in the acquisition and processing of

pressure and temperature values and system void volumes calibration. In this way the experimental setup requires hardware (H) and software (S) solutions in order to minimize all the error sources. The equation (1.12) can be utilized only for pure gases, since high gas purity is required. To summarize the following experimental details has to be considered and discussed critically:

2.1.2 Gas Purity

Two main sources can contaminate the adsorbed gas: intrinsic gas purity (H) and oil from low vacuum pumps (H). The first problem is due to the nominal purity of the gas set from the vendor company. For instance hydrogen 5.0 means H_2 with purity of 99,999%. If the reservoir void volume V0 is filled with H_2 at P0 pressure and the H_2 moles are n_0, the contaminations moles are 10-5 times n0. Because of the adsorbed moles into the samples pores range in between ~10-3 - 10-4, the error made in the adsorbed hydrogen moles evaluation can range between 1-10% which is an enormous value compared to the error made in the P, V and T measurements (see chapter 2.1.3.5, the propagation error evaluation). The second one could be related to the use of classical rotary pumps.

2.1.2.1 Thermal gradients

The equation (1.12) can be utilized in gas thermal equilibrium. Therefore all the system thermal gradients have to be removed. The thermal gradients can

be divided in intrinsic (S) and extrinsic (H). The former are produced from the electrovalves which warm up during their opening. The latter can appear when the measurements are not carried out in stable conditions (i.e. at room temperature).

2.1.2.2 Pressure measurements

The accuracy in pressure measurements does not depend only on the pressure manometer nominal error, but evaluation on the manometers calibration and analogical signal acquisition has to be spent.

2.1.2.3 System void volumes calibration

The calibration of system void volumes (H and S) is not a trivial task to deal. The normal procedure utilized in the literature is the gas expansions into the sample holder void volume filled with a specific solid material with well know density. Usually to obtain error less than 1% in the estimation of the adsorbed moles, error of 0.1-0.5 % should be obtained in the void volumes evaluation (see chapter 2.1.3.5, error evaluation).

2.1.2.4 Sample Properties

In order to obtain the adsorbed moles, several sample properties has to be known: sample skeleton density (H and S), adsorbed gas density (S) and surface specific area (SSA) (H).

2.1.3 Experimental Considerations

2.1.3.1 Gas purity

Usually the gas used for adsorption experiments contains intrinsic impurities whose quantities can be reduced to ppb. An additional source of contaminant gases derives from oil vapours back-streaming from the vacuum system. Even though those quantities are small, their sticking coefficient is usually high as they chemisorb on the pores' walls and, thus, they are selectively adsorbed reducing and/altering the physisorption properties of the material with respect to the main gas. To reduce the extent of these problems we adopted the following solutions. When gases with low liquefaction temperature are used, as in the case of H_2 and CH_4, a void volume, connected to the gas-in pipe and filled with zeolites molecular sieve (Zeolite Trap, ZT), is merged in a liquid nitrogen bath during the measurements in order to absorb the gas contaminations (mainly H_2O, CO_2 and light hydrocarbons) increasing in this way the gas purity. Previously to each experimental run, the ZT is heated and evacuated to remove the contaminations that are physisorbed or chemisorbed in the zeolite pores. To exclude contaminations coming from the pumping system, we make use of an oil-free turbo/drag/membrane system. In this way, in the normal operation as well as in the worst conditions as a vacuum system failure, the system manifold is not contaminated from oil vapours back-streams.

2.1.3.2 Pressure measurements

The accuracy in pressure measurements is one of the most important parameter in gas adsorption experiment. The precise knowledge of gas pressure is fundamental in order to be accurate about the quantity of gas

adsorbed on the storing materials. However accurate pressure value does not depend only on the pressure manometer nominal error, but evaluation on the manometers calibration and analogical signal acquisition has to be spent.

The calibration of our apparatus to get the best adsorption measurement needs some considerations. First of all, because of adsorption isotherms from 0.0 up to 8.0 MPa will be acquired, we need the best accuracy over the entire pressure range. To get this result, we decided to use pressure manometer with the similar nominal error. The former works in the range (0 – 0.1) MPa, usually used for small pressure adsorption measurements, and the latter in the range (0 – 10) MPa to reach higher pressure.

2.1.3.3 Real gas law and compressibility

At high pressure measurement the representation of the real gas law by compressibility factor Z is very important for the meaning of the data. If the compressibility is neglected significant error can be done in the calculation of the wt% adsorbed .

The equation considered during the experiments is the real gas law in the formulation taking into account the compressibility factor Z(P,T).

In order to obtain an accurate evaluation of gas adsorbed moles (n_{ads}), small errors in the measurements of temperatures, pressure and volumes are required. An accurate evaluation of the compressibility factor is of great importance in the determination of n_{ads}, too.

However the compressibility of the gases presents different behaviour by changing the temperature and the pressure. In figures 2.3a and 2.3b are reported the compressibility factor of H_2 at liquid nitrogen temperature (LN_2) and room temperature respectively. In the second case because of the

temperature value can range in (288 – 298) K, three different curves are taken into account.

As an example, in figure 2.2 the wt% of H_2 adsorbed from ZSM-like powder is represented taking into account the real and ideal gas laws.

If the contribution of the compressibility is removed, the curve of the wt% is over-estimated. In fact, at high pressure and low temperatures, the real hydrogen gas is denser into the respect to the ideal case. For the same gas at low pressure (< 0.1 MPa), the ideal and real gas laws are practically identical, as expected.

In the case of methane adsorption measurements, the compressibility factor evaluation is more complex. In fact in our case, the normal procedure considers PcT isotherms at different temperature ranging in (283 – 323) K. In this way the compressibility factor of methane consists of a complex dependence in pressure and temperature which can be well reproduced by non trivial two dimensional fitting results.

Many works outlined the importance of this correction [1,3,8] and to be more accurate we compared the data sheet of NIST [9] and Perry's handbook data[8] resulting in a fair agreement. The contribution of the compressibility has been considered also in the system void volumes calibration and sample density evaluation, depending on the gas and the pressure range utilized.

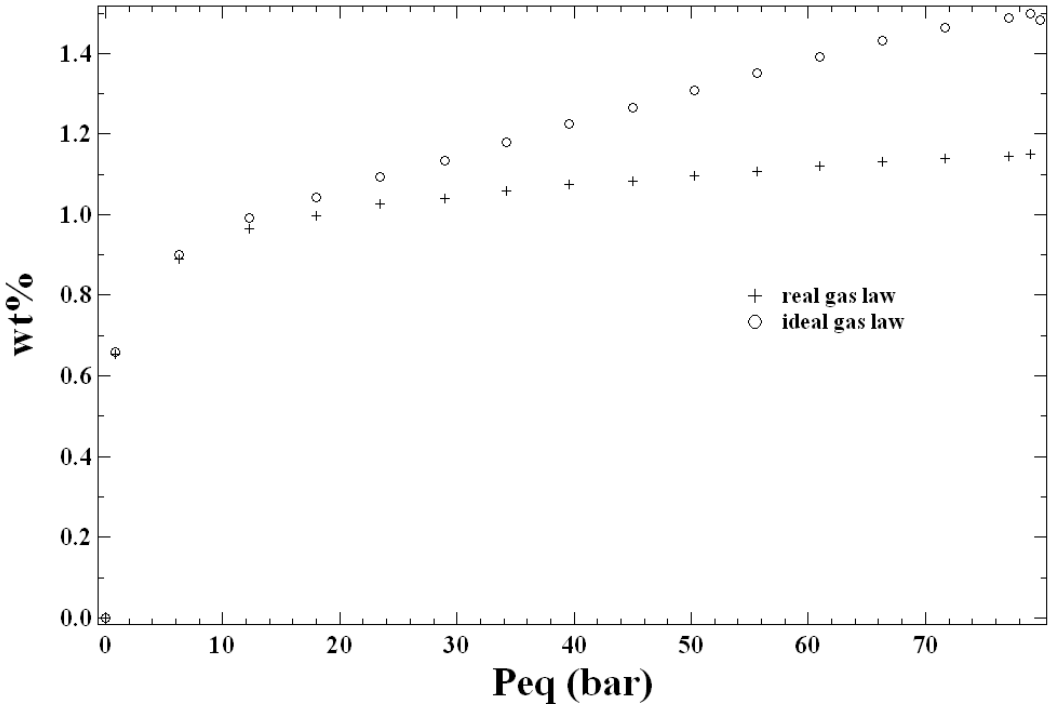

Figure 2.2. Adsorbed H_2 (wt%) in ZSM-like zeolite taking into account the real and ideal gas laws.

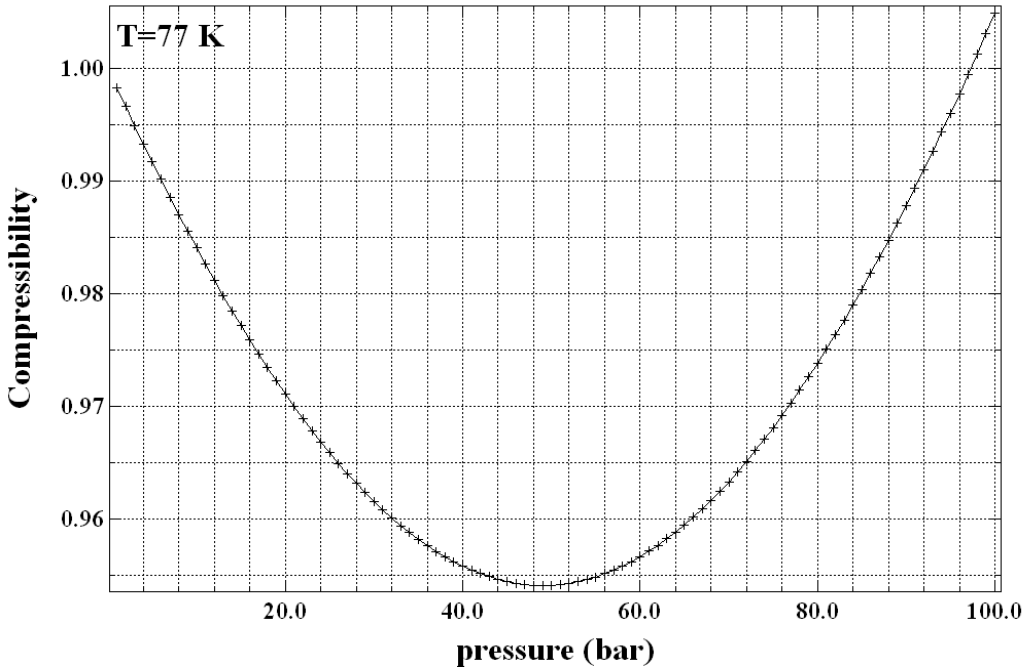

(a)

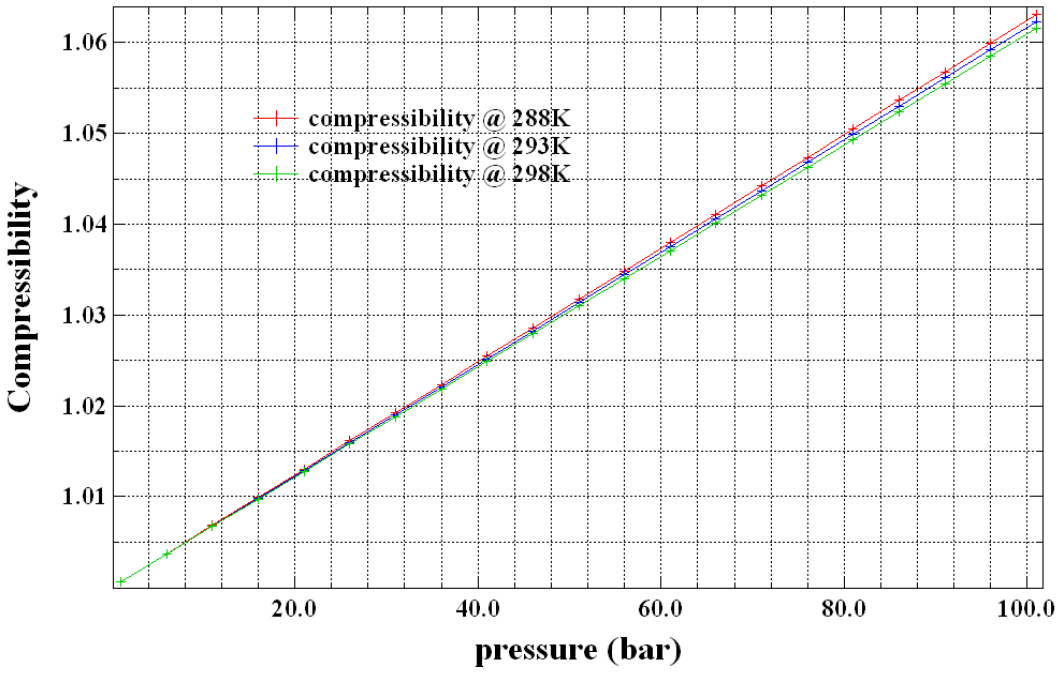

(b)

Figure 2.3. Compressibility factor of H_2 **(a)** at 77 K and **(b)** at 288 K, 293 K and 298 K.

2.1.3.4 Temperature measurements and thermal gradients

The right knowledge of the gas temperature is an important task to resolve. Considering relation (1.12), if gas temperature is under- or over-estimated, the adsorbed gas moles will be over- or underestimated. In the literature several experimental works deal with the temperature measurements[10-14] but only few of them discuss about the thermal gradient between the reservoir and the SH [1,3,7,8].

The gas presence in the apparatus at high pressures should facilitate the achievement of equilibrium temperature. In fact, the thermal conductivity of helium and hydrogen are ranging, at room temperature and in the pressure range (0 – 10) MPa, between (0,156 – 0,162) W/(m K) and (0,186 – 0,194) W/(m

K) respectively, while at LN2 temperature and (0 – 10) MPa pressure range it changes between (0,062 – 0,076) W/(m K) and (0,054 – 0,092) W/m K respectively [9]. If the average speed of the two gases are, at 273 K and 0.1 MPa, 1200 m s-1 and 1700 m s^{-1} respectively,[15] the gas expansion will be very fast and its thermalization optimized according to the relation:

$$k = \frac{n\bar{v}\lambda c_v}{3N_A} \qquad (2.1)$$

where **k** is the thermal conductivity, **n** the molecules per unit volumes, **v** the mean molecules speed, **λ** the mean free path, $\mathbf{c_v}$ the molar heat capacity and **NA** the Avogadro's number.

Keeping in mind those values, the thermal transpiration effect can be neglected if helium and hydrogen gases are utilized [16].

In order to stabilize efficiently the temperature, the calibrated reservoir is enclosed in a box where the temperature is measured with an accuracy of ca. 0.005 K (figure 2.4). This section of the gas line is fixed in thermal equilibrium with the room temperature and monitored during the experiments.

However, we believe the main problem derived from the management of the

thermal gradient between the RT section and the controlled temperature one. This thermal gradient has to involve a small part of the gas line volume in order to minimize the uncertainty of the temperature determination and thus of the gas moles in the gas line. Rouquerol et al. [16] pointed out how this problem has important consequences in the calibration of the volumes with different temperatures.

To efficiently reduce this problem, we let the temperature gradient involve a short section of a 1/8" steel pipe.

To keep a more stable temperature profile when very low temperatures are concerned, we use a control on the cooling liquid level with a feed-back system that maintain it at a fixed position with respect to the gas line.

A further source of temperature gradients is due to the use of electromagnetic valves (see the paragraph 2.1.3.5 concerning the volumes). In fact, the solenoid and the internal ferromagnetic cylinder are heated in proportion to the electric power absorption and the time of use. We minimized this effect, which was not discussed in the literature [10], by both hardware (increase of the heat exchange area) and software (reduction of the "power on" time) solutions.

All the described work on the temperature control allowed us to obtain very stable conditions as depicted by figure below. (Δt=0.035)

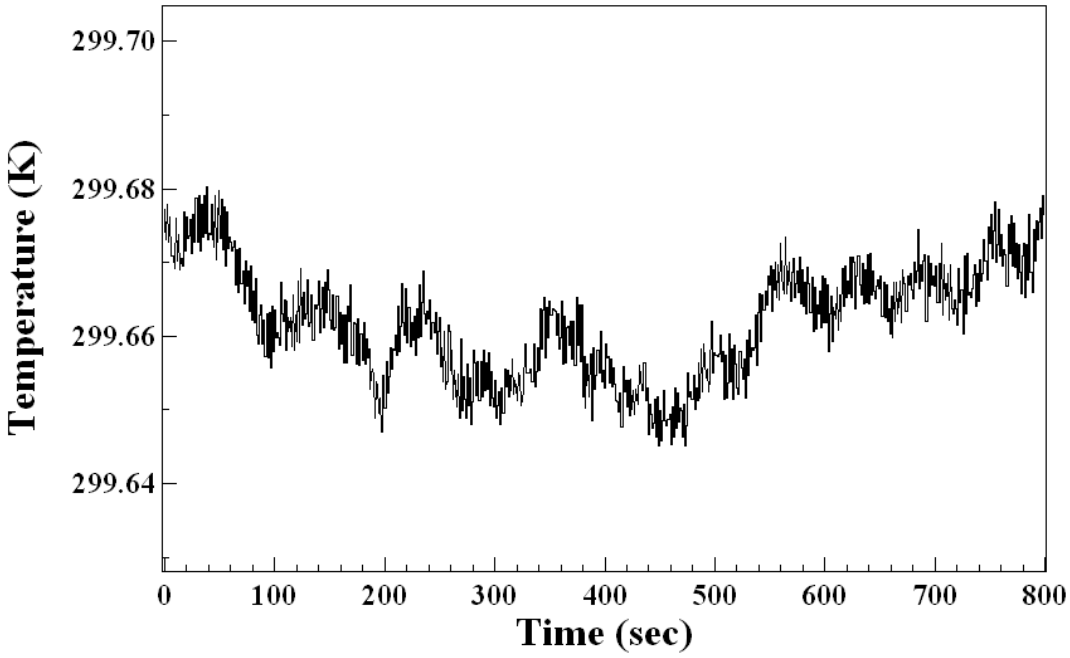

Figure 2.4. Evolution of system temperature during a generic measurement.

2.1.3.5 System void volumes: calibration, sample weight-to-volume optimization and error propagation

The evaluation of void volumes is one of the main problems in volumetric apparatus for gas storage measurements [1,3,10,18,19]. However the volume calibration procedure was not critically dealt in the past leaving several opened question about its determination and errors.

As a starting point, the inner volumes of the gas piping must be accurately measured. The standard procedure reported in the literature is the expansion of the gas between the reservoir and either the empty or filled sample holder [10, 16]. We actually used as a first trial, a procedure in which an object with calibrated volume (an accurately weighted copper cylinder) is introduced in the sample holder volume allowing the determination of its volume by comparison of the gas expansion data. The uncertainty on the copper density and the corrugation of its surface can determine volume errors greater than 1% which propagate to adsorbed moles error bigger than 100% at 8.0 MPa! As an example, in the literature, this procedure has been carried out filling the sample holder void volume with sea sand [20] or stainless steel rood [2] and expanding hydrogen gas. We point out that, even though the used materials do not uptake significant hydrogen molecules, it is difficult to carefully measure the samples density and roughness. In addition, the procedure gives optimal results when the calibrated volume has a similar size of the void volume [16] while the fittings pipeline connecting the SH and the reservoir volume is a significant fraction of it. This fact introduces a significant source of error, too.

Thus, we developed an alternative procedure for the void volume calibration involving two steps: in the first, we utilize MFC to measure the total void volume (avoiding in this way the use of the calibrated sample). The second

step involve the expansion of the gas from the reservoir to the SH volume. The MFC use allows us to determine the gas moles introduced into the different system void volumes by flux measurements. In fact, the mass of the gas admitted by the MFC (*VN gas*), in terms of normal volume, is the integral of the measured flux (Φ):

$$\int \Phi(P,T,t)dt = V_{gas}(P,T) \tag{2.2}$$

The volume ***VN gas*** is related to the gas pressure ***P*** and system void volume ***Vtot*** by:

$$V_N^{gas} = V_{tot}\,(T_N P) / (P_N T) \tag{2.3}$$

where T_N and P_N are temperature and pressure in normal conditions and **T** is the system void volume temperature.

Thus the evaluation of the slope of the *VN gas (P)* curve allows the determination of $Vtot=V_{SH}+V_{CR}+V_{MFC}$ (figure 2.5). The calculation of the three void volumes needs two more relations that are obtained by monitoring the pressure variation following the gas expansion from the calibrated reservoir to either the sample holder or the MFC void volumes. Following this calibration procedure we calculate volume values within the error of 0.5%.

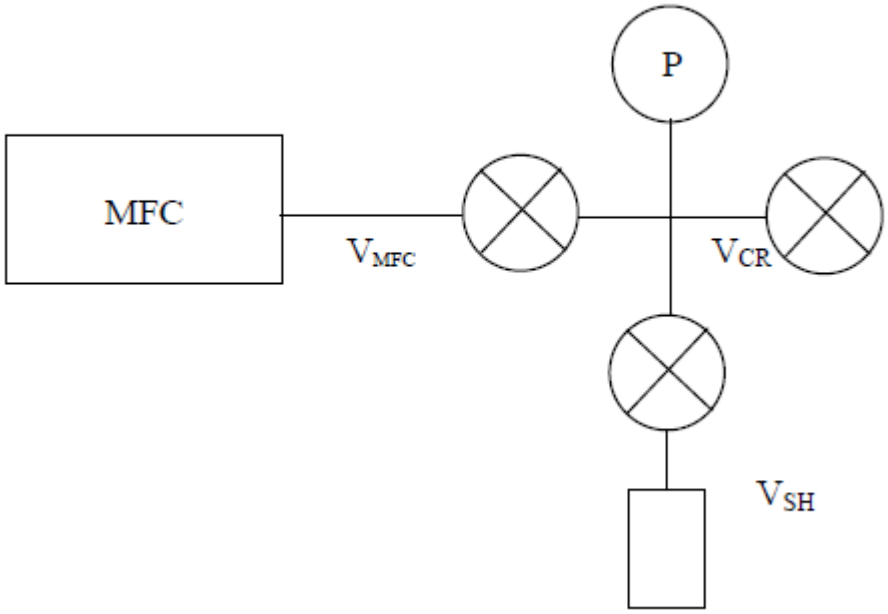

Figure 2.5. Schematic representation of the system void volumes involved during the calibration procedures.

Finally, to calculate the evaluation error on the adsorbed gas moles, an error propagation procedure has to be performed. In a step-by-step isothermal adsorption curve measurement, for each equilibrium pressure step, the expansion of a known quantity of gas from the calibrated reservoir (V_{CR}) to the sample holder (V_{SH}) volumes is monitored and the adsorbed gas moles n_{ads} are calculated taking into account the real gas law [9, 21] by means of the following relation:

$$n_{ads} = \rho_1[V_{CR}(\rho_0/\rho_1 - 1) - V_{SH}] + \rho_1' V_{SH} \qquad (2.4)$$

where $\boldsymbol{\rho i}=Pi/(Z(Ti,Pi)\ \mathrm{RTi})$ is the molar densities of the gas, with $Z(Ti,Pi)$ the compressibility factor of the measured gas at the temperature $\boldsymbol{Ti}$ and the pressure $\boldsymbol{Pi}$. $\boldsymbol{\rho 0}$ is the molar density in the calibrated reservoir before the gas expansion, $\boldsymbol{\rho 1}$ is the molar density after the gas expansion in the SH volume

and the consequent adsorption in the sample. **ρ*1'*** is obtained as ρ*1* in the previous step. Naturally, in this evaluation the sample volume is removed from the sample holder volume $\mathbf{V_{SH}}$.

The maximum error on the adsorbed moles is:

$$\Delta n_{ads} = (V_{SH} + V_{CR})\Delta\rho_1 + V_{CR}\Delta\rho_0 + (\rho_0 - \rho_1)\Delta V_{CR} + \rho_1\Delta V_{SH} + V_{SH}\Delta\rho_1' + \rho_1'\Delta V_{SH} \quad (2.5)$$

where $\mathbf{\Delta V_1} = \Delta V_0$, $\Delta P_1 = \Delta P_0 = \Delta P_1' = 0.01/RT$ cc^{-1}

In figure 20, the behavior of the relative error $\mathbf{\Delta n_{ads}/n_{ads}}$ vs pressure at different relative error $\Delta V_i/V_i$ is shown in the case of H_2 adsorption measurement in ZSM-like zeolites reported in figure 2.2.

The maximum error values in the adsorbed moles evaluation increase dramatically at high pressure. A 0.2% relative error in the system void volumes evaluation implies a maximum error in the calculation of n_{ads} ranging from 1.5% to 10% in the 0.0÷8.0 MPa, an acceptable value for volumetric measurements on gram-scale samples. As a consequence, the evaluation error on the piping and valves dimensions in a typical volumetric system, whose void volumes range between 10 cm^3 and 800 cm^3 [3, 10, 13,22], should be as low as 0.02 cm^3 for the minimum value.

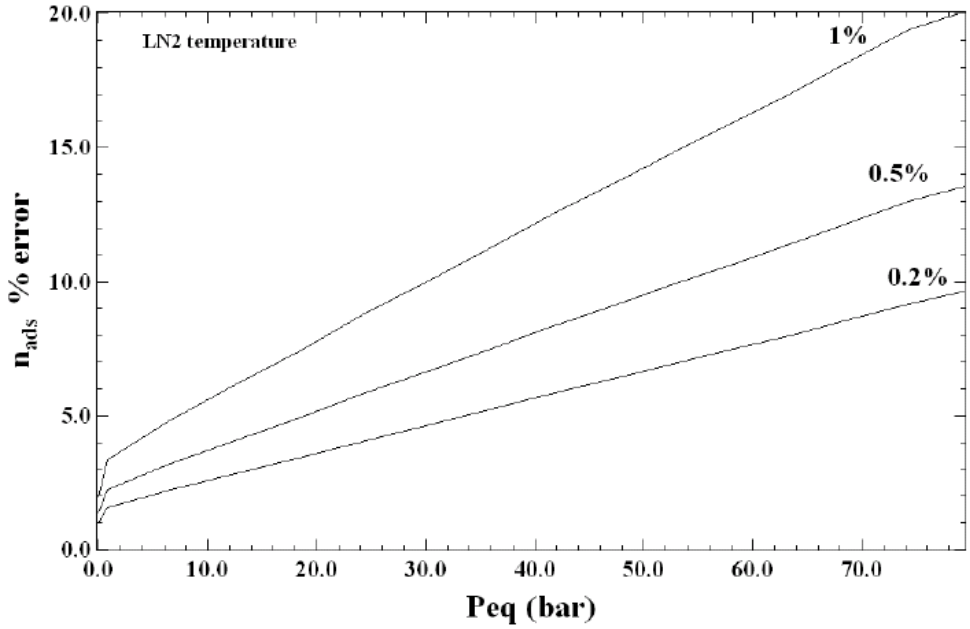

Figure 2.6. % error of n_{ads} evaluated at different error of the void system volumes at LN2 temperature. The sample is ZSM-like zeolite.

On the other hand, by using a pressure manometer with 0.1 kPa sensitivity, an order of magnitude below the value for the *f*-PcT one, the maximum error decreases more than the 50%.

Additional critical aspects have to be considered as possible error sources in the system void volumes calibration.

The system volumes are connected with two different valves: manual valves (MV) and electric valves (EV). The employ of those valves is due to the involved volumes during the experiments. The MV are utilized only in the gases-in line and on the ZT, the EV are used to divide the SH and the reservoir volumes from the rest of the system. The use of EVs is made to fix the system void volume independently if the valves are open or closed, which is, from our point of view, extremely important for the success of the

experiments. In literature the most utilized valves are the pneumatic (PV) [7, 23], bellows [11] and needle valves [14].The internal volume of those valves, as it is shown in figure 2.7a, changes between its opening and closure. On the other hand, the volume of solenoid valves remains constant between the on- and off-status (see figure 2.7b).

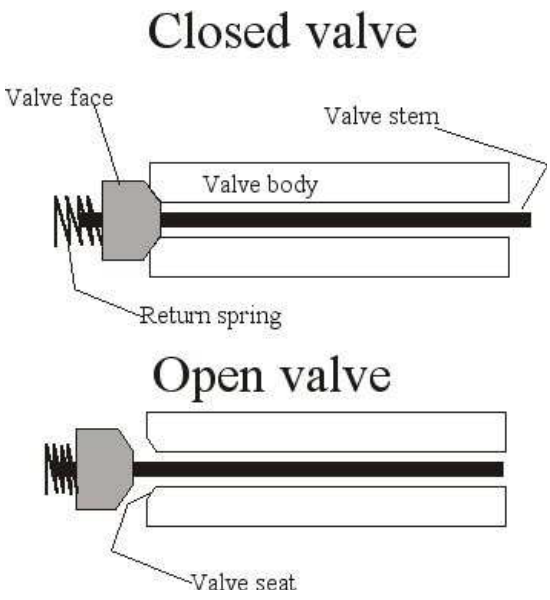

(a)

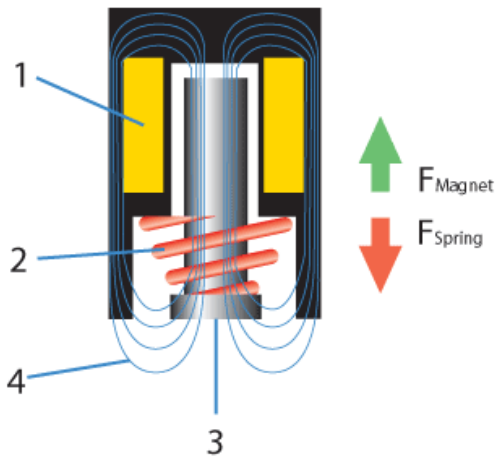

(b)

Figure 2.7. Schematic view of on and off status in (a) PV and (b) EV.

In the *f*-PcT apparatus, variable-volume valves are utilized only in the gases-in line and on the ZT, while solenoid valves are used to separate the SH and the calibrated reservoir volumes from the rest of the system. Fixing in this way the values of the internal volumes, we obtain a reliable evaluation of those crucial parameters in the adsorbed moles determination.

In fact, the alternative choice of variable-volume valves can give rise to a volume measurement uncertainty of 1% which results in an error of the order of 20% or greater in the calculation of the adsorbed gas wt%.

For the volume calibration procedure, Rouquerol et al. [16] advise the use of gases with the same virial coefficient $\mathbf{B_m}$ as the adsorptive specie, since the correction due to this coefficient can be significantly different from one gas to the other. Furthermore, to be more accurate, sample holder with a smooth internal surface should be utilized otherwise it will behave as porous material and it could alter the measured equilibrium and dynamical sorption properties. Due to the favorable conditions for our system (very low gas condensation at RT, very smooth internal surface area of the piping), we prefer to perform the calibration with the same gas utilized in the sorption measurements and not helium gas as reported in the literature [1]. Cross testing the volume evaluation results by using either He or H_2, we found identical volume values.

To be more accurate in the volume calibration procedure, sample holder with

smooth surface should be utilized otherwise it will behave as porous material and it could changes the equilibrium and dynamical sorption properties of the investigated sample. In addition the expanded gas could condensates easily on the sample holder with rough surface during the sorption measurements at low temperature.

The choice of the system void volumes values fulfill two requirements:

1. the gas adsorbed moles are less than the moles expanded into the void volume (Wang and Suda relation [7]),

2. the reservoir and sample holder void volumes do not differ too much.

The first condition requires $n_{exp} \geq n_{ads}$, where the n_{exp} are the gas moles expanded to the sample holder void volume. If $PV = Zn_{exp}RT$ we obtain the relation:

$$\mathbf{V \geq wt\%(Z(T,P)*R*T*m_{sample}*)/(MP)} \qquad (2.6)$$

where **M** is the gas molecular weight.

In silicalite-1 the wt% of hydrogen adsorbed at 0.1 MPa and 77 K is 0.7%, if 0.2 mg are measured, the sample holder void volume has to fulfil the relation V ≥ 4.5 cc. In our case the sample holder void volume is 5.8 cc.

The second condition has to be fulfilled because considering formula (2.5), the error made on the evaluation of the wt% depends on the pressures difference between the reservoir volume before the valve opening and the sample holder volume after the valve opening. In particular, if the reservoir and sample holder void volumes are too different, the pressures difference enhances and thus, the error made on the adsorbed moles evaluation increases.

2.1.3.6 Sample properties

In order to perform accurate experiments and calculate exactly the gas adsorbed moles, different sample properties have to be evaluated: sample volume, adsorbed gas density, gas compressibility, gas diffusion time and SSA.

The insertion of the sample in the apparatus causes a reduction of the relative sample holder volume [8]. According to this reduction, a non trivial question raises in the volumetric evaluation of the sorbed gas concerning the sample volume. In principle, this volume has to be considered as volume inaccessible to the sorbed gas specie. In addition, the same sample has different apparent volumes if gases with different "molecular radius" are considered.

Furthermore, when meso- and micro-porous materials are concerned, several other points have to be considered such as regarding the empty internal volumes originated from the material porous structure. In particular for material with high specific surface area (SSA), it is usual to refer the sample volume to the material skeleton density. To overcome these problems, we implemented an "in-situ" gas pycnometry technique by using He gas [17]. As a first step, after the sample insertion and eventual under vacuum heating procedure, we perform a series of gas expansion at low pressure (below 1 atm) and RT. Using low pressures, we avoid the effects described by Malbrunot et al. [22], i.e. the He gas partial adsorption from the sample at higher pressures. Error less than 1% in the skeleton sample volume evaluation has been obtained.

An additional topic to be considered when high SSA samples are investigated is the increment of the sample volume during the adsorption of gas molecules (moles in excess, n_{exc}) [16,17]. Naturally, this extra-volume is negligible for low SSA samples due to the very small thickness of the adsorbed layer. In general the volume occupied from the physisorbed molecules is

$$V_{ads} = v_o * n_{ads} \qquad (2.7)$$

where $\mathbf{v_o}$ is the volume occupied from 1 mole of condensed gas (molar volume).

As an example, in literature there are many works about the density of physisorbed hydrogen on carbon materials [24] or MOF [25] which show values close to the liquid hydrogen value (v_0 = 28.25 cm^3/mol; density = 70.8 kg/m^3) [24] or even lower (v_0 = 37.73 cm^3/mol; density = 53 kg/m^3) [25]. In order to find a general rule for determining this value, we tried to find out the lowest density (highest molar volume) for the liquid phase on the basis of the following consideration: the physisorption temperatures (77 K or even more) is usually largely higher than the H_2 critical temperature (T_c = 33.145 K) while the measured H_2 pressures go beyond the critical pressure (P_c = 1.2964 MPa). For those reasons, we estimate as a minimal value for the adsorbed film molar volume, the liquid hydrogen value at the melting point (T_m = 14.1 K), i.e. 28.25 cc/mol. Having this as a boundary, the molar volume could increase by changing the H_2/surface interaction: well packed liquid-like hydrogen films are expected to be characterized from high physical interaction energies. In any case, the usually low interaction energies (few meV/molecule) will be effective in physisorption leaving a high lateral mobility of the adsorbed molecules whose density could be at maximum that of the liquid phase of the molecular specie [26]. Attempts to evaluate this parameter by molecular dynamics calculations are not totally reliable because the modelled internal surface of the porous sample does not represent strictly the real structure.

Considering a typical mesoporous sample with 0.7 g/cm^3 apparent density (i.e. the mass of powder filling a unit volume) adsorbing up to 1wt% of H_2, we obtain a maximum value of V_{ads} = 0.10÷0.12 cm^3 of condensed H_2 per each cm^3 of the sample holder V_{SH} which is consistent fraction of its value. The fact that these volumes are comparable, make strictly necessary to take V_{ads} into account for the evaluation of the volume for the free diffusion of the gas in the evaluation of the n_{ads} by formula (2.4). At this point, we deal with two strictly related quantities, V_{ads} and n_{ads}, whose evaluation is not independent. We

adopted a recursive routine that allowed to calculate these quantities in self-consistent way. This routine converges rapidly (7-9 loops) making it a reliable tool to avoid the effects of the apparent sample volume expansion due to the adsorbed gas layer. Figure 2.8 shows how the H_2 adsorption isotherms for silicalite-1 present different behavior taking into account the n_{exc} contribution, as expected.

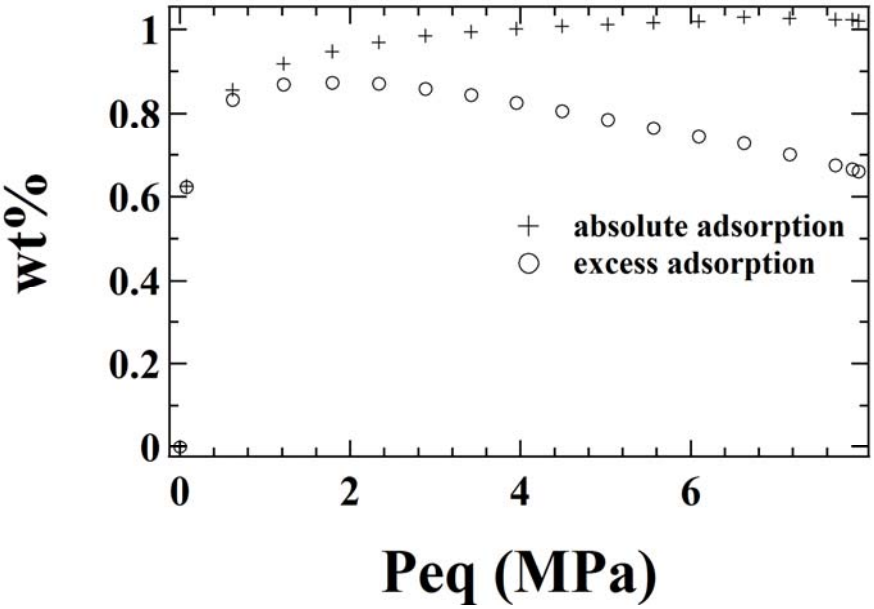

Figure 2.8. PcT isotherms of silicalie-1 considering the n_{exc} contribution to the sample apparent volume.

2.2 Brunauer, Emmett, Teller method (BET)

Specific surface area S_{BET} and porosity were determined with the BET method [27] using adsorption data points in the relative pressure P/P_o range 0.01 to 0.30. Surface areas S_t were also determined from t-plots which were constructed using nitrogen adsorption data. The desorption branches of the isotherms were used for the pore size calculations according to the Kelvin

equation r_k ~ 4.146/log P_o/P (Å), where P_o is the saturated vapour pressure in equilibrium with the adsorbate condensed in a capillary or a pore, *P* is the vapour pressure of a liquid contained in a cylindrical capillary, and r_k is the Kelvin radius of the capillary or pore. The Kelvin equation was used according to BJH method for calculation of core radii from the pressure values of the isotherm, the pore radius combining the last with the t-values from the standard isotherm and finally the pore size distribution (PSD) of the samples. All samples used for the surface analysis were outgassed at around 523 K for 10 h under high vacuum (10^{-5} mbar) before measurement.

2.3 Scanning Electron Microscopy (SEM)

Scanning electron microscope [28] is one of the most versatile instruments for examining the microstructural characteristics of porous solids. High resolution that can go beyond 2,5 nm and three-dimensional view are characteristic principles of this instrument. The variety of the attained signals (x-rays, Auger electrons etc) provides rich information regarding surface's composition and additionally can be studied crystallographic, magnetic and electronic characteristics of the materials. A scanning electron microscope is composed of:

- ✓ the luminescence source: Electron gun;
- ✓ the vacuum system;
- ✓ the electromagnetic lenses;
- ✓ the deflection coil;
- ✓ the object's lens;
- ✓ the signal detector;

- ✓ the signal transformation system to images;
- ✓ the sample holder area;

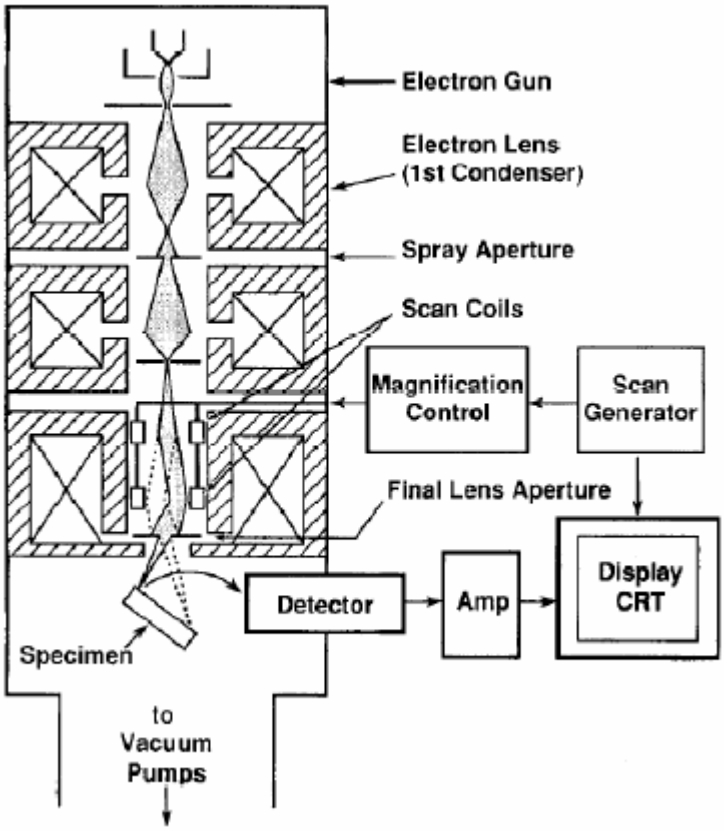

Figure 2.9. Schematic presentation of a SEM apparatus.

The scanning procedure takes place through interactions between sample's surface and the electronic beam. Between the produced signals there are: secondary electrons, electrons diffusing inside the surface, a continuum characteristic of the X rays, auger electron emissions and photons of various energies. The resolution of a particular SEM signal is determined primarily by the excitation volume and not by the magnitude of the secondary probe. The energy of the beam electrons lies in between (1 – 30) keV. When the beam arrives in the surface there can be either elastic or inelastic diffusion. The first

results from the interactions between the beam electrons and the atoms of the material provoked by significant deviations on the occurring directions. The second is produced from the inelastic interaction between the beam's electrons and the material's bonds.

The inelastic diffusion is directly responsible for the production of the signals used for the surface's examination. In fact, the interaction with the Coulomb field of the atoms verifies energy loss and emission of characteristic x-rays.

Below 10 nm the electrons diffusing from the primary beam get strongly absorbed through recombination with the gap that is created during the diffusion process and in some insulator materials there are produced photons with wave lengths in the visible or the near infrared giving therefore a visible luminescence. The intensity of backscattered electrons can be correlated to the atomic number of the element within the sampling volume. Hence, some qualitative elemental information can be obtained. The analysis of characteristic X-rays emitted from the sample gives more quantitative elemental information. Such X-ray analysis can be confined to analytical volumes as small as 1 cubic micron.

The Scanning Electron Microscope we used (Quanta FEG 400 (FEI)) operates in the e- SEM mode, which is environmental-SEM and allows operation in very low vacuum conditions (≤ 20 Torr) with the possibility to collect secondary electron with an appropriate detector (GSED). The gas ionization process on the sample allows the compensation of the charge product by the electron beam on the surface. In this way it is possible to analyze also non conductive sample without a pre-metallization.

Moreover, operating in a relative high pressure permits to study sample with a high content of volatile substances, like water, polymer and etc. Cooling the sample close to or below 0 °C is possible to work in a condition of 100% relative humidity.

2.4 X-ray Powder Diffraction

Morphological investigation is linked to the long range order probed by XRD [29].

The X-ray powder diffraction (XRD) data were collected using Cu K_α radiation of a Bruker Axs Diffractometer/Reflectometer (D8) equipped with a Dynamic Scintillation Detector, NaI and with a Gobel mirror. The measurements are made in transmission: the sample powder is put in special glass capillaries (ϕ=1mm, Hilgenberg GmbH) and the latter in a handmade sample holder. All measurements have been done at room temperature (298 K). The spectra were recorded in the 2Θ range from 2 to 40°. The step was $0{,}03^o$ and the counting time was 1s/step. The effect of void capillary has been taken into account.

Bibliography Chapter 2

[1] Broom DP. International Journal of Hydrogen Energy. 2007;32:4871-88

[2] Lee YW, Clemens BM, Gross KJ. Journal of Alloys and Compounds. 2008;452(2):410-3

[3] Zielinski JM, Coe CG, Nickel RJ, Romeo AM, Cooper AC, Pez GP. Adsorption-Journal of the International Adsorption Society. 2007;13(1):1-7

[4] Panella B, Hirscher M, Roth S. Carbon. 2005;43:2209-14

[5] Voskuilen T, Zheng YA, Pourpoint T. International Journal of Hydrogen Energy.35(19):10387-95

[6] Weinberger B, Lamari FD. International Journal of Hydrogen Energy. 2009;34(7):3058-64

[7] Wang, X. L.; Suda, S. Journal of Alloys and Compounds, 1995, 231, 660-665

[8] Blach, T. P.; Gray, E. M. Journal of Alloys and Compounds, 2007, 446, 692-697

[9] http://webbook.nist.gov. The compressibility was calculated taking into account the inverse of H2 molar density in the NIST data, multiplied for pressure and divided for the ideal gas constant and temperature

[10] Belmabkhout, Y.; Frere, M.; De Weireld, G. Measurement Science & Technology, 2004, 15, 848-858

[11] Blackman, J. M.; Patrick, J. W.; Snape, C. E. Carbon, 2006, 44, 918-927

[12] Checchetto, R.; Trettel, G.; Miotello, A. Measurement Science & Technology, 2004, 15, 127-130

[13] Ramaprabhu, S.; Rajalakshmi, N.; Weiss, A. International Journal of Hydrogen Energy, 1998, 23, 797-801

[14] Sun, J., Jarvi, T. D., Conopask, L. F. et al. Energy & Fuels, 2001, 15, 1241-1246

[15] Hirschfelder, J.O.; Curtiss, C.F.; Bird, R.B. ed., Wiley, New York, 1954

[16] Rouquerol, F.; Rouquerol, J.; Sing, K. ed., Academic Press, London, 1999

[17] Sircar, S. Aiche Journal, **2001**, 47, 1169-1176

[18] Broom, D. P.; Moretto, P. Journal of Alloys and Compounds, 2007, 446, 687-691

[19] Beeri, O., Cohen, D., Gavra, Z. et al. Journal of Alloys and Compounds, 1998, 267, 113-120

[20] Panella B, Kossykh L, Dettlaff-Weglikowska U, Hirscher M, Zerbi G, Roth S. Synthetic Metals. 2005;151(3):208-10

[21] Perry RH, Green DW, Maloney JO. Perry's chemical engineers' handbook. 7th edition ed. New York: McGraw-Hill 1997

[22] Malbrunot P, Vidal D, Vermesse J, Chahine R, Bose TK. Langmuir. 1997;13(3):539-44

[23] Checchetto R, Trettel G, Miotello A. Measurement Science & Technology. 2004;15(1):127-30

[24] Zuttel, A., Wenger, P., Sudan, P. et al. Materials Science and Engineering BSolidState Materials for Advanced Technology, 2004, 108, 9-18

[25] Lee, J. Y., Pan, L., Kelly, S. R. et al. Advanced Materials, 2005, 17, 2703

[26] Karger, J; Ruthven, D.M. Diffusion in zeolites and other microporous solids, ed., John Wiley & Sons, 1992

[27] Stephen Brunauer, P. H. Emmett, Edward Teller, J. Am. Chem. Soc., 1938, 60 (2), pp 309–319

[28] J.I.Goldstein, H.Yakovitz Practical Scanning Electron Microscopy, 1rst ed., Plenum Press, New York, 1975

[29] Klein, Cornelis and Cornelius Hurlbut Jr. Manual of Mineralogy, 20th ed., Wiley, 1985.

3. Synthesis

3.1 Periodic Nanoporous Organosilicas (PNOs)

3.1.1 Phenylene Bridged PNOs

3.1.1.1 Synthesis procedure

All solutions were prepared with analytical grade chemicals and ultra pure water. Decyltrimethylammonium bromide (C_{10}TABr, 99%, Aldrich), dodecyltrimethylammonium bromide (C_{12}TABr, 99%, Aldrich), cetyltrimethylammonium bromide (C_{16}TABr, 99%, Fluka), and octadecyltrimethylammonium bromide (C_{18}TABr, Aldrich) as structure-directing agents and 1,4-bis(triethoxysilyl)benzene (BTB, 96%, Aldrich) as organosilica source reagents were used. Sodium hydroxide pellets, ammonium hydroxide solution (25%) as catalysts, absolute ethanol (99.9% (v/v) and hydrochloric acid (36%), were supplied from Aldrich. BTB was used as the silica source without further purification.

The PNO samples were synthesized by a typical synthesis procedure using the follow ratio of 5(mmol) BTB : 2.8(mol) H2O : 20(mmol) NaOH (6M) : 4.9(mmol) surfactant. Trimethyl ammonium bromide was dissolved in water and sodium hydroxide at 50-60^{o}C in a closed polypropylene bottle until the solution become clear. Then, BTB precursor was slowly added to the surfactant solution under vigorous stirring at room temperature. The mixture was sonicated for 20 minutes and stirred for 20 hours. The solutions were aged at 95^{o}C for 20 hours in closed polypropylene bottles. The white powder was collected by centrifugation, washed thoroughly with water, and air-dried under ambient conditions. In order to remove the surfactants creating open structures the as-synthesized sample was stirred for 24h in a refluxing solution of 10g HCl (36% wt.) and 70g of ethanol. The same procedure was

repeated three times. The corresponding porous material was collected by centrifugation and air-dried under ambient conditions.

3.1.1.2. Organisilica synthesis using BTB and TEOS as precursors

The typical synthesis procedure is the same as the one described above. In a second polypropylane bottle, mixtures of BTB over tetraethoxysilane (TEOS) are inserted in ratios of 0%, 25%, 75% and 100% BTB:TEOS and stirred for 30 minutes. Precursors are added into initial solution drop by drop while solution being stirred. Following this, procedure continues as above. Removal of surfactants takes place as described above.

3.1.1.3. Organosilica synthesis with 4,4 Bis-Triethoxysilyl-Biphenyl (DBTB) as precursor

The synthetic procedure is carried out like this: in a polypropylene bottle of 150 ml there are added 59.4 g H2O (3.3 mol), 5.06 ml NaOH (6M) (30.4 mmol) and lastly 1.16 g (3.2 mmol) of the surfactant. Then, 1.16 ml (3.2 mmol) of the precursor is added drop by drop under vigorous stirring in ambient temperature. Solution is stirred for 20 hours and after it is sealed airproofly is placed in 95 ˚C for 22 hours under static conditions. Following this, solution is left to cool down in ambient temperature and is centrifugated. Centrifugation is repeated 2 times with distilled water washing to take place between each centrifugation. (Centrifugation parameters: t=10 minutes, speed: 3.5 krpm). Surfactant removal was carried out with H+ cation exchange as described above.

3.1.1.4. Doping with Li+ cations

0.5 g of sample synthesized under the procedure described in section 3.0.2.1 or 3.0.2.3 was introduced into a bottle and have been through reflux at 70 °C for 8 hours, with 125 ml of LiCl solution in ethanol 1N.

3.1.2 Naphthalene PNOs

1-Naphthyl(triethoxy)silane (substance: Naph-Si) was synthesized as follows:

Periodic nanoporous organosilica was synthesized with a one step direct co-condensation of TEOS and Naph-Si in a 6.33:1 ratio. 12.525 g H_2O, 8.058 g NH_3 (25%wt) and 0.315 g CTAB were stirred for 15 min in a 30 ml polypropylene bottle. 1.425 g TEOS (6.84 mmol) and 0.3138 g Naph-Si (1.08 mmol) were added and the solution was vigorously stirred for another 30 minutes. The beige product was retrieved after heat treatment at 80 °C for 96 hrs, which can be slightly considered as a hydrothermal treatment. It was filtered, rinsed with H_2O and cold ethanol (EtOH) and finally placed on a plate for air-drying (sample: Naph-PNO). 600 mg Naph-PNO were treated with 4.5 g HCl 37%wt in 100 ml EtOH for 1 h at 70 °C. The product was then filtered, rinsed with cold EtOH and afterwards was placed on a plate for air-drying (sample: Naph-PNO-H^+). 240 mg Naph-PNO were placed in a porcelain crucible and were heat treated at 350 °C for 5 hrs with a 1.5 °C/min heating rate (sample: Naph-PNO-350).

3.2 Zeolite-like carbon materials

Zeolite beta powder was obtained by Tosoh Corporation (Japan). The porous carbon materials were prepared as follows: a ceramic boat with 0.5 g of zeolite beta (pretreated in air at 923K for 2 hours), was placed in a flow through tube

furnace. The sample was then heated up to the desired temperature (1023 K, 1073K and 1123K) under argon atmosphere. When the targeted temperature was reached, acetylene as a carbon precursor was admixed (for 15 min) with the carrier gas (argon) at flow rates of 10 cm^3/min and 90 cm^3/min, respectively. After the completion of acetylene flow, the ceramic boat was cooled down to room temperature under argon atmosphere. The resulting zeolite/carbon composites were recovered and washed with 10 wt% HF for 3 days in order to remove the zeolite framework. Finally, the resulting carbon materials were dried in air in an oven at 393K (samples denoted as CZ1023, CZ1073 and CZ1123 correlated to the three temperatures used during the CVD method).

3.3 Zeolites

3.1 Sapo-34

SAPO-34 crystals were prepared by using tetraethylammonium hydroxide, dipropylamine as primary and secondary structure-directing agents, respectively and methylene blue as crystal growth inhibitor, with different N/Si ratio (0.5 and 0.27, for crystals synthesized respectively with and without methylene blue). The synthesis has been carried in two steps as reported for MFI crystals: the first at low temperature to favour crystal nucleation; the second one at high temperature for the crystal growth.

3.2 Silicalite-1

The silicalite-1 zeolites have been prepared from a synthesis mixture of the following composition (in oxides): 8.8 $(C_3H_7)_4NBr$: 5 Na_2O : 0,125 Al_2O_3 : 100 SiO_2 : 1250 H_2O obtained by dissolving the right amount of

tetrapropylammonium bromide (>99%, Fluka, purum) in a freshly prepared 30% sodium hydroxide solution (pellets, 98,6%, Baker analyzed), followed by the addition of the rest of distilled water and finally by precipitated SiO_2 (BHD). Aluminum was contained as an impurity mainly in the silica, and its content measured by means of atomic absorption spectroscopy (Perkin Elmer AAS 380). The homogenized gel was loaded in a Teflon lined stainless steel autoclave and heated at 170 ^oC for 30 hours. The solid was filtered and washed with plenty of water up to a neutral pH, and dried at 100 ^oC for 12 hours.

The silicalite-1 has been modified with different organosilane molecules: Cl_3SiCH_3, $Cl_2Si(CH_3)_2$ and $Cl_3Si(CH_2)_2(CF_2)_8F$. For the sake of clarity the sample modified with the last molecules will be called fluorinated silicalite-1.

4. Results and Discussion

4.1 Periodic Nanoporous Organosilicas (PNOs)

Before each adsorption measurement, the samples were heated up to 200°C under vacuum for 12 hours in order to remove water and other possible impurities.

For each sample PcT isotherms were obtained at 287K, 298K and 313K, and the experimental data fitted by Tóth equation [1]. From the fitting parameters results we can have estimation about the trend of the samples adsorption properties. The number of molecules per nm^2 and the isosteric heat of adsorption will be evaluated for all samples.

Furthermore, the Specific Surface Area (SSA) and porosity were measured with the common Brunauer-Emmet-Teller (BET) technique with N_2 as the probing molecule.

Density was measured with pycnometry measurements with He as a probe molecule (see experimental part). Images with Scanning Electron Microscopy (SEM) and X-ray diffraction patterns were received to extract more information on the morphology and crystallinity of the samples structure.

The combination of all the experimental results will be discussed in order to extract the relation between adsorption and structural/morphological properties.

4.1.1 Phenylene Bridged PNOs

4.1.1.1 Surfactant's main chain length variation (BTB) **[2]**

According to the PNOs samples' synthesis procedure (see paragraph 3.1.1.1), a multiplicity of pores ordering has been obtained, which ranges between fully disordered to fully ordered packaging. In particular, we observed that the surfactant chain length is the key parameter in order to tune the morphology and the porosity of the synthesized materials which are strictly related to the sample adsorption properties [3].

The XRD patterns reveal an amorphous structure of the BH_C10_100 sample while a certain degree of order is visible for the other samples (figure 4.1 a-d). Particularly, the XRD pattern of the BH_C12_100 shows the (100) diffraction of the hexagon symmetry at 2.45° while the (110) and (200) diffractions are not well observed indicating a low degree of long-range ordering. Thus the distance between (100) planes, d_{100}, is 36.2 Å (the centers of the tubular pores are 41.8 Å apart). A similar pattern is present for the BH_C18_100 sample with the main peak centered at 1,92° revealing an increase of the lattice parameter, d_{100} = 46.0 Å, due to the longer surfactant chain. Finally, the XRD pattern of the BH_C16_100 sample shows the (100) diffraction at 2.07° (d_{100} = 42.6Å), while the (110) and (200) diffraction are clearly observed indicating that the hexagonal symmetry is retained on domains extended for several unit cell, i.e. in the 100 nm range.

The XRD patterns do not vary after methane adsorption (data not shown), towards several adsorption/desorption cycles and thermal treatments, revealing the stability of the samples.

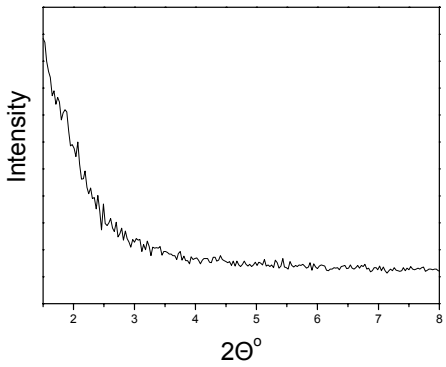

Figure 4.1a. *XRD pattern of the BH_C10_100.*

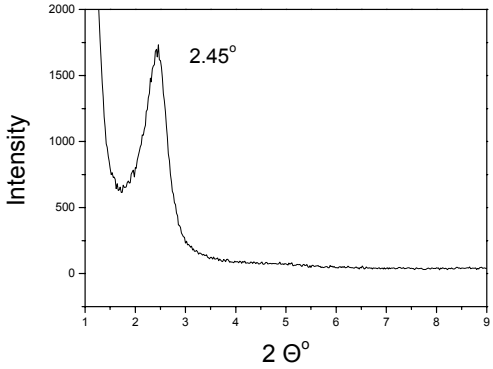

Figure 4.1*b*. *XRD pattern of the BH_C12_100*

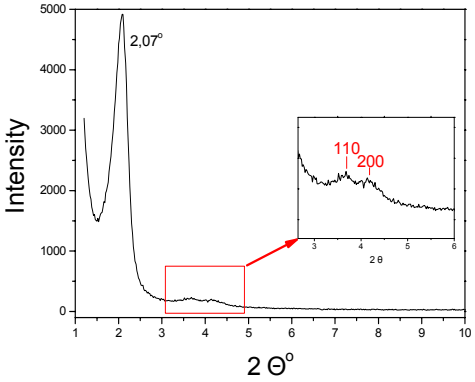

Figure 4.1c. *XRD pattern of the BH_C16_100*

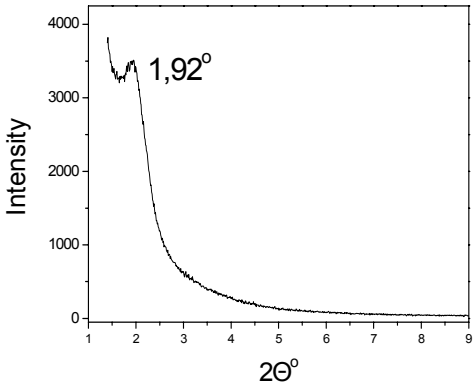

Figure 4.1d. *XRD pattern of the BH_C18_100*

SEM images (see figure 4.2 (a-d)) present the morphology of PNOs at the μm-scale. In particular, we observe that BH_C10_100 sample shows an open structure with no definite grain boundaries while few-micrometer sized particles are visible for all the other samples. BH_C16_100 particles, in some cases, show the hexagonal shape as expected from their sharper XRD pattern, i.e. their wider long range ordering.

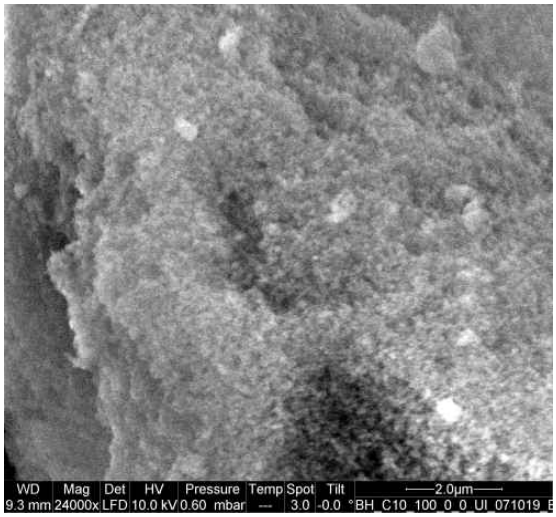

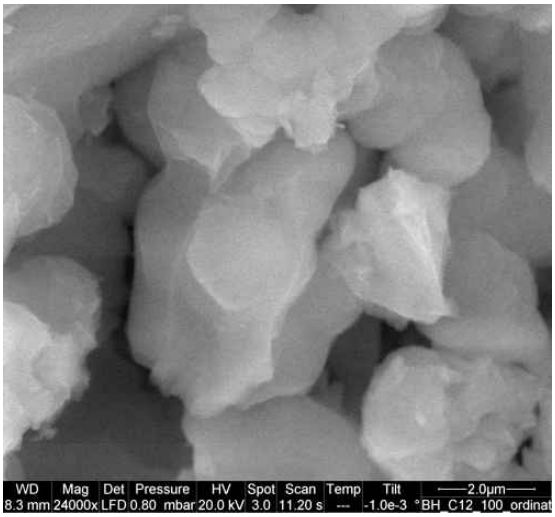

Figure 4.2a. *SEM image of the BH_C10_100 sample.* **Figure 4.2*b***. *SEM image of the BH_C12_100 sample*

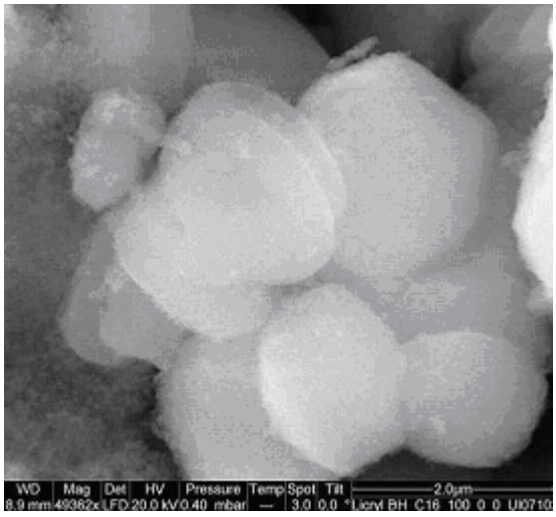

Figure 4 2 c. *SEM image of the BH_C16_100 sample* ***Figure 4.2 d***. *SEM image of the BH_C18_100 sample*

The SSA evaluation by means of the BET method, allowed us to determine its dependence on the surfactant's chain length. BH_C16_100 sample shows the highest SSA value if compared to the other samples which, in turn, are quite similar. On the other hand, the BH_C10_100 sample owns the higher value of mean pore size if compared to the rest of the sample. A resume of the samples' structural characteristics is presented in Table 4.1.

SAMPLE	Skeletal Density (g/ccm)	SSA (m^2/g)	Mean pore diameter (Å)	Crystallinity	d_{100} (Å)
BH_C10_100	1.51 ± 0.03	654	24.0	Fully Disordered	=
BH_C12_100	1.35 ± 0.05	642	17.0	Partly Ordered	36.2
BH_C16_100	1.41 ± 0.03	783	18.8	Ordered	42.6
BH_C18_100	1.54 ± 0.03	686	19.2	Partly Ordered	46.0

Table 4.1: Structural properties of all the samples.

Figure 4.3 (a) shows the adsorption (close symbols) and the desorption (open symbols) isotherm curves of methane on PNOs obtained at 298K. The overall shape of the curves is also representative of the isotherms behaviors obtained at 286 K and 313 K on the same samples (figure 4.3b, here presented only for the BH_C10_100 sample) revealing that an enhancement in the storage capacity is obtained at lower temperature, as expected; decreasing the temperature increases the heat removal and increases the storage capacity.

The isotherm curves shape is in agreement with the type I IUPAC curve [4], as all the adsorption isotherms that will be presented in this work, which are fitted adopting the Tóth schema where the saturation is reached with a monolayer coverage. The desorption isotherm curves follow exactly the adsorption isotherms which proves the fully reversibility of the CH_4

adsorption [5]. Considering all the samples, the BH_C10_100 has higher methane uptake up to 5.5 wt% while the rest of the PNO materials present similar storage capacity.

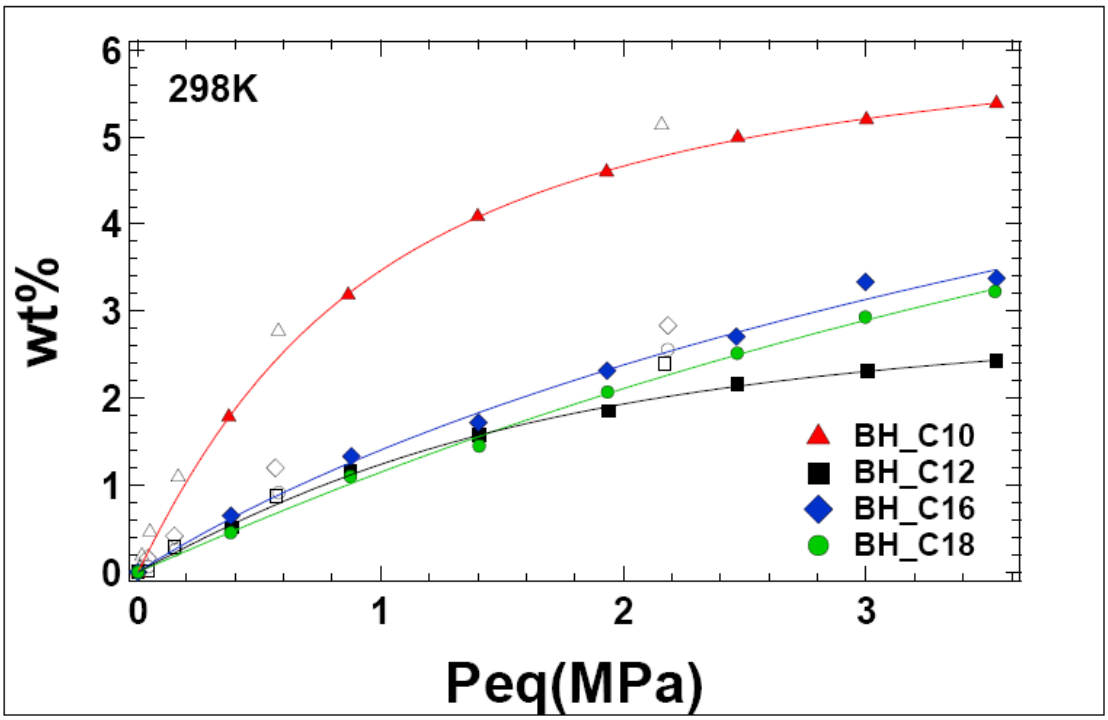

Figure 4.3 a : PcT adsorption isotherms obtained at 298K up to 3.6 MPa for all the samples (markers). Lines between points represent the data fitting procedure based on the Tóth model.

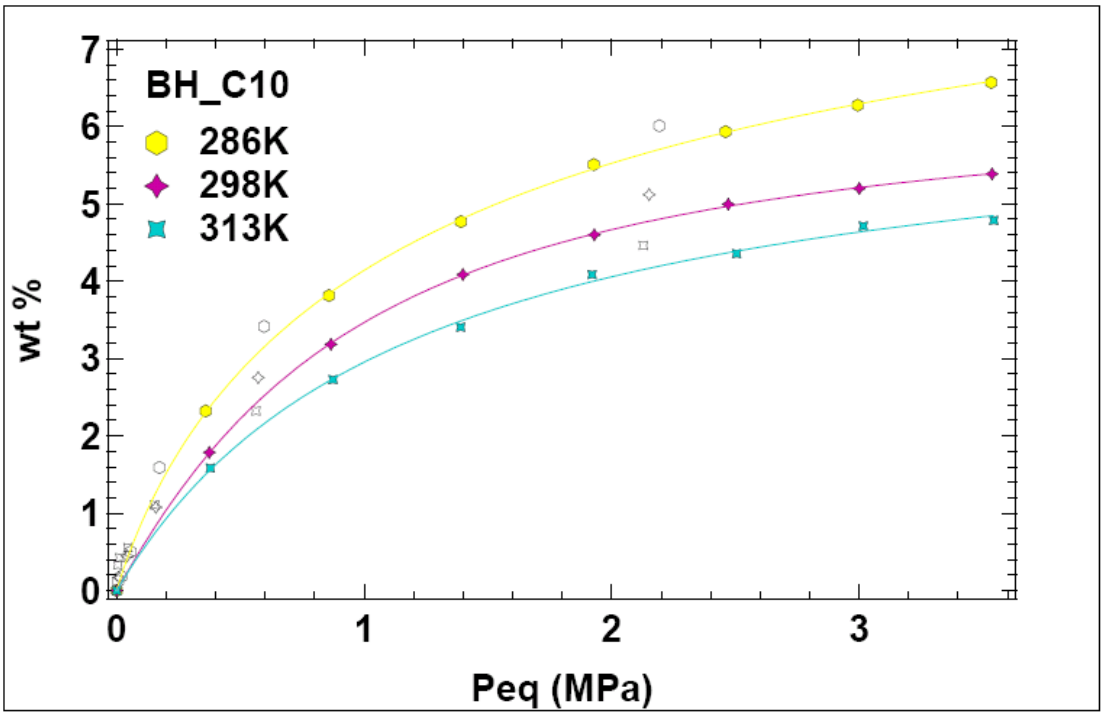

Figure 4.3 b :PcT adsorption and desorption isotherms obtained at 286K, 298K and 313K up to 3.5 MPa for the sample BH_C10_100 (markers). Lines between points represent the data fitting procedure based on the Tóth model.

After evaluating the adsorbed molecules per nm^2 (figure 4.4) it was observed that at the higher pressure reached in the experiment, the BH_C10_100 sample adsorbs a number of molecule/nm^2 close to the formation of one monolayer. On the contrary, the other samples at 3.6 MPa store similar values of number of molecules/nm^2 which correspond to a coverage of half a monolayer of adsorbed methane molecules [6].

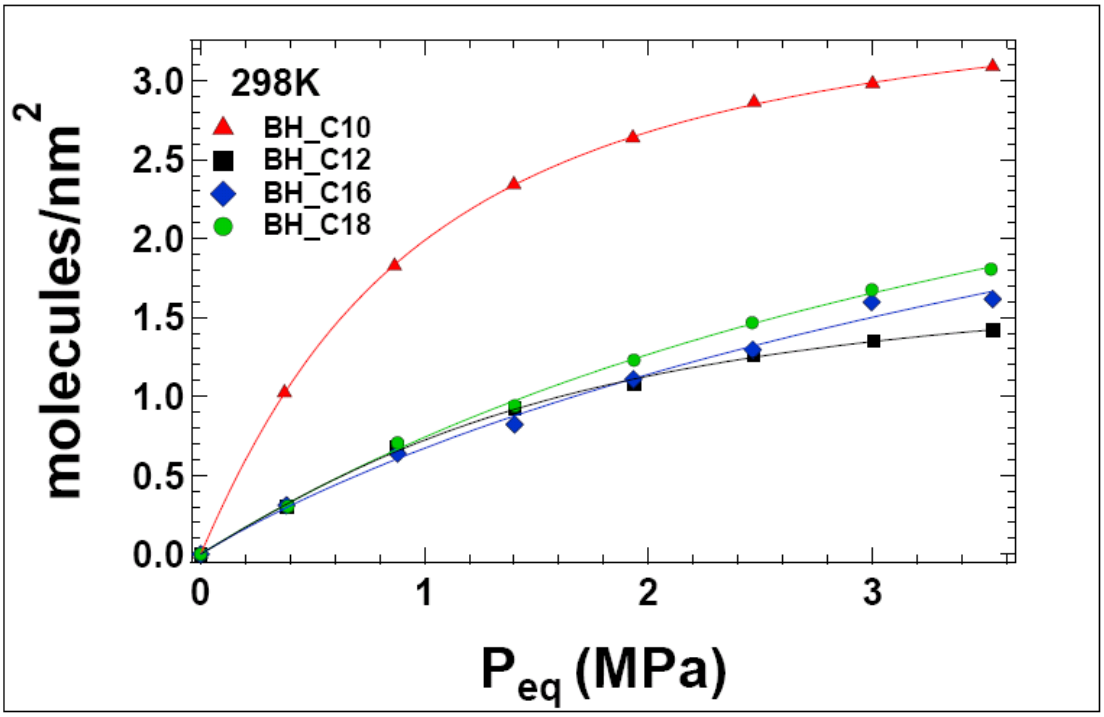

Figure 4.4: Number of molecules per surface's nm^2 for all the samples (markers). Lines between points represent the data fitting procedure based on the Tóth model.

Considering the mean pore size of the samples reported in table I (calculated from the pore size distribution, obtained by BET isotherms), we obtain that the use of the chain length C10 gives an optimum pore size distribution which allow to attract more efficiently the methane molecules compared to the other samples.

The isosteric heat calculated on BH_C10_100 (figure 4.5) is the highest one between the investigated samples (see table 4.2), which is related to greater binding energy between the PNOs surface and the CH_4 molecules in low pressures. In particular, its value is circa twice the isosteric heat calculated on the other samples, which could also explain its higher methane storage capacity (see figure 4.3) and higher amount of adsorbed molecules/nm^2 (see

figure 4.4) at higher pressure values. Specifically, on the other samples, similar methane storage capacities at 3.6 MPa corresponds to comparable isosteric heat (see table 4.2).

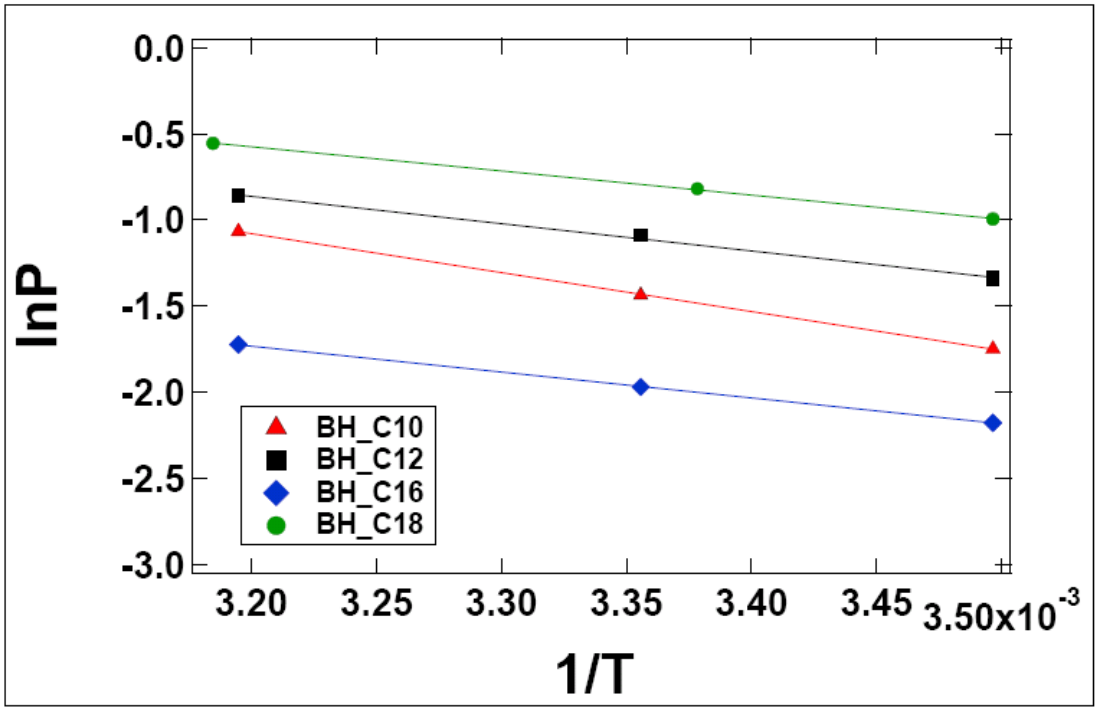

Figure 4.5: lnP vs T^{-1} graph of all the samples and fitting results by using the Clausius-Clapeyron relation.

SAMPLE	ΔH (kJ/mol) Low coverages	ERROR (kJ/mol)
BH_C10_100	19.00	± 0.20
BH_C12_100	13.00	± 0.90
BH_C16_100	12.50	± 0.15
BH_C18_100	12.00	± 0.30

Table 4.2: Calculated isosteric heat of adsorption and its error for all the samples.

The homogeneity grade of the porous sample surface has been evaluated by means the analysis of the adsorption isotherms by Tóth. Considering the Tóth equation and the isotherm curve obtained at room temperature for BH_C10_100, we obtained fitting results as shown in figure 4.6. In particular, at room temperature, we determined the same t-value within the error, for all the investigated samples, with a value close to unity indicating a high grade of surface homogeneity regardless to the samples' structural properties (see Table 4.3). Thus, we can deduce that the CH_4 adsorption sites on the samples surface are energetically equivalent and that the inter-molecular interaction does not affect the adsorption behavior even at high coverages.

On the other hand, the equilibrium constant K calculated in BH_C10_100 is up to six times larger than in the other samples, which is related to its higher isosteric heat value as calculated by Clausius-Clapeyron equation.

The sample BH_C10_100 has the higher theoretical maximum storage capacity as expected.

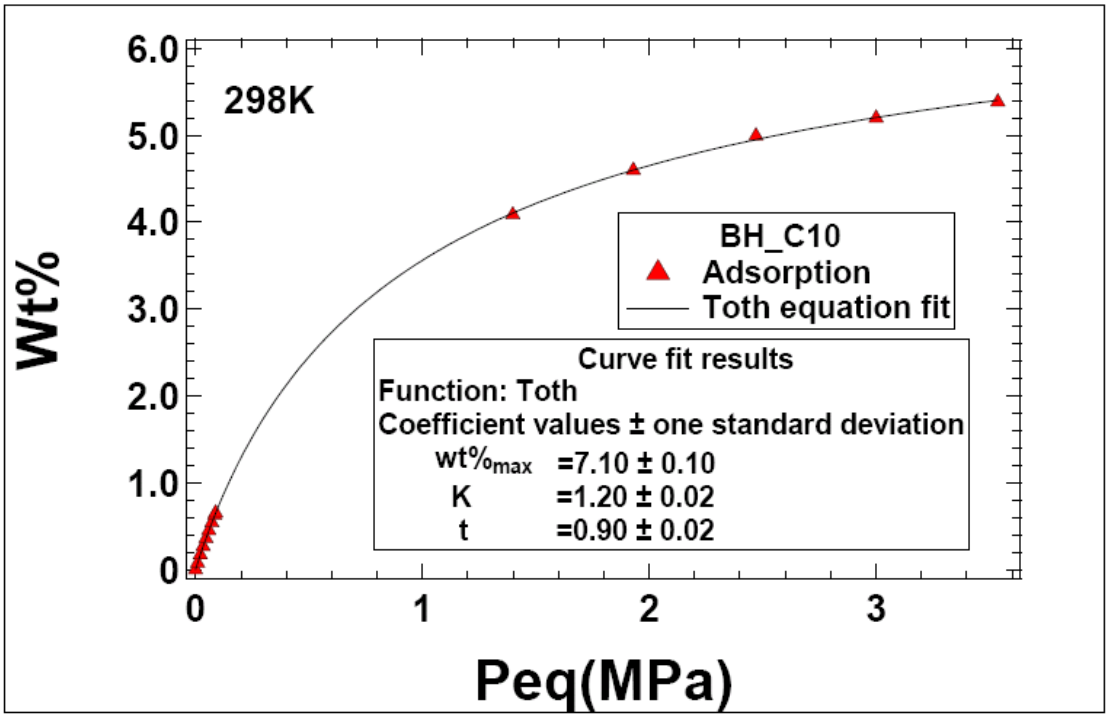

Figure 4.6 :PcT adsorption isotherm obtained at 298 K up to 3.6 MPa for the sample BH_C10_100, fitted with the Tóth model according to the formula. Note that a wider data range is used to obtain a reliable evaluation of the Tóth parameters

SAMPLE	$Wt\%_{max}$	$K \pm \Delta K$ (bar^{-1})	$t \pm \Delta t$
BH_C10_100	7.10 ± 0.10	1.20 ± 0.02	0.90 ± 0.02
BH_C12_100	3.10 ± 0.30	0.20 ± 0.04	0.80 ± 0.04
BH_C16_100	4.50 ± 0.20	0.50 ± 0.08	0.90 ± 0.02
BH_C18_100	4.20 ± 0.10	0.40 ± 0.05	0.90 ± 0.03

Table 4.3: Tóth equation fitting parameters for the samples.

As a consequence, the observed differences of the methane uptake properties of the samples can only be attributed to most favorable binding energy between the methane molecules and the BH_C10_100 pore walls. This higher affinity can be related to the lower curvature of the pore walls which enhances the binding energy between the PNOs walls and the CH_4, as expected [7]. In this explanation framework, a role could be also played by the long range ordering of the samples provided that the BH_C10_100 sample is the only amorphous sample.

4.1.1.2 Effect of aromaticity in the walls of PNOs

PNOs samples were obtained by using the same surfactant chain length (C16) and increasing ratios of BTB and TEOS precursors. Samples are denoted based on the percentage of BTB precursor used (*0%, 25%, 50%, 75%,100%*).

The XRD patterns reveal ordered structures when only one precursor is present : BH_C16_0 and BH_C16_100 (figure 4.7 a,e) while a high degree of disorder is visible for the other samples (figure 4.7 b-d).

Particularly, the XRD pattern of the BH_C16_0 sample shows the (100) diffraction of the hexagonal symmetry at 2.20° while the (110) and (200) diffraction are clearly observed indicating that the hexagonal symmetry is maintained on extended for several unit cell. Thus the distance between (100) planes, d_{100}, is 46.40 Å.

The XRD pattern of the BH_C16_25, after a smoothing, shows the (100) diffraction of the hexagonal symmetry at 2.07° while the (110) and (200) diffractions are not well observed indicating a low degree of long-range ordering. The distance between (100) planes, d_{100}, is 42.60 Å.

A similar pattern is present for the BH_C16_50 sample with the main peak centered at 1,92° and the distance between (100) planes is calculated to be d_{100} = 46.0 Å. For the sample BH_C16_70 a low intensive peak is observed at 2.21° and d_{100} = 46.16 Å. Finally, the XRD pattern of the BH_C16_100 sample shows the (100) diffraction at 2.07° (d_{100} = 42.6Å), while the (110) and (200) diffraction are clearly observed indicating that the hexagonal symmetry is kept on domains extended for several unit cell.

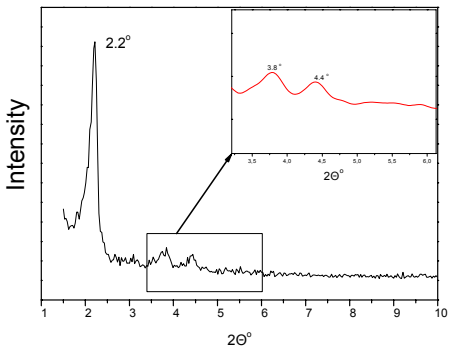

Figure 4.7a. *XRD pattern of the BH_C16_0*

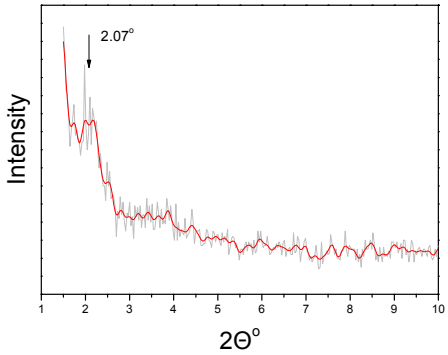

Figure 4.7*b*. *XRD pattern of the BH_C16_25*

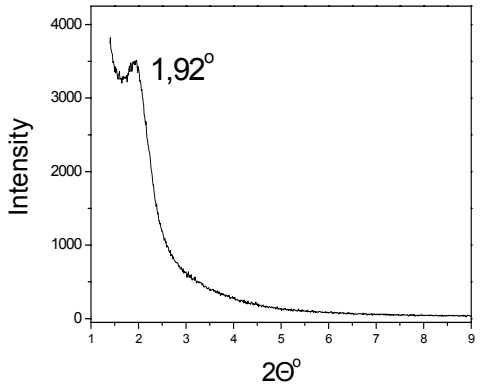

Figure 4.7c. *XRD pattern of the BH_C16_50*

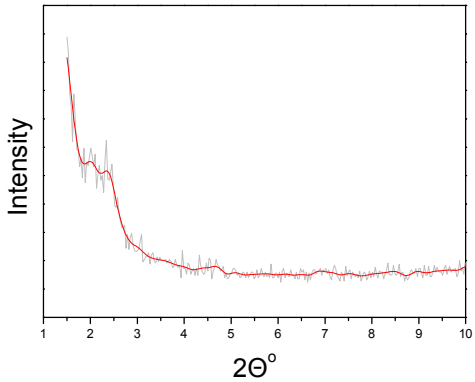

Figure 4.7d. *XRD pattern of the BH_C16_75*

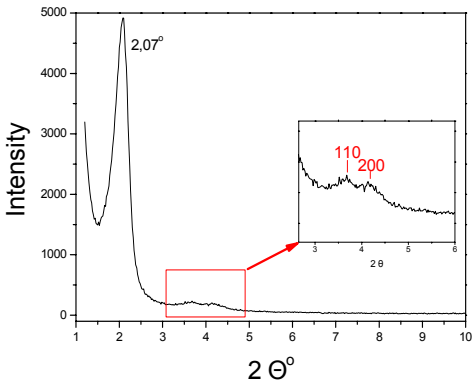

Figure 4.7e. *XRD pattern of the BH_C16_100*

SEM images (see figure 4.8 (a-d)) present the morphology of PNOs at the μm-scale. In particular, we observe that BH_C16_0 and BH_C16_100 samples show the hexagonal shape as expected from their sharper XRD pattern while the samples BH_C16_25, BH_C16_50 and BH_C16_75 show some small hexagonal crystals but also the presence of other micro-particles in different sizes and shapes.

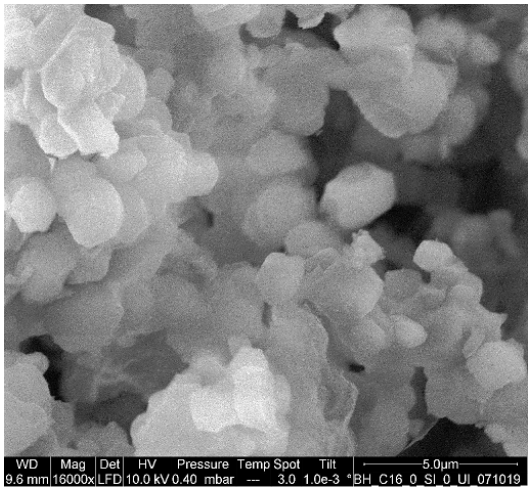

Figure 4.8 a. *SEM image of the BH_C16_0 sample.*

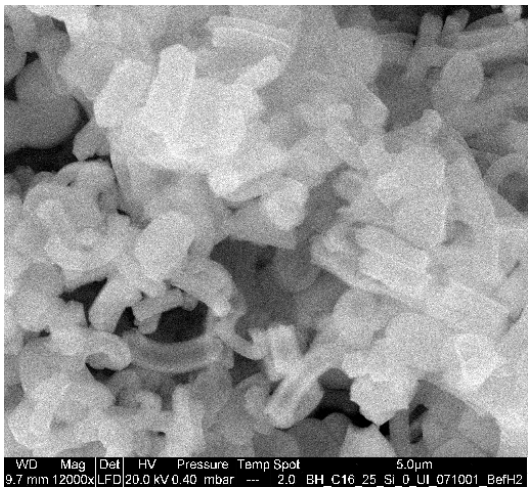

Figure 4.8b. *SEM image of the BH_C16_25 sample*

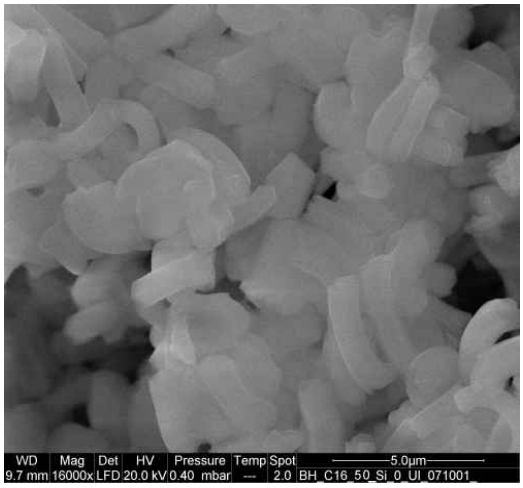

Figure 4.8 c. *SEM image of the BH_C16_50 sample*

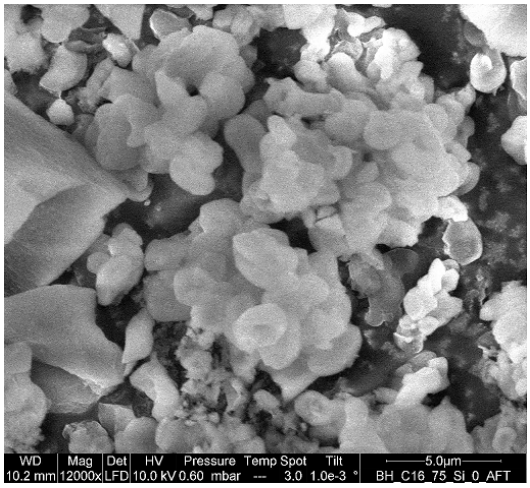

Figure 4.8 d. *SEM image of the BH_C16_75 sample*

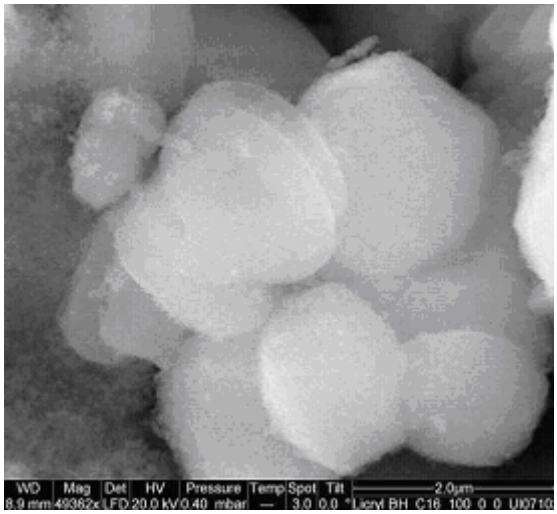

Figure 4.8 e. *SEM image of the BH_C16_100 sample*

In table 4.4 are presented the structural characteristics of this group of materials. As it is shown, the SSA of the samples varies depending the ratio BTB : TEOS. The sample BH_C16_75 (75% BTB and 25% TEOS), as well as the sample BH_C16_0 (0% of BTB and 100% of TEOS), own the higher values of SSA. It was noticed that the BH_C16_0 sample has a low mean pore size compared to the other samples even if the same surfactant chain length was used for al of them. This can be probably attributed to the absence of the BTB precursor from the specific sample, which may have an effect on the magnitude of the pores.

SAMPLE	Skeletal Density (g/ccm)	SSA (m^2/g)	Mean pore diameter (Å)	Crystallinity	d_{100} (Å)
BH_C16_0	2.43 ± 0.09	953	16.0	Ordered	46.40
BH_C16_25	1.90 ± 0.10	636	18.6	Partly Ordered	42.60
BH_C16_50	2.05 ± 0.04	800	18.8	Partly Ordered	46.00
BH_C16_75	2.02 ± 0.05	1220	18.0	Partly Ordered	46.16
BH_C16_100	1.41 ± 0.03	783	18.8	Ordered	42.60

Table 4.4: Structural properties of all the samples.

In figure 4.9a is presented the adsorption (close symbols) and the desorption (open symbols) isotherm curves of methane on the PNO samples obtained at 298K. The isotherm curves shape is in agreement with the type I IUPAC curve and the overall shape of the curves is also representative of the isotherms behaviors obtained at 286 K and 313 K on the same samples (figure 4.9b, here presented only for the BH_C16_75 sample) revealing that an enhancement in the storage capacity is obtained at lower temperature, as an increase in temperature will decrease the amount adsorbed due to the greater energy required by the adsorbed molecules to evaporate.

Also in this case, the desorption isotherm curves follow exactly the adsorption isotherms which indicates that the methane gas can be easily extracted from the samples. Considering all the samples, the BH_C16_75 has a higher methane uptake up to 4.2 wt%. Depending on the very high SSA (1220 m^2/g)

of this sample (the highest of the investigated PNOs samples in this work) we could expect a greater difference in its adsorption capacity compared to the other four samples of this group. A reason why this may does not happen will be given after the fitting of the adsorption isotherm of this sample using the Tóth equation.

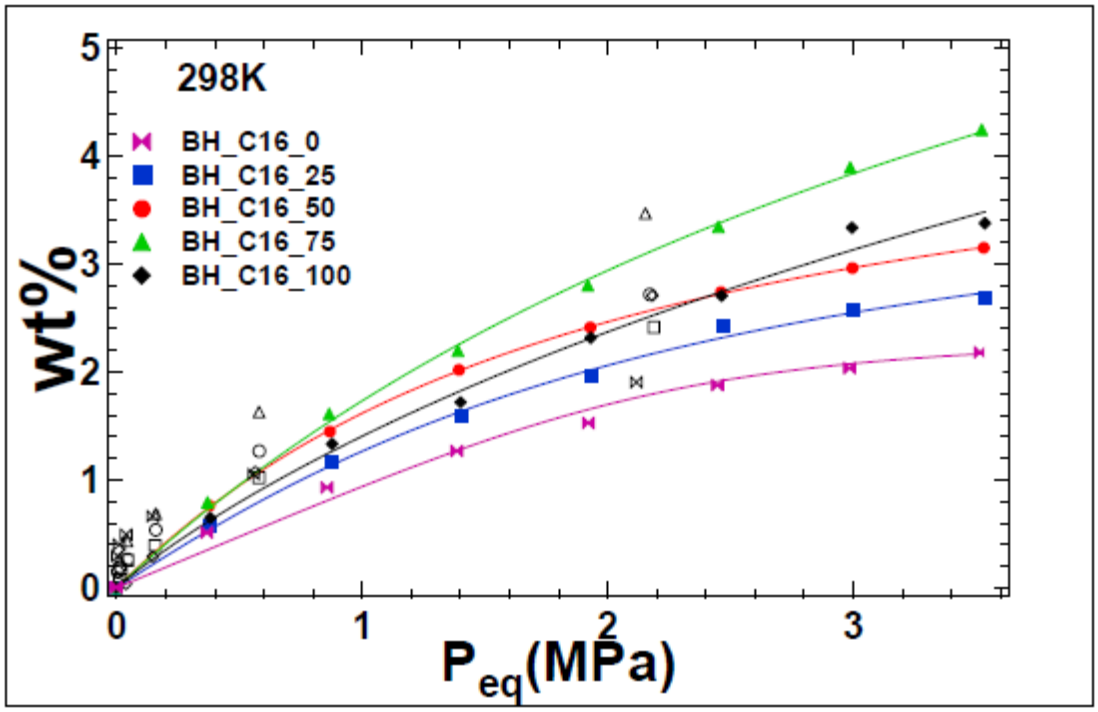

Figure 4.9 a : PcT adsorption isotherms obtained at 298K up to 3.6 MPa for all the samples (markers). Lines between points represent the data fitting procedure based on the Tóth model.

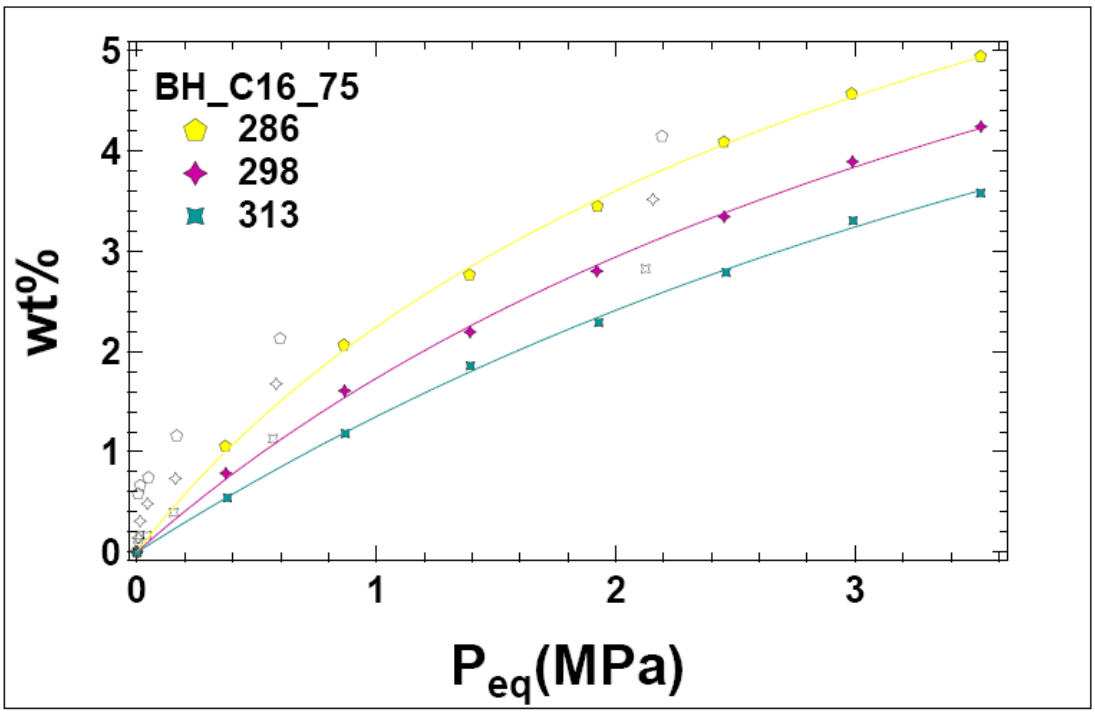

Figure 4.9 b :PcT adsorption and desorption isotherms obtained at 286K, 298K and 313K up to 3.5 MPa for the sample BH_C16_75 (markers). Lines between points represent the data fitting procedure based on the Tóth model.

The calculation of the adsorbed molecules per nm^2 (figure 4.10) shows that at the higher pressure reached in the experiment, none of the samples form a monolayer and in particular the sample BH_C16_0 adsorbs a very low number of molecule/nm^2 compared to the other samples. This fact is in correlation with its small mean pore size.

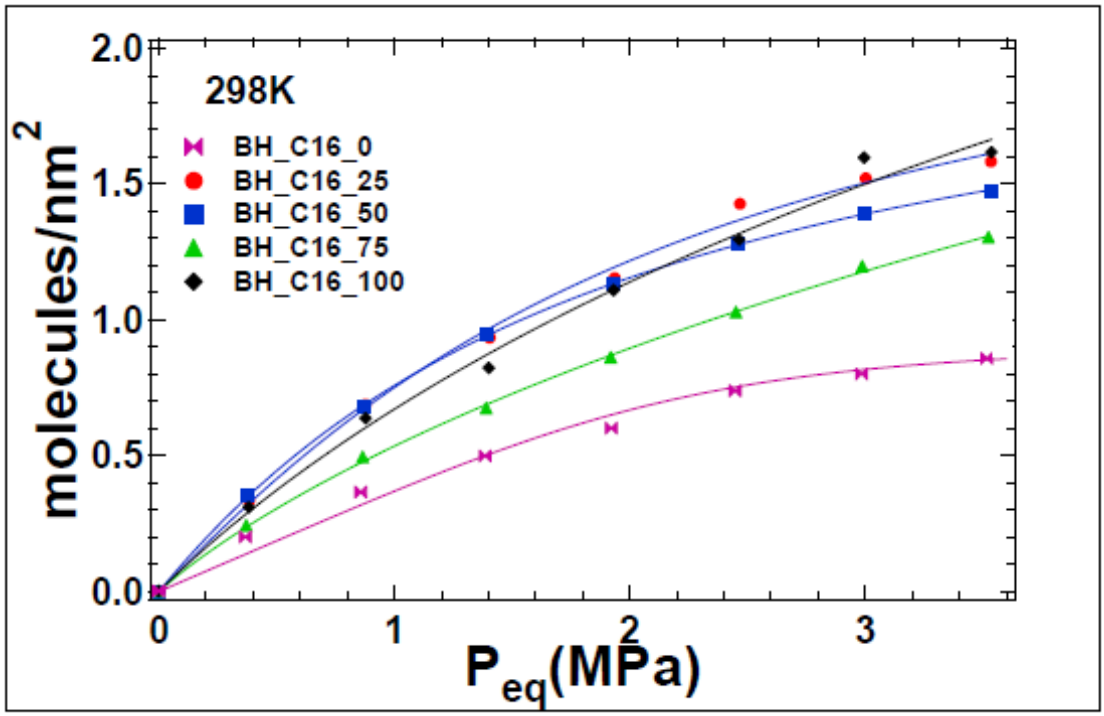

Figure 4.10: Number of molecules per surface's nm² for all the samples (markers). Lines between points represent the data fitting procedure based on the Tóth model.

Considering the Toth equation and the isotherm curve obtained at room temperature for BH_C16_75, we obtained fitting results as shown in figure 4.11. All samples' adsorption isotherms were fitted with the Tóth model and the results are shown in table 4.5. The BH_C16_75 sample shows the higher theoretical maximum storage capacity but at the same time a low K value indicating the weak interaction between the methane molecules and the surface. This may explain the relatively low adsorption capacity of this sample respect to its high SSA.

All the samples that contain a certain degree of TEOS as precursor show similar but none very high values of t. On the other hand the absence of TEOS

(sample BH_C16_100) increases the surface homogeneity as it demonstrated in table 4.5.

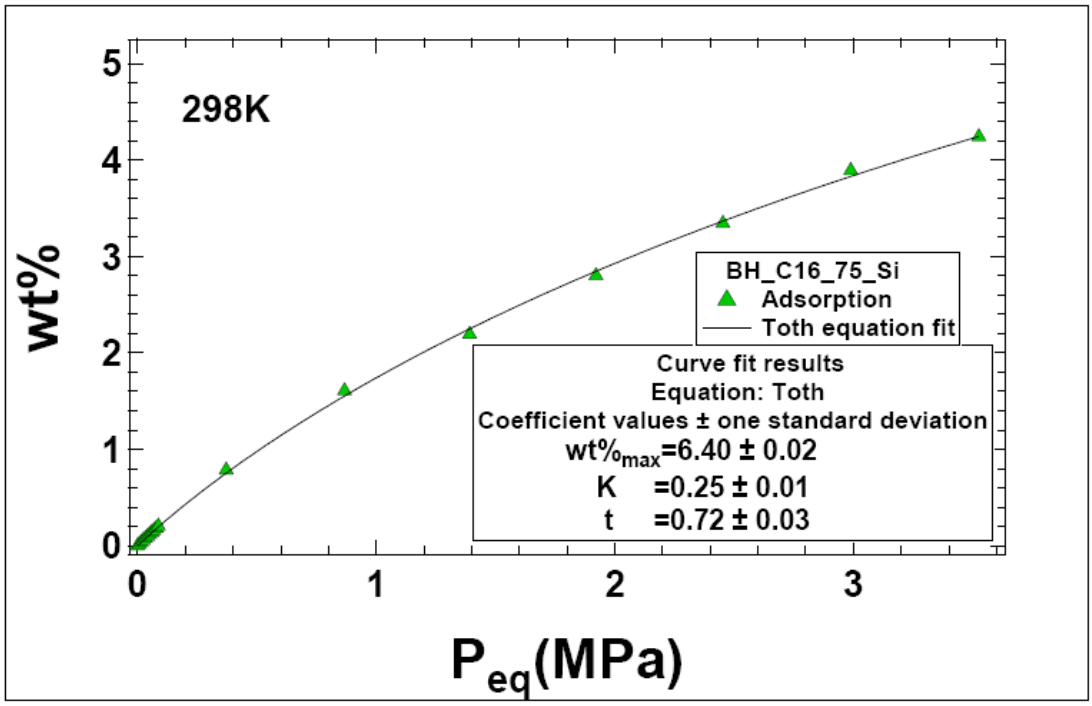

Figure 4.11 :PcT adsorption isotherm obtained at 298 K up to 3.6 MPa for the sample BH_C16_75, fitted with the Tóth model according to the formula. Note that a wider data range is used to obtain a reliable evaluation of the Tóth parameters

SAMPLE	$Wt\%_{max}$	$K \pm \Delta K$ (bar^{-1})	$t \pm \Delta t$
BH_C16_0	3.50 ± 0.90	0.20 ± 0.05	0.70 ± 0.10
BH_C16_25	4.00 ± 0.40	0.50 ± 0.07	0.60 ± 0.15
BH_C16_50	5.20 ± 0.06	0.45 ± 0.02	0.75 ± 0.05
BH_C16_75	6.40 ± 0.02	0.25 ± 0.01	0.72 ± 0.03
BH_C16_100	4.50 ± 0.20	0.50 ± 0.08	0.90 ± 0.02

Table 4.5: Tóth equation fitting parameters for the samples.

Similar values of isosteric heat of adsorption within the error were found for all the five investigated samples indicating that in low pressures and coverages the different ratio between BTB and TEOS precursors didn't play an important role in the adsorption capacity of the samples unlike to the extracted results for higher pressures presented above.

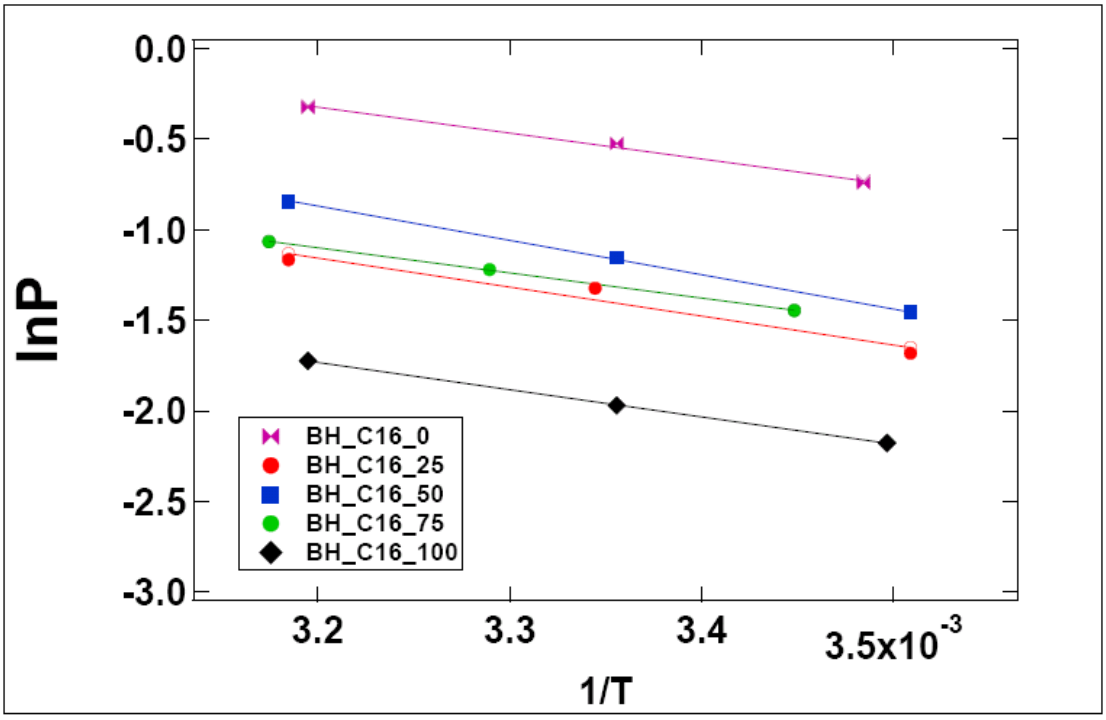

Figure 4.12: lnP vs T^{-1} graph of all the samples and fitting results by using the Clausius-Clapeyron relation.

SAMPLE	ΔH (kJ/mol) Low coverages	ERROR (kJ/mol)
BH_C16_0	12.00	± 1.00
BH_C16_25	14.00	± 0.20
BH_C16_50	15.00	± 0.70
BH_C16_75	11.50	± 0.20
BH_C16_100	12.50	± 0.15

Table 4.6: Calculated isosteric heat of adsorption and its error for all the samples.

4.1.1.3 Surfactant's main chain length variation (DBTB)

The XRD patterns reveal an amorphous structure of the DH_C10_100 sample while a certain degree of order is visible for the other samples (figure 4.13 a-d). Particularly, the XRD pattern of the DH_C12_100 shows the (100) diffraction of the hexagonal symmetry at 2.45° while the (110) and (200) diffractions are not well observed indicating the low hexagon symmetry structure. Thus, the distance between (100) planes, d_{100}, is 36.2 Å. Similar patterns are presented for the DH_C16_100 and DH_C18_100 samples with their main peaks centered at 2.07° and 1.9° respectively while the distance of the (100) planes d_{100} is 49.1 Å and 53.7 Å respectively.

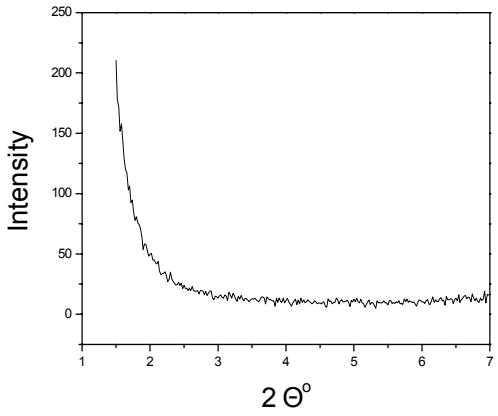

Figure 4.13 a. *XRD pattern of the DH_C10_100.*

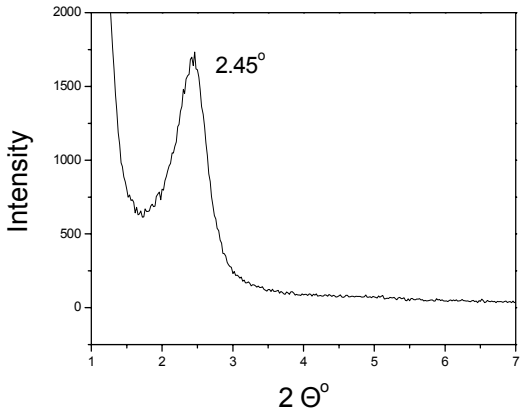

Figure 4.13 *b*. *XRD pattern of the DH_C12_100*

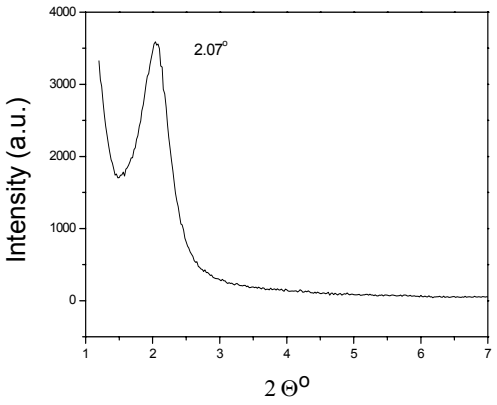

Figure 4.13 c. *XRD pattern of the DH_C16_100*

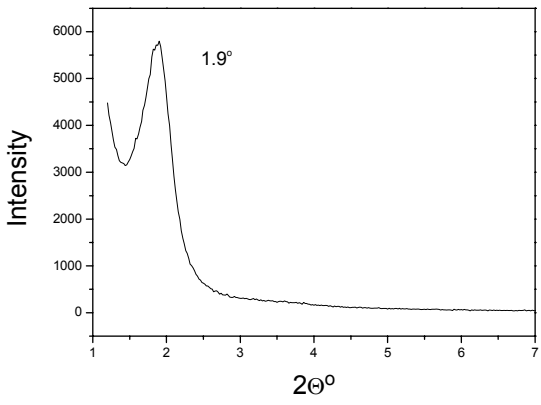

Figure 4.13 d. *XRD pattern of the DH_C18_100*

SEM images (see figure 4.14 (a-d)) present the morphology of PNOs at the μm-scale. In particular, we observe that DH_C10_100 sample shows an open structure with no definite grain boundaries while few-micrometer sized particles are visible for all the other samples. DH_C12_100, DH_C16_100, DH_C18_100 particles, in some cases, show the hexagonal shape as expected from their sharper XRD pattern, i.e. their wider long range ordering.

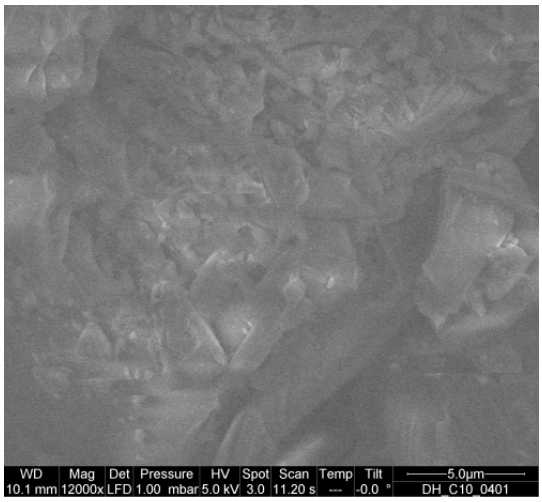

Figure 4.14a. *SEM image of the DH_C10_100 .*

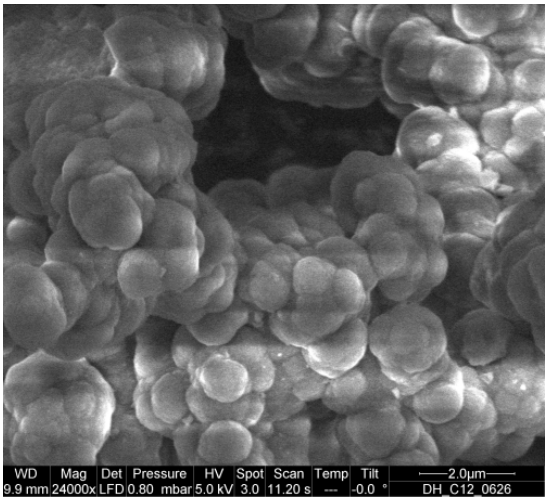

Figure 4.14b. *SEM image of the DH_C12_100*

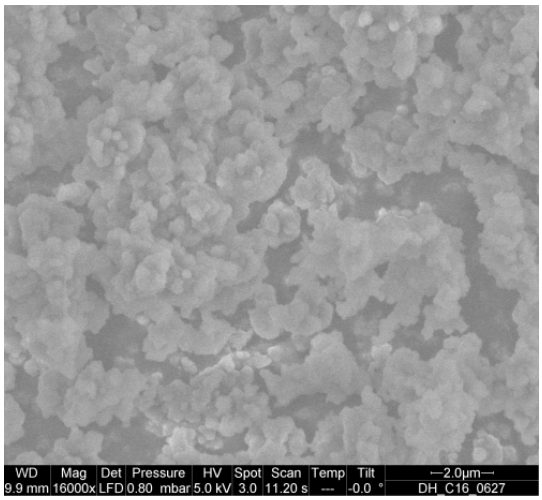

Figure 4.14 c. *SEM image of the dH_C16_100*

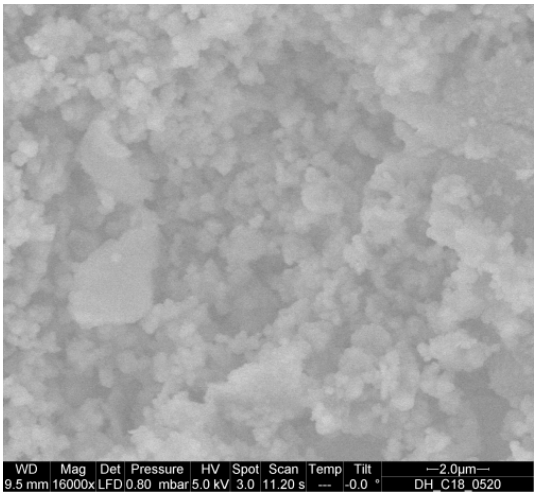

Figure 4.14 d. *SEM image of the BH_C18_100*

As the surfactant's chain length is increasing, an increase of the pore diameter is observed. The case of DH_C10_100 sample cannot be taken into account as it is an amorphous material. The crystallinity varies between fully disordered to partly ordered. A resume of the samples' structural characteristics is presented in Table 4.7.

SAMPLE	Skeletal Density (g/ccm)	SSA (m^2/g)	Mean pore diameter (Å)	Crystallinity	d_{100} (Å)
DH_C10_100	1.41 ± 0.02	795	21.0	Fully disordered	=
DH_C12_100	1.45 ±0.04	720	18.6	Partly Ordered	36.2
DH_C16_100	1.25 ± 0.06	827	19.0	Partly Ordered	49.1
DH_C18_100	1.35 ± 0.07	723	19.5	Partly Ordered	53.7

Table 4.7: Structural characteristics

In figure 4.15a is presented the adsorption (close symbols) and the desorption (open symbols) isotherm curves of methane on the PNO samples obtained at 298K. The isotherm curves shape is in agreement with the type I IUPAC curve and the overall shape of the curves is also representative of the isotherms behaviors obtained at 286 K and 313 K on the same samples (figure 4.15b, here presented only for the DH_C10_100 sample). Also in this case, it is demonstrated that an enhancement in the storage capacity is obtained at lower temperature, as expected.

As shown before for other groups of PNOs samples, the desorption isotherm curves follow exactly the adsorption isotherms which indicates that the methane gas can be easily extracted from the samples. Considering all the

samples, the DH_C10_100 has a higher methane uptake up to 5.5 wt% while the rest of the PNO materials present similar storage capacity.

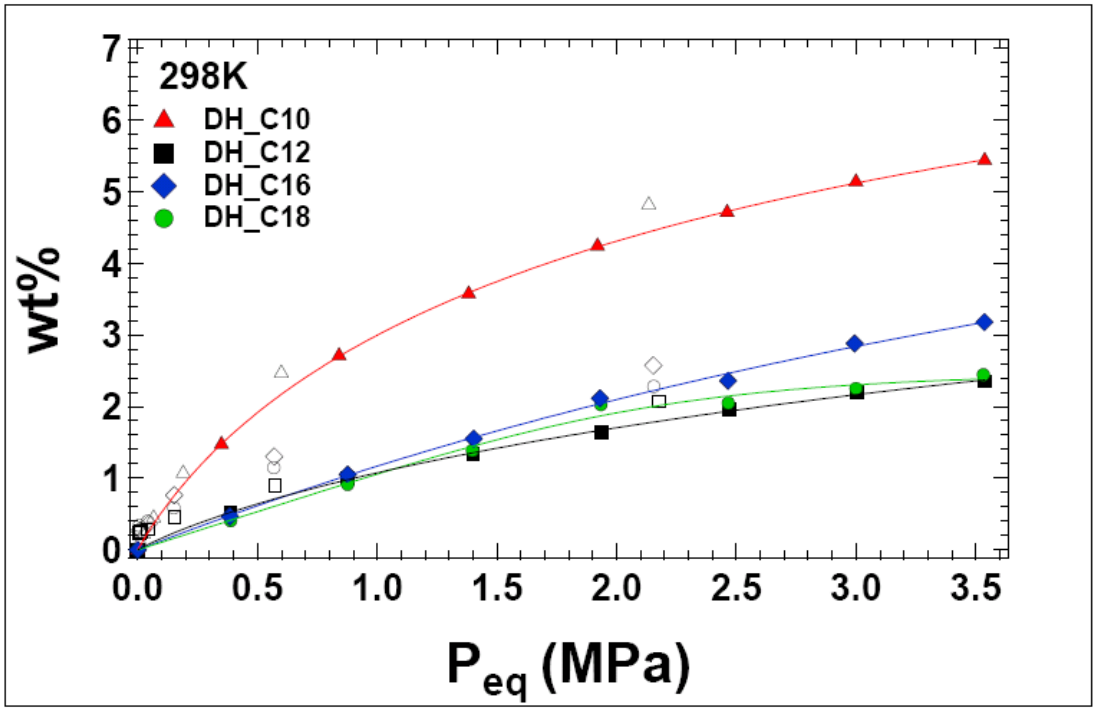

Figure 4.15a: PcT adsorption isotherms obtained at 298K up to 3.6 MPa for all the samples (markers). Lines between points represent the data fitting procedure based on the Tóth model.

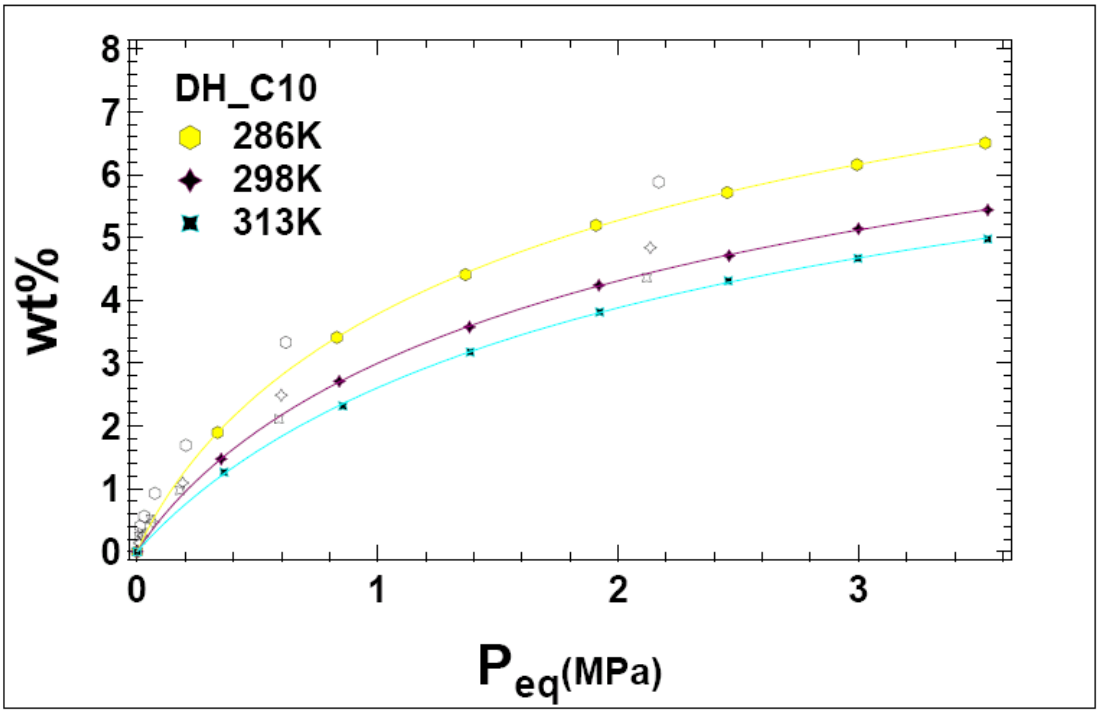

Figure 4.15 b: PcT adsorption and desorption isotherms obtained at 286K, 298K and 313K up to 3.5 MPa for the sample DH_C10_100 (markers). Lines between points represent the data fitting procedure based on the Tóth model.

None of the samples forms a monolayer of adsobed molecules / nm^2 (figure 4.16). None the less, the sample DH_C10_100 adsorbed more molecules per nm^2 compared to the others, which is in agreement with its higher methane storage capacity and relatively high SSA (795 m^2/g).

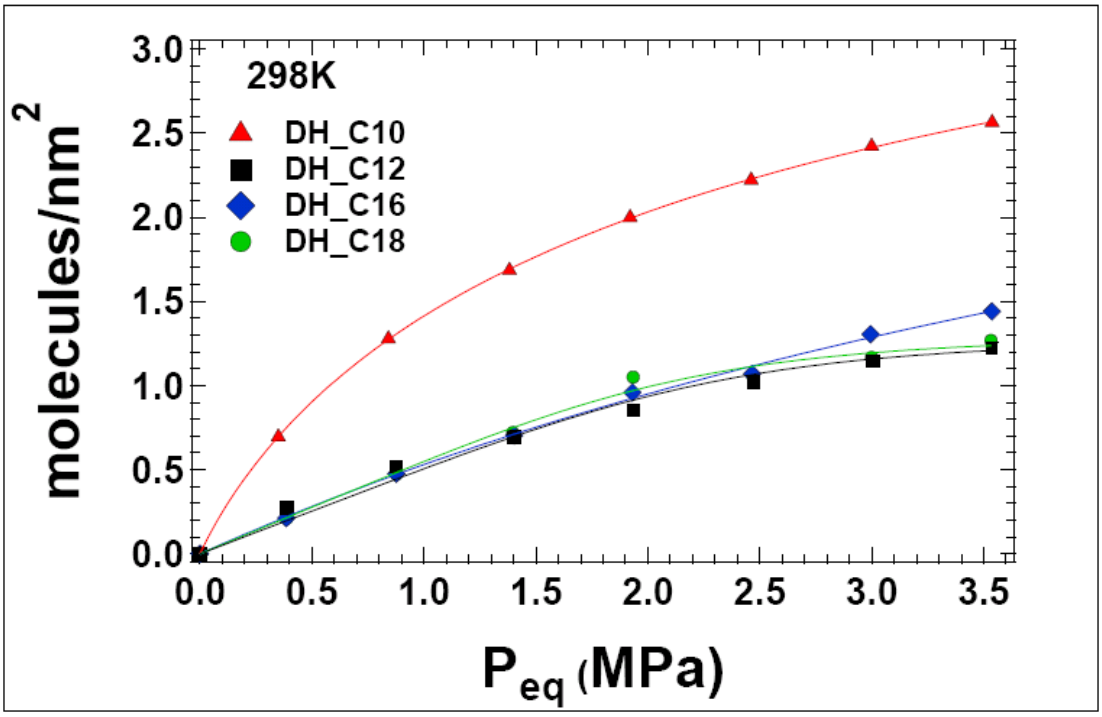

Figure 4.16: Number of molecules per surface's nm² for all the samples (markers). Lines between points represent the data fitting procedure based on the Tóth model.

The evaluation of the enthalpy showed that the sample DH_C10_100 presents a higher value of enthalpy comparing to the other three samples that within the error show the same capacity of attracting methane molecules in low coverages (table 4.8).

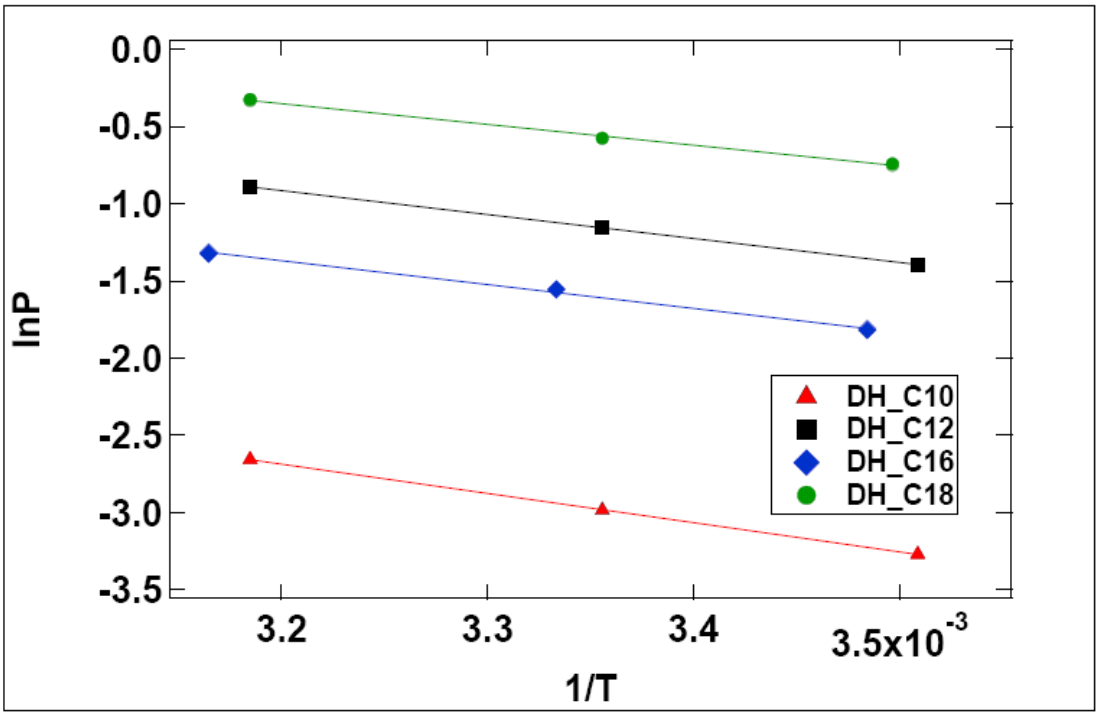

Figure 4.17: lnP vs T^{-1} graph of all the samples and fitting results by using the Clausius- Clapeyron relation

SAMPLE	ENTHALPY (kJ/mol)	ERROR (kJ/mol)
DH_C10_100	16.0	± 0.1
DH_C12_100	13.0	± 0.5
DH_C16_100	13.0	± 0.9
DH_C18_100	11.0	± 0.7

Table 4.8: Calculated isosteric heat of adsorption and its error

Finally, in table 4.9 the values of Tóth equation parameters are summarized. By increasing the surfactant's chain length, a decrease in the theoretical maximum capacity is occurred. The K-value is higher for the sample DH_C10_100, therefore higher surface's attraction to methane molecules, while all samples of this series present the same high grade of homogeneity within the error.

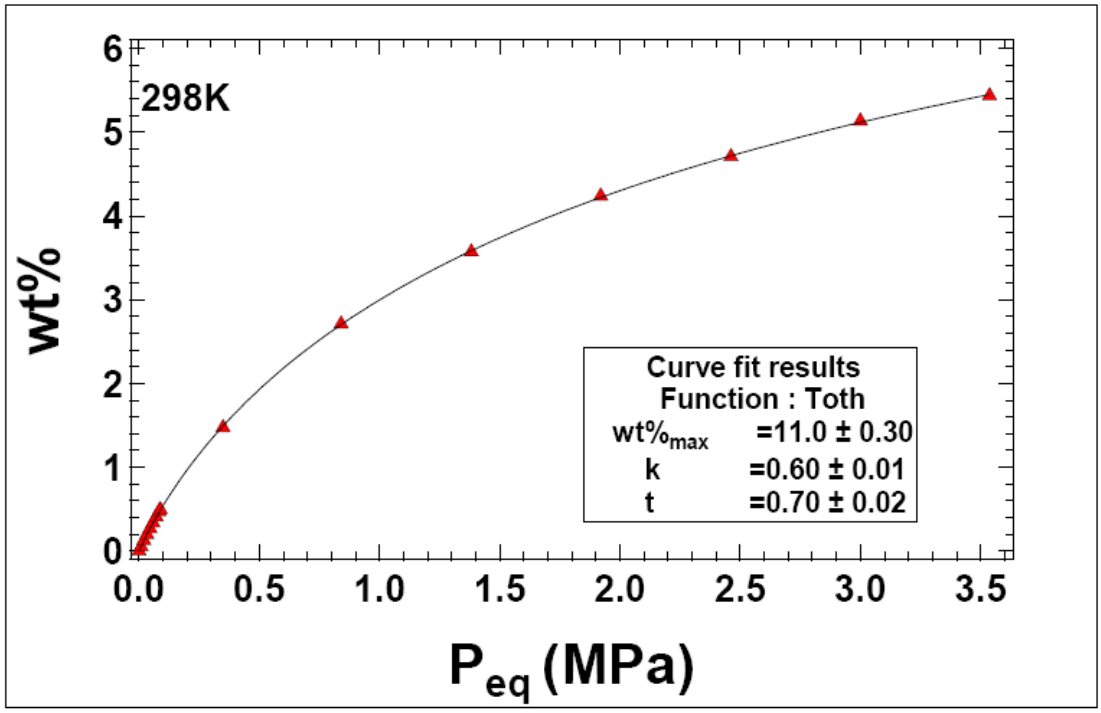

Figure 4.18 : PcT adsorption isotherm obtained at 298 K up to 3.6 MPa for the sample DH_C10_100, fitted with the Tóth model according to the formula. Note that a wider data range is used to obtain a reliable evaluation of the Tóth parameters

SAMPLE	$wt\%_{omax}$	$K \pm \Delta K$ (bar^{-1})	$t \pm \Delta t$
DH_C10_100	11.0 ± 0.30	0.60 ± 0.01	0.70 ± 0.02
DH_C12_100	3.50 ± 0.02	0.30 ± 0.09	0.70 ± 0.15
DH_C16_100	5.00 ± 1.00	0.40 ± 0.07	0.80 ± 0.09
DH_C18_100	3.00 ± 0.20	0.40 ± 0.03	0.70 ± 0.05

Table 4.9: Tóth equation fitting parameters

4.1.1.4 Doping with Li^+

The XRD pattern (figure 4.19) reveal the fact that the amorphous structure of the DH_C10_100 sample was maintained as expected also after the insertion the Li+ cations.

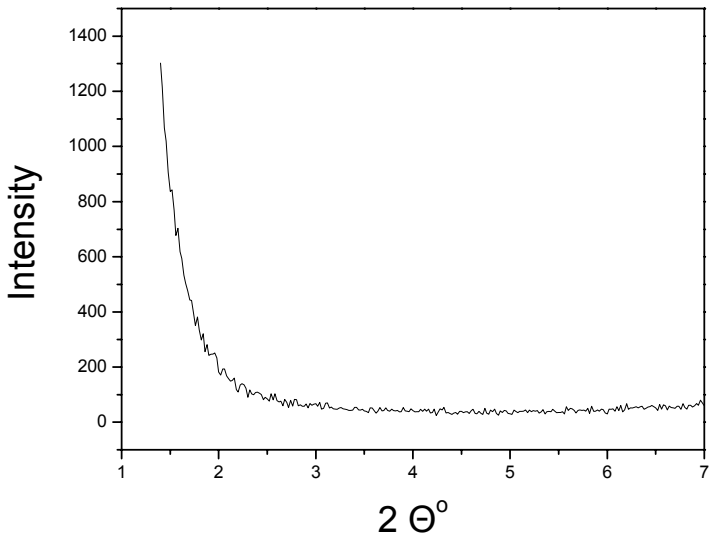

Figure 4.19 : XRD pattern of DH_C10__100_Li sample

SAMPLE	Skeletal Density (g/ccm)	SSA (m^2/g)	Mean pore diameter (Å)	Crystallinity	d_{100} (Å)
DH_C10_100	1.41 ± 0.02	795	21.0	Fully disordered	=
DH_C10__100 _Li	1.54 ± 0.03	223	18.1	Fully disordered	=

Table 4.10 :Structural characteristics

After doping the initial material with Li^+, is noticed an increase in the density indicating the presence of the Li^+ cations (table 4.10). Nevertheless, the SSA and therefore the storage capacity of the doped material is remarkably decreased (figure 4.20a). This can be due to the non - successful insertion of the cations and likely the coverage of the internal pore walls by Li atoms.

In figure 4.20b are presented the adsorption and desorption isotherms obtained at 286 K and 313 K demonstrating an expected increase in adsorption capacity with the decrease of the temperature.

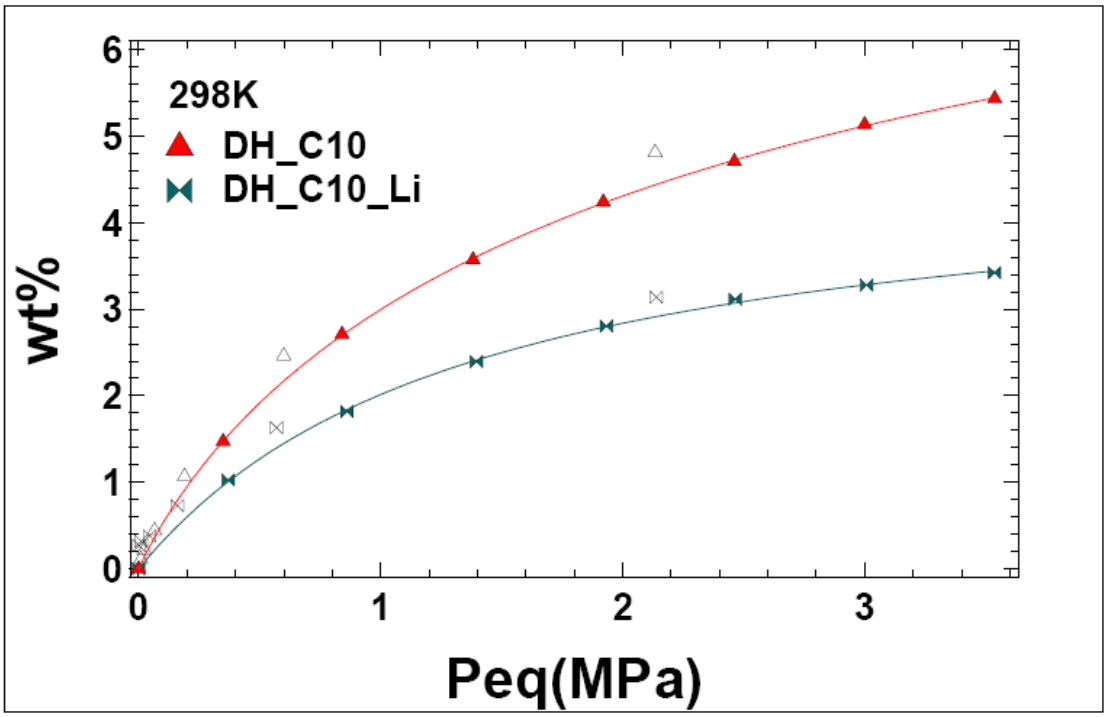

Figure 4.20 a: PcT adsorption isotherms obtained at 298K up to 3.6 MPa for the samples DH_C10_100 and DH_C10_100_Li (markers). Lines between points represent the data fitting procedure based on the Tóth model.

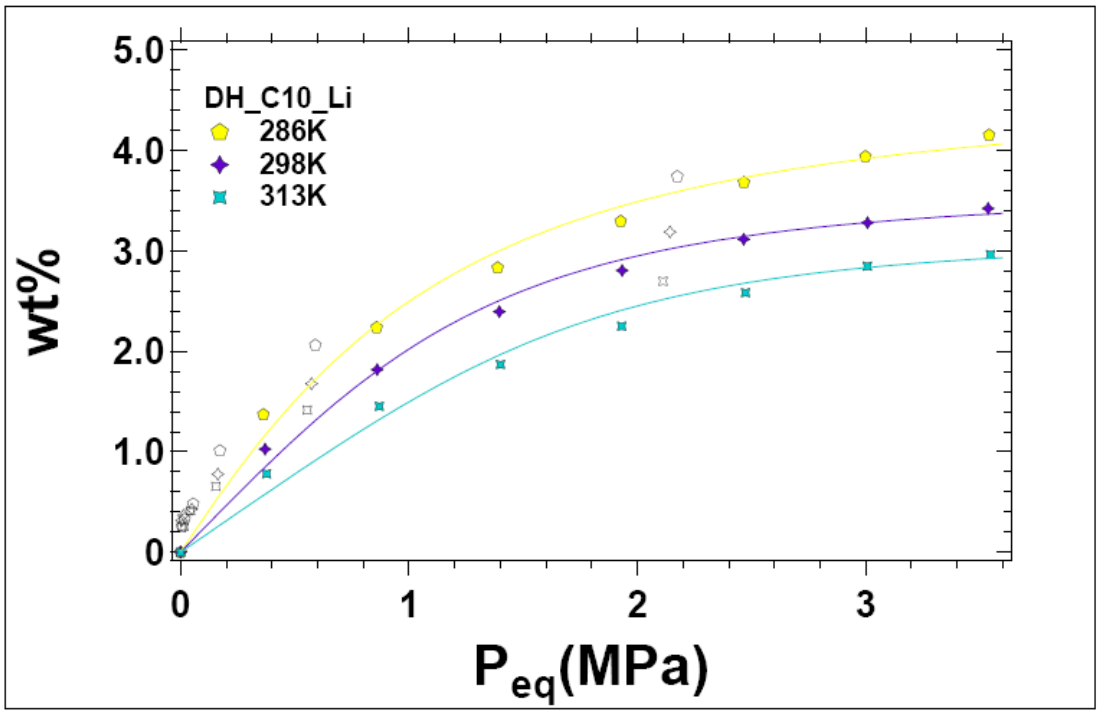

Figure 4.20b: PcT adsorption and desorption isotherms obtained at 286K, 298K and 313K up to 3.5 MPa for the sample DH_C10_100_Li (markers). Lines between points represent the data fitting procedure based on the Tóth model.

A comparison between the adsorbed molecules per nm^2 for the two materials shows that the surface of the doped material can host three times more molecules per nm^2 forming more than one monolayer (figure 4.21). Nevertheless, as mentioned before, the reduced SSA that Li+ cations insertion caused, is responsible for the lower methane storage capacity. Therefore, the insertion of Li^+ probably "blocked" a large amount of the pore walls (small SSA) but the remained "open" sites became more active and capable to attract methane molecules because of the point charge of Li^+.

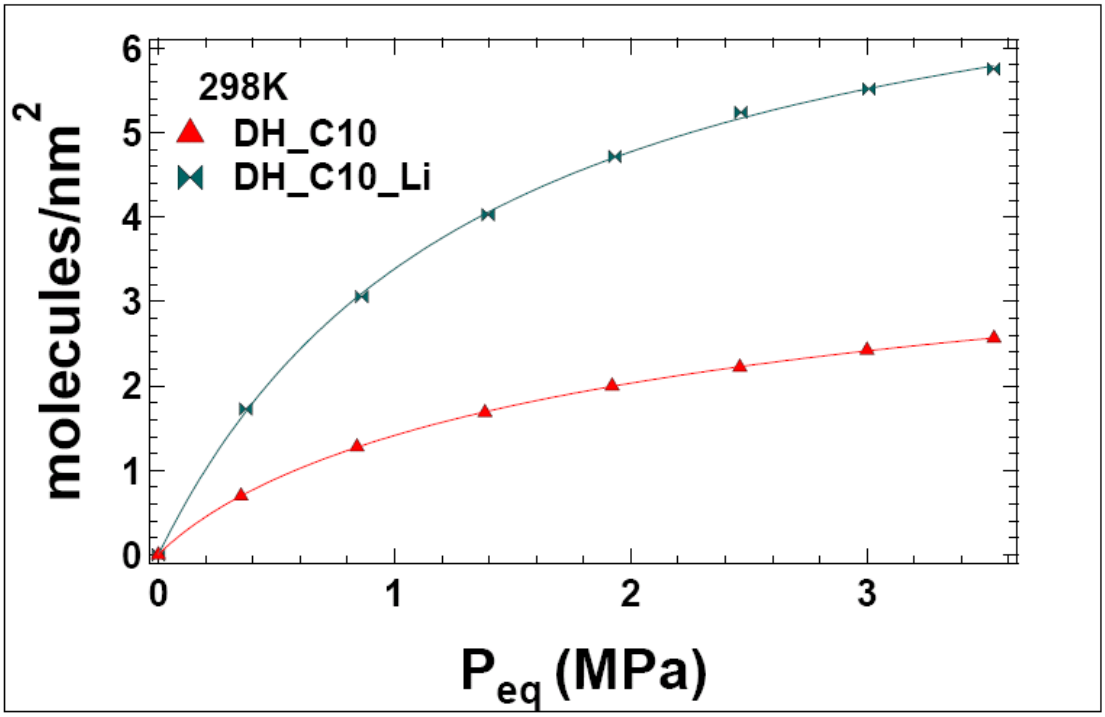

Figure 4.21: Number of molecules per surface's nm² for the samples DH_C10_100 and DH_C10_100_Li (markers). Lines between points represent the data fitting procedure based on the Tóth model.

The DH_C10_100 _Li sample has, expectedly, a lower theoretical maximum storage capacity while the t-value parameter remained in the same magnitude for both samples indicating same surface homogeneity. On the other hand the K value of the doped sample is higher revealing a higher interaction between the adsorbate and the pore walls (table 4.11).

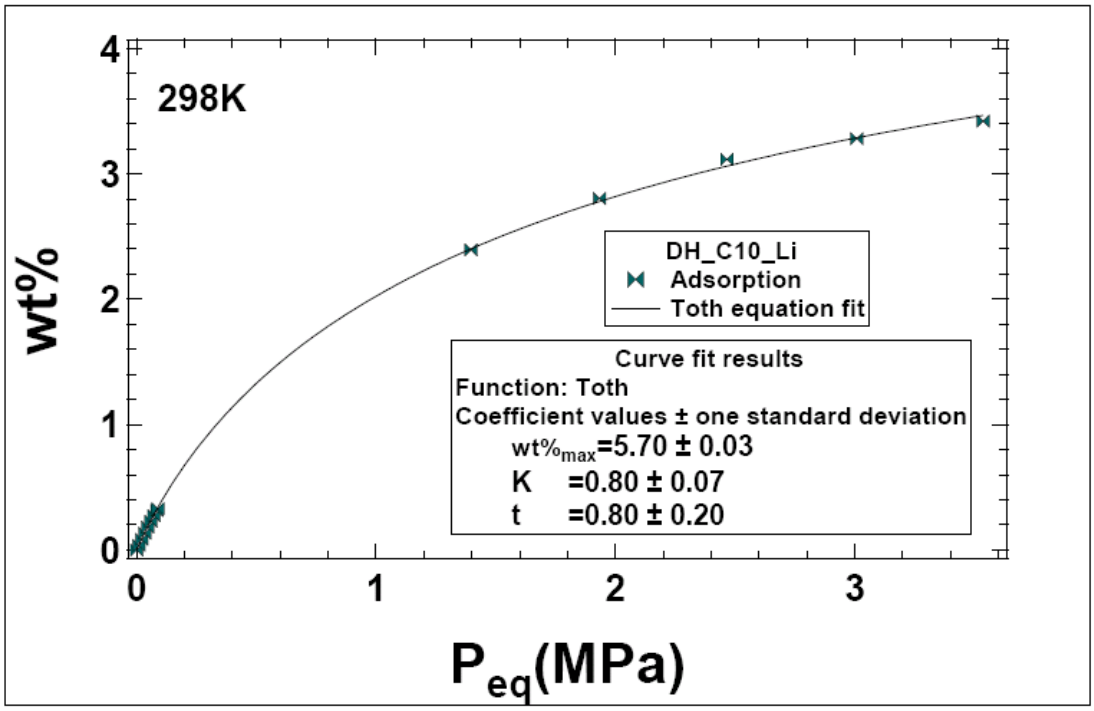

Figure 4.22: PcT adsorption isotherm obtained at 298 K up to 3.6 MPa for the sample DH_C10_100_Li, fitted with the Tóth model according to the formula. Note that a wider data range is used to obtain a reliable evaluation of the Tóth parameters

SAMPLE	$wt\%_{max}$	$K \pm \Delta K$ (bar^{-1})	$t \pm \Delta t$
DH_C10_100	11.0 ± 0.30	0.60 ± 0.01	0.70 ± 0.02
DH_C10_100 _Li	5.70 ± 0.03	0.80 ± 0.07	0.80 ± 0.20

Table 4.11: Tóth equation fitting parameters

The evaluation of the enthalpy showed a small change in low coverages between the initial and doped material. Therefore, the insertion of Li+ did not

affect the bonding energy between the methane molecules and the surface of the materials in low pressures.

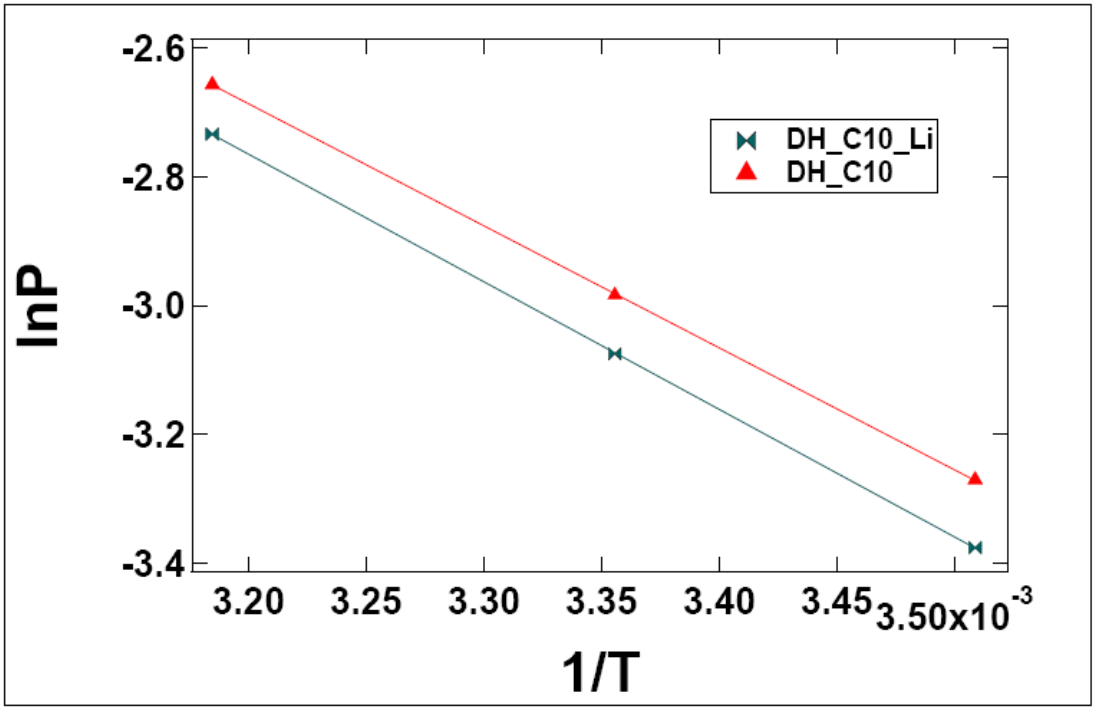

Figure 4.23: lnP vs T^{-1} graph of the two samples and fitting results by using the Clausius- Clapeyron relation

SAMPLE	ENTHALPY (kJ/mol)	ERROR (kJ/mol)
DH_C10_100	15.70	± 0.10
DH_C10_100 _Li	16.40	± 0.08

Table 4.12: Calculated isosteric heat of adsorption and its error

4.1.2 Naphthelene PNOs [8]

In the following paragraphs will be presented all the results regarding hydrogen and methane adsorption/desorption analysis performed on our samples: Naph-PNO-H^+ and Naph-PNO-350.

The helium pycnometry measurements were performed in order to evaluate the samples' skeletal density, while the specific surface area (SSA) and the pore volume were obtained by the Brunauer-Emmett-Teller (BET) method [9]. Then, the adsorption/desorption isotherms were collected by the *f*-PcT apparatus. Before each adsorption measurement, the samples were treated up to 200 °C under high vacuum for 12 hours in order to remove water and other possible impurities.

Results

After chemical, structural and morphological characterization we shown that the final materials, Naph-PNO-H^+ and Naph-PNO-350, exhibit high crystallinity, high naphthalene content up to 17 wt%, surface areas above 1000 m^2/g and pore size distributions in the microporous/mesoporous boundary [9].

X-ray powder diffraction (XRD) patterns in the low angle region of the samples Naph-PNO, Naph-PNO-H^+ and Naph-PNO-350 are shown in figure 4.24 All three patterns are typical of materials with hexagonal arrangement of uniform pores displaying the characteristic strong reflection at low scattering angles 2θ as well as the next two reflection peaks. All three samples are classified in the p6mm space group which means that the first reflection peak is attributed to Miller (100) lattice planes. Specifically, XRD pattern of sample Naph-PNO (a) displays three reflection peaks corresponding to d_{100}, d_{110} and

d_{200} spacings. Applying Bragg's law for the first reflection peak is resulted that d_{100} spacing is 41.6 Å. Pattern (b) of sample Naph-PNO-H^+ shows also the first three reflection peaks with a d_{100} spacing of 42.4 Å, while d_{100} spacing of sample Naph-PNO-350 in pattern (c) is 38.1 Å suggesting a small shrinkage in the pore diameters due to the heat treatment in spite of maintaining the wide range hexagonal pore ordering [10].

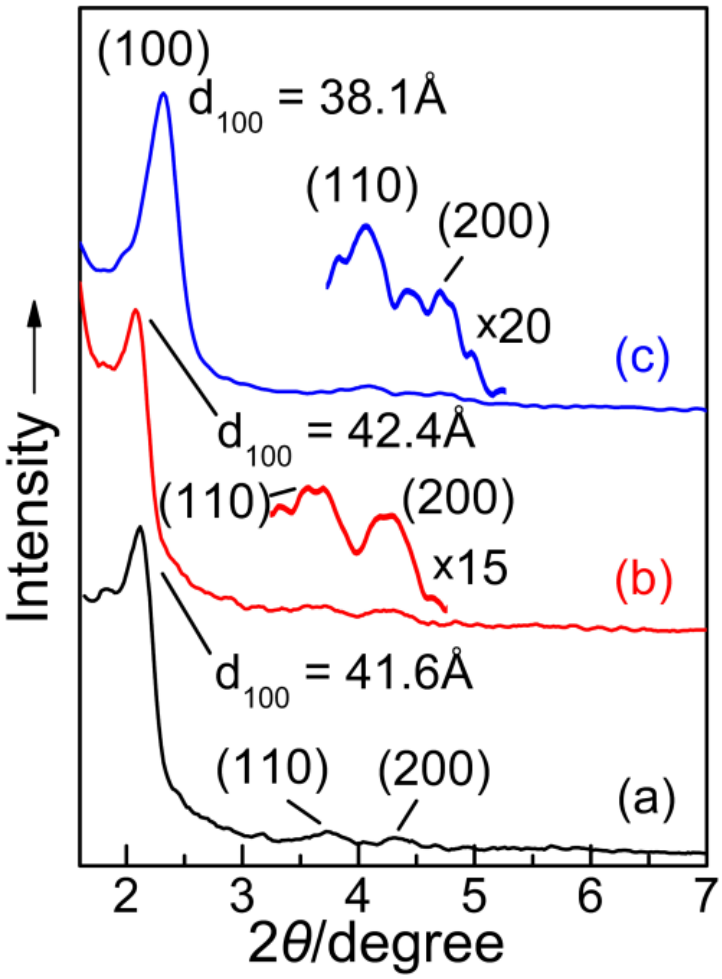

Figure 4.24 X-ray powder diffraction patterns in the low angle region for samples Naph-PNO (a), Naph-PNO-H^+ (b) and Naph-PNO-350 (c).

A higher SSA and pore volume is observed for the sample Naph-PNO-350, see Table 1. This fact could be related to the different procedure adopted for the pore evacuation from the surfactant for each sample during the synthesis [9].

Sample	S_{BET} (m^2/g)	V_{pore} (mL/g)	d_{BJH} (Å)	a_o (Å)	$d_{skelet.}$ (g/mL)
Naph-PNO-H^+	1016	0.43	20.4	48.9	2.068
Naph-PNO-350	1076	0.57	22.0	44.0	1.96

[a] Data taken from Ref. [9].

Table 4.13. Structural properties of the Naph-PNO-H^+ and Naph-PNO-350 samples. Pore parameters derived from X-ray diffraction patterns, nitrogen adsorption data and helium pycnometry.[a]

Figure 4.25 shows the methane adsorption (closed symbols) and desorption (open symbols) isotherms of the investigated samples obtained up to 3.5 MPa and at 298K. As it's shown, the isotherm curves are in agreement with the type I IUPAC curve; the desorption isotherms follow the adsorption isotherms (no large hysteresis loop is observed) proving the fully reversibility of the methane adsorption and consequently the fact that methane can be easily extracted from the material.

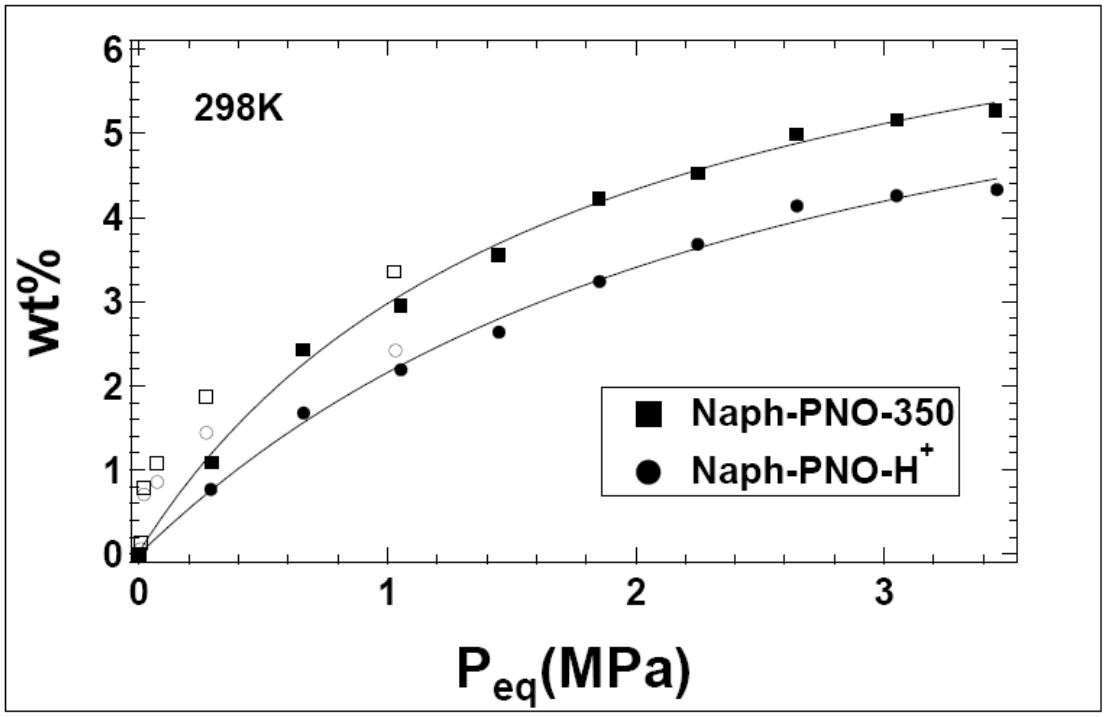

Figure 4.25 PcT adsorption isotherms obtained at 298K up to 3.5 MPa for Naph-PNO-H^+ and Naph-PNO-350 samples (markers). Lines between points represent the data fitting procedure based on the Tóth model.

Considering the two samples, Naph-PNO-350 has higher methane uptake reaching up to 5.2 wt% at 3.5 MPa, as expected taking into account its higher SSA and pore volume values (Table 4.13). The better adsorptive characteristics of this sample are observed for the whole range of pressures (Figure 4.25).

However, the ability of Naph-PNO-350 to store higher values of methane compared to Naph-PNO-H^+, may not only depend on the SSA but also to the possibility to form more than one monolayer of adsorbed methane molecules.

For this reason, the evaluation of the adsorbed molecules per nm^2 could be useful to indicate the efficacy of the sample to create more than one monolayer.

As shown in Figure 4.26, none of the samples form one monolayer at room temperature, nevertheless the sample Naph-PNO-350 seems to adsorb more molecules per nm^2 (1.8 mol/nm^2) proving again its higher capacity to store methane molecules compared to Naph-PNO-H^+. By means of this evaluation we can derive a higher affinity of the Naph-PNO-350 pore surfaces towards the methane adsorption process showing a 12% increase of the adsorbed molecules per unit surface area in the same conditions.

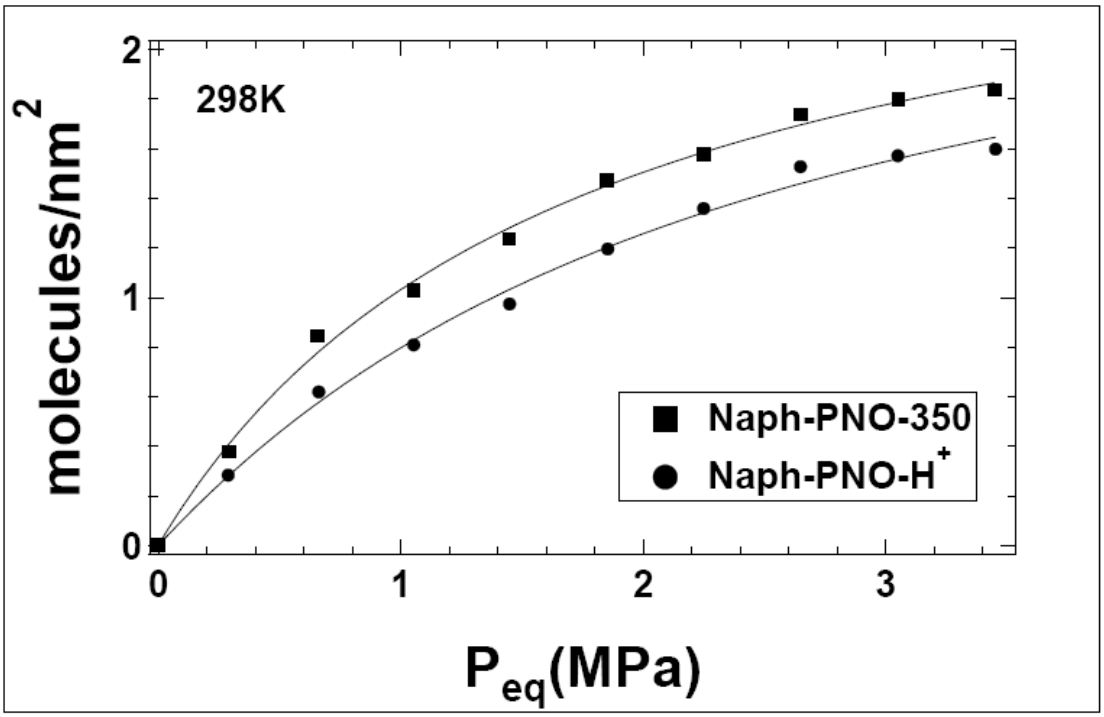

Figure 4.26 Number of molecules per surface's nm^2 for Naph-PNO-H^+ and Naph-PNO-350 samples up to 3.5 MPa and at 298K. Lines between points represent the data fitting procedure based on the Tóth model.

The theoretical maximum storage capacity, the equilibrium constant and homogeneity grade of the samples have been evaluated by means of analysis of the adsorption isotherms by using the Tóth model. The higher K-value of

the sample Naph-PNO-350 reveals its ability to attract more efficiently the methane molecules. Nevertheless, both samples own low K-values and no saturation is reached in the probed pressure range (Figure 4.27). Finally, we obtained the same t-value, for both samples, which is close to unity (within the error) indicating a high grade of surface homogeneity (Table 4.14) and very low dependence of the CH_4/surface interaction on the coverage.

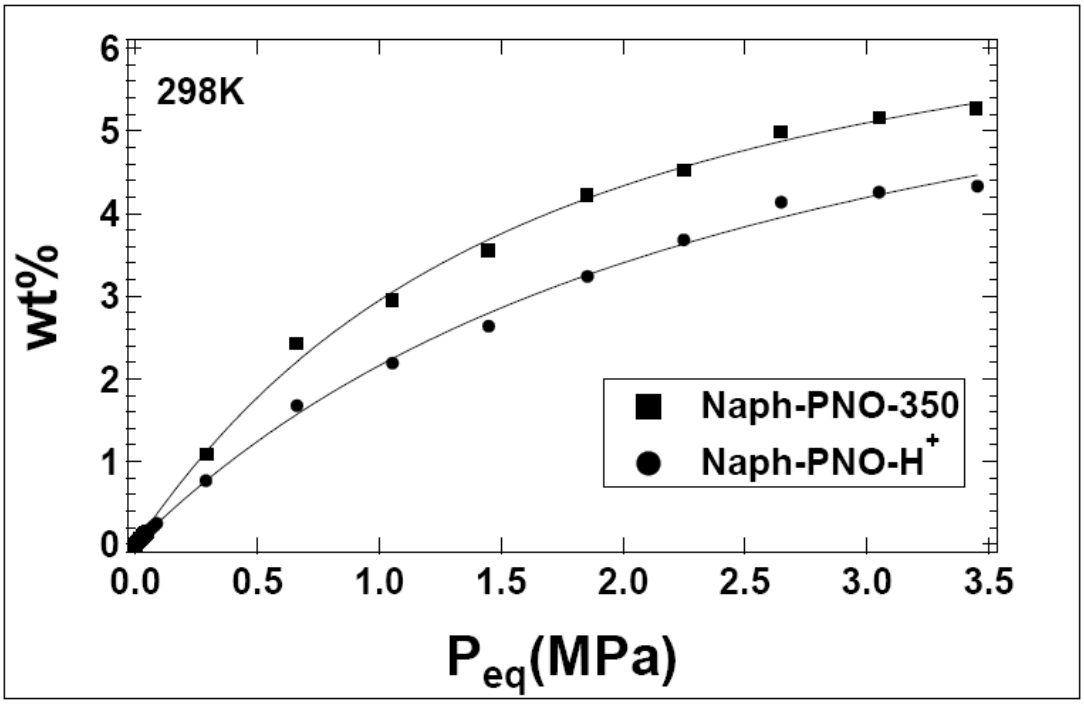

Figure 4.27 PcT adsorption isotherm obtained at 298 K up to 3.5 MPa for the Naph-PNO-H^+ and Naph-PNO-350 samples, fitted with the Tóth model according to the formula. Note that a wider data range is used to obtain a reliable evaluation of the Tóth parameters.

Sample	$wt\%_{omax}$	K (bar^{-1})	t
Naph-PNO-H^+	7.50 ± 1.50	0.40 ± 0.05	1.00 ± 0.20
Naph-PNO-350	7.40 ± 0.70	0.60 ± 0.03	1.00 ± 0.20

Table 4.14. Theoretical maximum storage capacity, equilibrium constant and homogeneity grade for Naph-PNO-H^+ and Naph-PNO-350 samples obtained as Tóth equation fitting parameters.

In Figure 4.28 we show the linear fitting of the adsorption data for both samples while Table 4.15 reports the isosteric heat results.

As expected, the value for the Naph-PNO-350 is slightly higher confirming the higher affinity of its pore surfaces towards the methane adsorption.

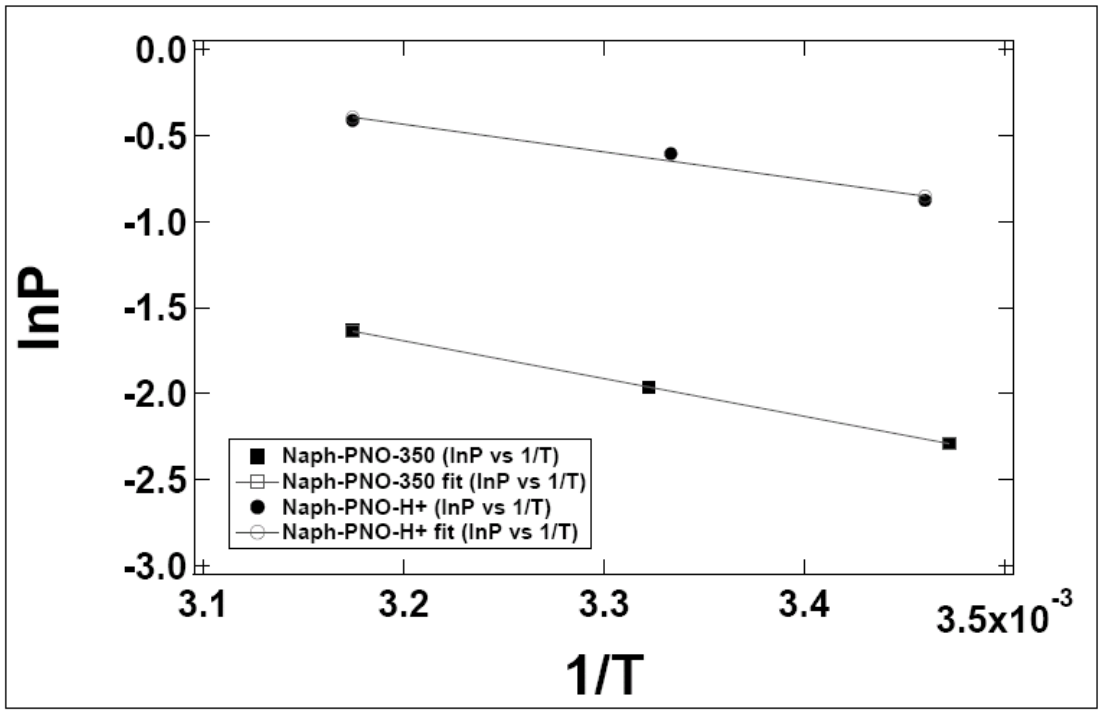

Figure 4.28 lnP vs T^{-1} graph of the Naph-PNO-H^+ and Naph-PNO-350 samples and fitting results by using the Clausius-Clapeyron relation.

Sample	ΔH(kJ/mol) low coverages	error(kJ/mol)
Naph-PNO-H^+	14.0	± 2.0
Naph-PNO-350	18.0	± 0.2

Table 4.15. Calculated isosteric heat of adsorption and its error for Naph-PNO-H^+ and Naph-PNO-350 samples.

As a consequence, the observed differences of the methane uptake properties of the samples could be attributed to both the higher SSA and pore volume values of the Naph-PNO-350 sample, which settle it as more efficient to attract methane molecules.

4.2 Carbon nanostructured materials [11]

For each resulting sample, will be presented the combined morphological and structural characterization by SEM, BET and XRD techniques.

Density was measured with pycnometry measurements with He as a probe molecule.

Before each adsorption measurement, the samples were heated up to 200°C under vacuum for 12 hours in order to remove water and other possible impurities.

Afterwards the adsorption isotherms, obtained by PcT apparatus, will be analysed by Tóth equation and number of molecules per nm^2. Then the isosteric heat of adsorption will be evaluated for all samples.

The combination of all the experimental results will be discussed in order to extract the relation between adsorption and structural/morphological properties.

Results

The structure and morphology of the carbon products were studied by powder XRD and SEM. SEM images (figure 4.29 (a-d)) offer an excellent morphological overview of the carbon materials on the sub-micrometer scale. The morphology of the zeolite particles is replicated in the carbon samples produced under the three different temperatures (1023 K, 1073 K and 1123 K). As a matter of fact, all the carbon samples show several hundred nm wide flat particles whose morphology replicates the zeolite one in terms of the overall shape of the particles and their internal texture.

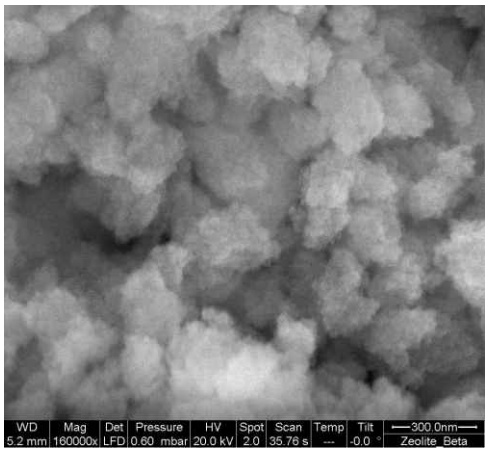

Figure 4.29 (a) zeolite beta

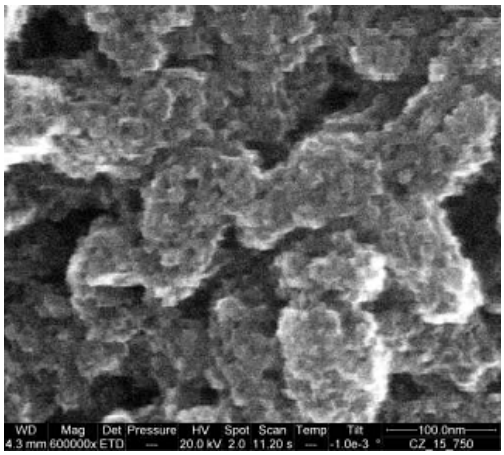

Figure 4.29 (b) CZ1023

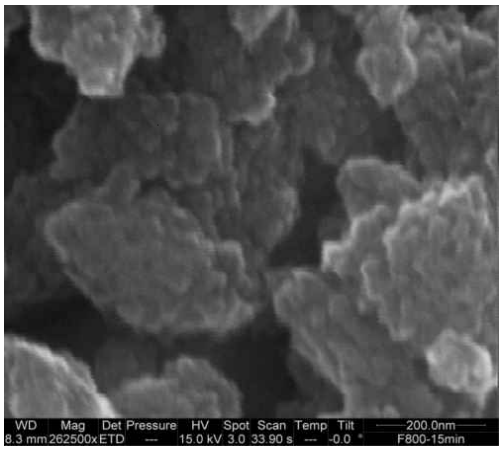

Figure 4.29 (c) CZ1073

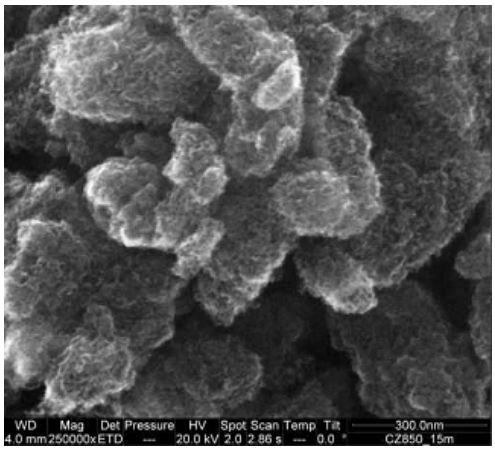

Figure 4.29 (d) CZ1123

The XRD patterns of pristine material and the final carbon products were compared in order to determinate the existing crystalline phases. In figure 4.30 the XRD patterns of zeolite beta and the final carbon samples are presented. When the CVD was performed at 1073 K and 1123 K, the resulting carbon samples exhibit a structural ordering that partly resembles that of zeolite beta as the presence of a broad peak at $2\theta=7^{o}$ indicates. This feature is, in fact, associated to the ordering on the basal plane and describes the pore ordering. On the other hand, when CVD was performed at 1023 K the structural ordering of zeolite beta seems not to have been readily replicated in the final sample, as the peak at $2\theta=7^{o}$ misses. All three carbon samples exhibit a low and broad peak at $2\theta=25^{o}$ which is similar to the (002) diffraction from turbostratic carbon indicating that a certain degree of local ordering resembling graphite is kept. A peak at $2\theta=18^{o}$ is observed for all three samples. In the literature, for similar samples, this peak is attributed to the (105) diffraction of zeolite beta or to the possibility that it may arise from other carbon contaminants [12].

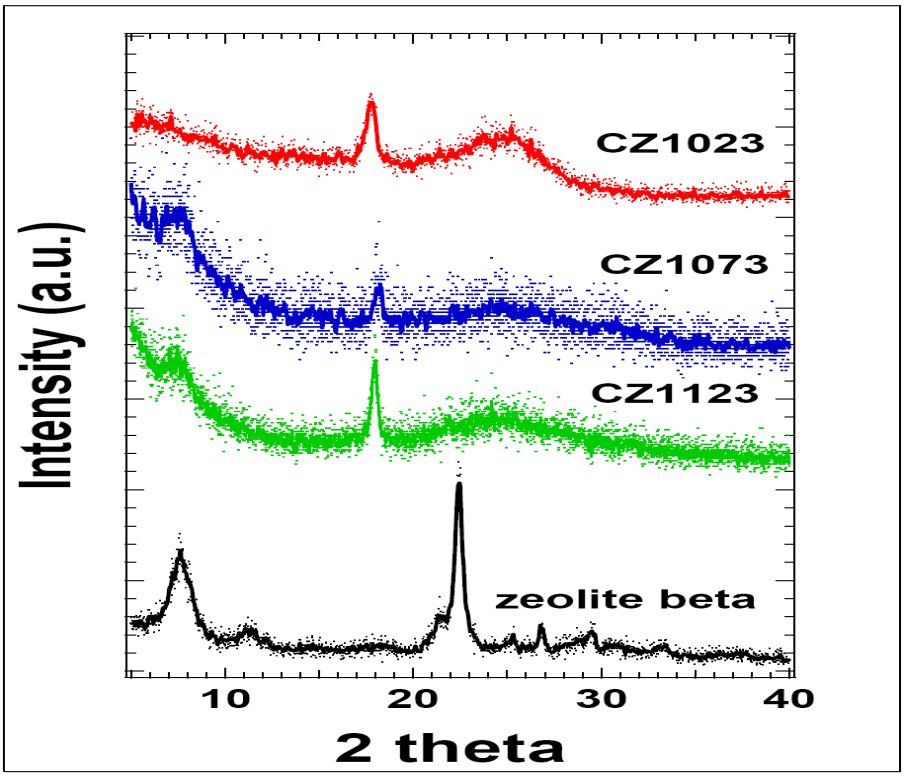

Figure 4.30 XRD patterns of zeolite beta, CZ1023, CZ1073 and CZ1123

In Table 4.16 we report samples' structural characteristics. The CZ1073 sample presents the highest specific surface area while the CZ1023 sample has the smallest pore size compared to the other two samples that have the same pore size. These characteristics have played an important role on the adsorption capacity of the samples.

SAMPLE	SSA (m^2/g)	MEAN PORE SIZE (nm)	DENSITY (g/ccm)
CZ1023	730	0.4	1.7
CZ1073	980	0.6	1.5
CZ1123	700	0.6	2.0

Table 4.16: Structural properties of all the samples

In figure 4.31 are presented the adsorption (close symbols) and the desorption (open symbols) isotherms of the investigated samples obtained at 298K. The overall trend of the curves depicted in figure 4.31(a) remains alike in the isotherms curves obtained at 287 K and 313 K on the same samples (see figure 4.31 b, here presented only for the CZ1073 sample). As expected, there is a clear enhancement in the storage capacity by decreasing the temperature.

As it's shown, the amount of adsorbed methane seems to increase according to the type I IUPAC curve. The desorption isotherm curves (open symbols in figure 4.31 a-b) follow exactly the adsorption isotherm indicating that the adsorption process is fully reversible and that the gas can be easily extracted from the material.

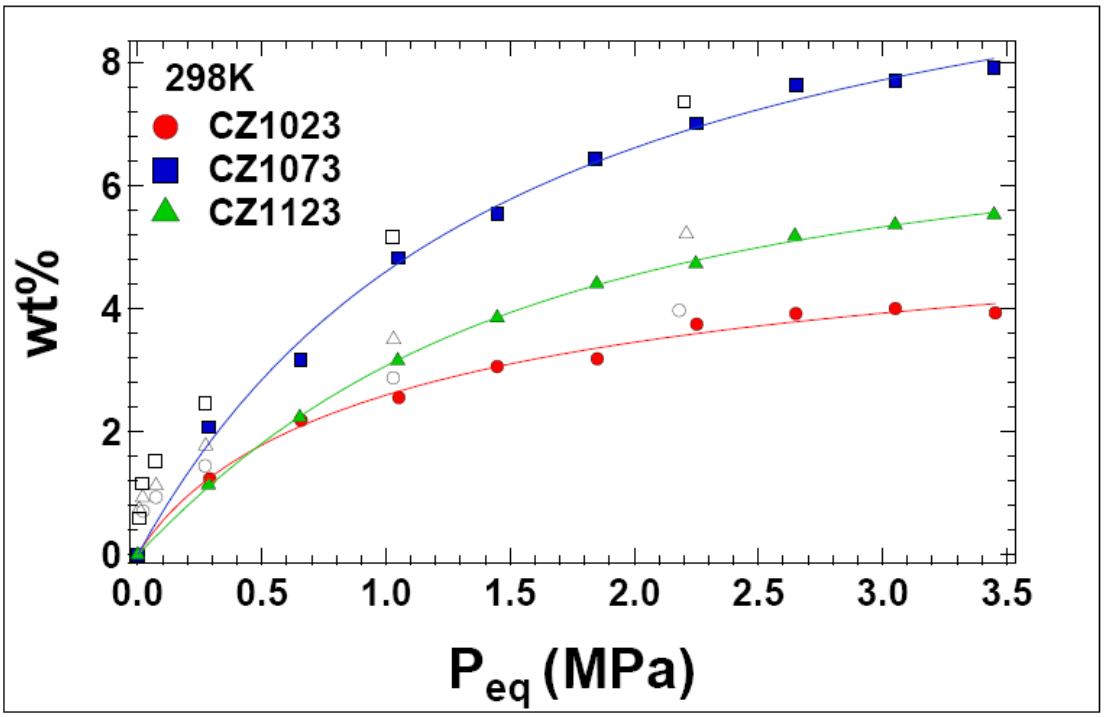

Figure 4.31(a) : PcT adsorption and desorption isotherms obtained at 298K up to 3.5 MPa for CZ1023, CZ1073 and CZ1123 (markers). Lines between points represent the data fitting procedure based on the Tóth model.

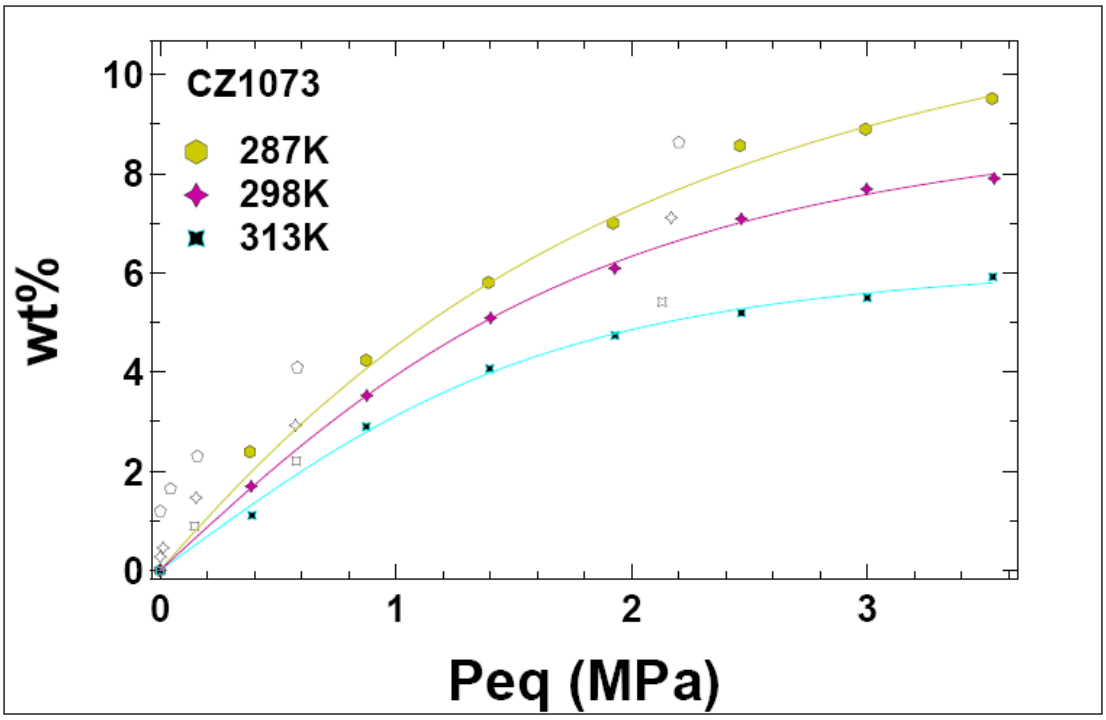

Figure 4.31(b): PcT adsorption and desorption isotherms obtained at 287K, 298K and 313K up to 3.5 MPa for the sample CZ1073 (markers). Lines between points represent the data fitting procedure based on the Tóth model.

The CZ1073 sample has the highest methane adsorption capacity just as the highest SSA (table 4.16). In particular its measured uptake is 8 wt% at 3.5 MPa. While, the sample CZ1123 stores more methane (5.6 wt% at 3.5 MPa) compared to the CZ1023 sample (4 wt% at 3.5 MPa) even if the second has higher SSA. This, can be related to the different pore size of these two samples (table 4.16) and can also be explained if we evaluate their degree of surface coverage in terms of adsorbed molecules per nm^2.

In figure 4.32 are presented the curves of the adsorbed molecules per nm^2 of the three carbon samples. The samples CZ1073 and CZ1123 form one monolayer at the highest pressure (about 3 molecules/nm^2, as the area occupied by a CH_4 molecule is about 0.3 nm^2), while the sample CZ1023 does

not. This, again, can be ascribed to the fact that the sample CZ1023 has a smaller pore size compared to the other two samples.

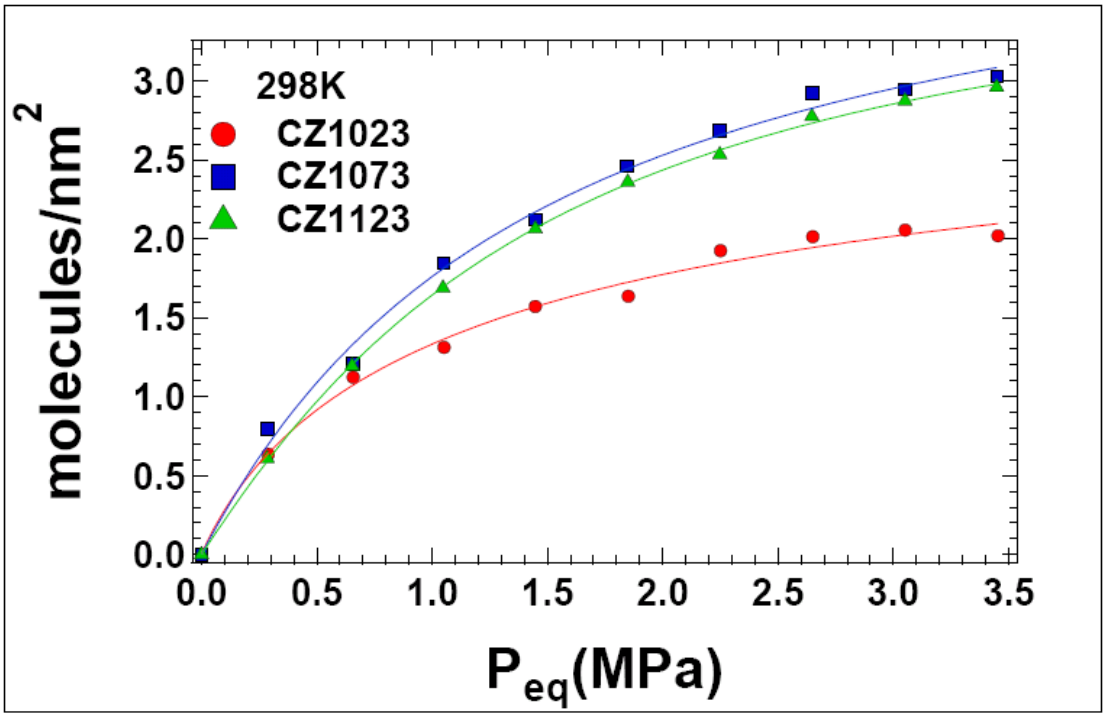

Figure 4.32: Number of molecules per surface's nm² for CZ1023, CZ1073 and CZ1123 (markers). Lines between points represent the data fitting procedure based on the Tóth model.

After fitting the adsorption isotherms with the Tóth model was found that the CZ1073 sample has a higher theoretical maximum storage capacity compared to the other two samples, as expected. The value of K for the samples CZ1073 and CZ1173 is the same within the error, while the value of K for the sample CZ1032 is higher (table 4.17). This can be related to the curvature of the isotherm of this sample (figure 4.33), indicating a quicker saturation of the adsorption sites for higher K. The grade of homogeneity is the same (close or

even equal to one), for all three samples, within the error, indicating very homogeneous surfaces and low CH_4/ CH_4 interaction (table 4.17).

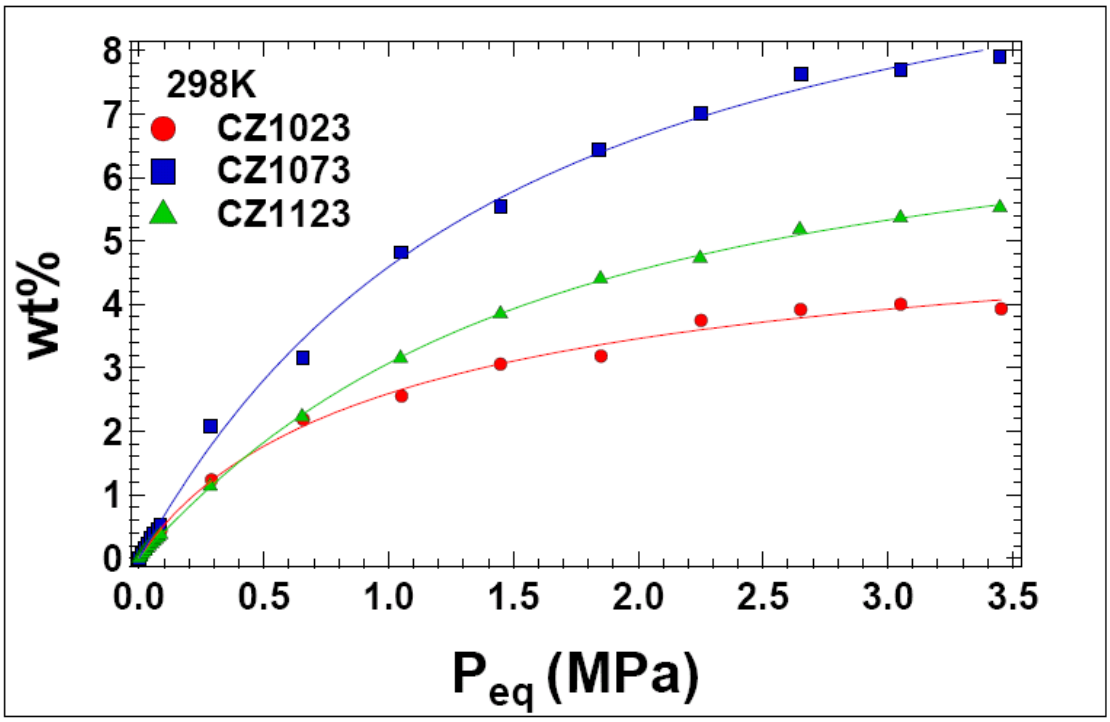

Figure 4.33: PcT adsorption isotherm obtained at 298 K up to 3.5 MPa for CZ1023, CZ1073 and CZ1123 fitted with the Tóth model according to the formula. Note that a wider data range is used to obtain a reliable evaluation of the Tóth parameters.

SAMPLE	wt% max	K ± ΔK (bar^{-1})	t ± Δt
CZ1023	6.0 ± 0.6	1.07 ± 0.10	0.80 ± 0.10
CZ1073	11.0 ± 1.2	0.60 ± 0.04	1.10 ± 0.20
CZ1123	7.5 ± 0.2	0.60 ± 0.01	1.20 ± 0.20

Table 4.17: Tóth equation fitting parameters for the samples

As it is shown in table 4.18 all three samples, within the error, have very close values of enthalpy, indicating a similar binding energy between the adsorbant and the adsorbent for low coverages.

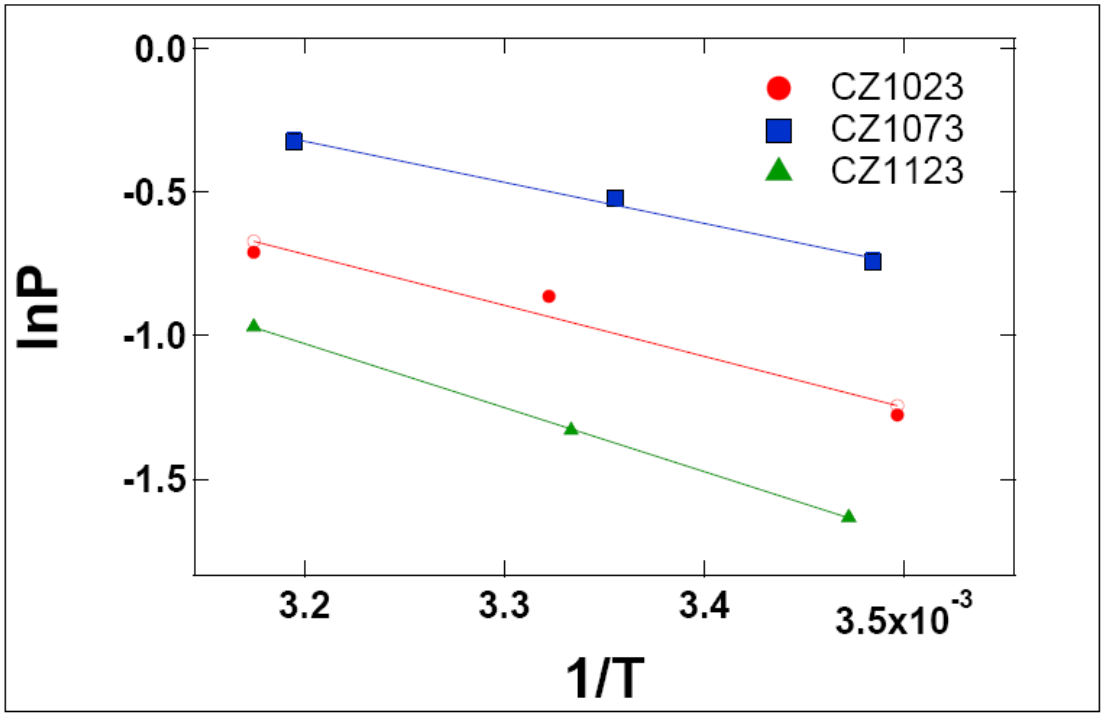

Figure 4.34: lnP vs T^{-1} graph of all the samples and fitting results by using the Clausius-Clapeyron relation.

SAMPLE	ΔH (kJ/mol) low coverages	Error (kJ/mol)
CZ1023	16.0	± 3.0
CZ1073	12.0	± 1.0
CZ1123	14.0	± 1.0

Table 4.18: Calculated isosteric heat of adsorption and its error for all the samples.

4.3 Zeolites

Before each adsorption measurement, the samples were treated up to 200°C under vacuum for 12 hours in order to remove water and other possible impurities.

For each sample PcT isotherms were obtained at 287K, 298K and 313K, and the experimental data fitted by Tóth equation. From the fitting parameters results we can have estimation about the trend of the samples adsorption properties. The number of molecules per nm^2 and the isosteric heat of adsorption will be evaluated for all samples.

Furthermore, SSA and porosity were measured with the common Brunauer-Emmet-Teller (BET) technique with N_2 as the probing molecule.

Density was measured with pycnometry measurements with He as a probe molecule (see experimental part). Images with Scanning Electron Microscopy (SEM) and X-ray diffraction patterns were received to extract more information on the morphology and crystallinity of the samples structure.

4.3.1 Sapo-34 [13]

4.3.1.1 Methane adsorption

SEM images (figure 4.35 a-b) show the different morphology obtained at different N/Si ratios (when methylene blue is present or not, SAPO-34 A.R. 9.0 and SAPO-34 AR 2.2 respectively). In the case of SAPO-34 A.R. 2.2 the particles demonstrate a cubic morphology while in the case of SAPO-34 A.R. 9.0 the particles have a layered morphology.

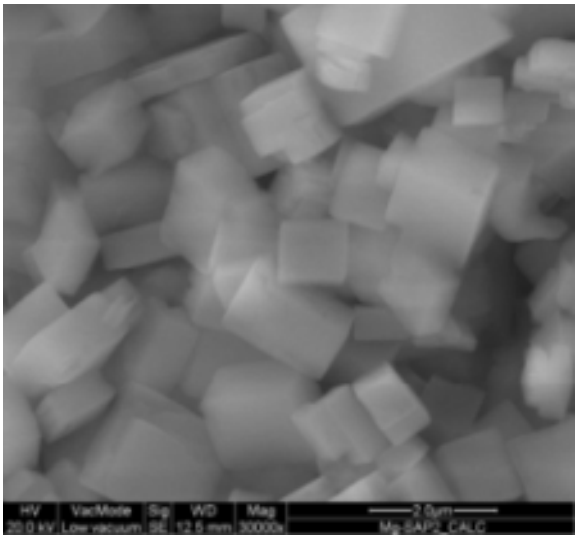

Figure 4.35 a SAPO 34 AR 2.2

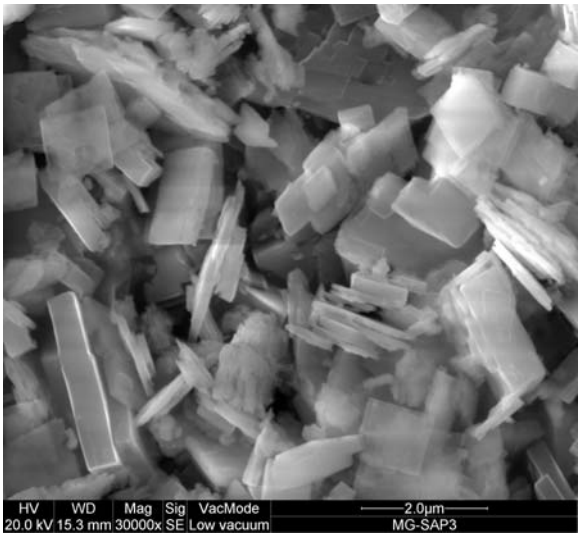

Figure 4.35 b SAPO 34 R 9.0

In Table 4.19 we report samples' structural characteristics. The SAPO 34 A.R. 9.0 sample presents higher specific surface area and pore volume values compared to the sample SAPO 34 A.R. 2.2 .

SAMPLE	**SSA (m^2/g)**	**Pore Volume (cm^3/g)**	**Si/Al ratio**	**N/Si ratio**	**Density (g/ccm)**
SAPO 34 R 9.0	581	0.25	0.27	0.50	2.5
SAPO 34 R 2.2	479	0.19	0.25	0.27	2.7

Table 4.19: Structural properties of all the samples

In figure 4.36a are presented the adsorption isotherms of SAPO 34 A.R 9.0 and SAPO 34 A.R. 2.2 at 298 K and up to 3.5 MPa. Both samples show very similar methane storage capacity up to 4.8 wt% even if they have a difference of about 100 m^2/g of SSA value. This, can be explained if we evaluate their degree of surface coverage in terms of adsorbed molecules per nm^2.

In figure 4.36(b-c) are shown the adsorption isotherms of the two samples at 287 K and 313 K.

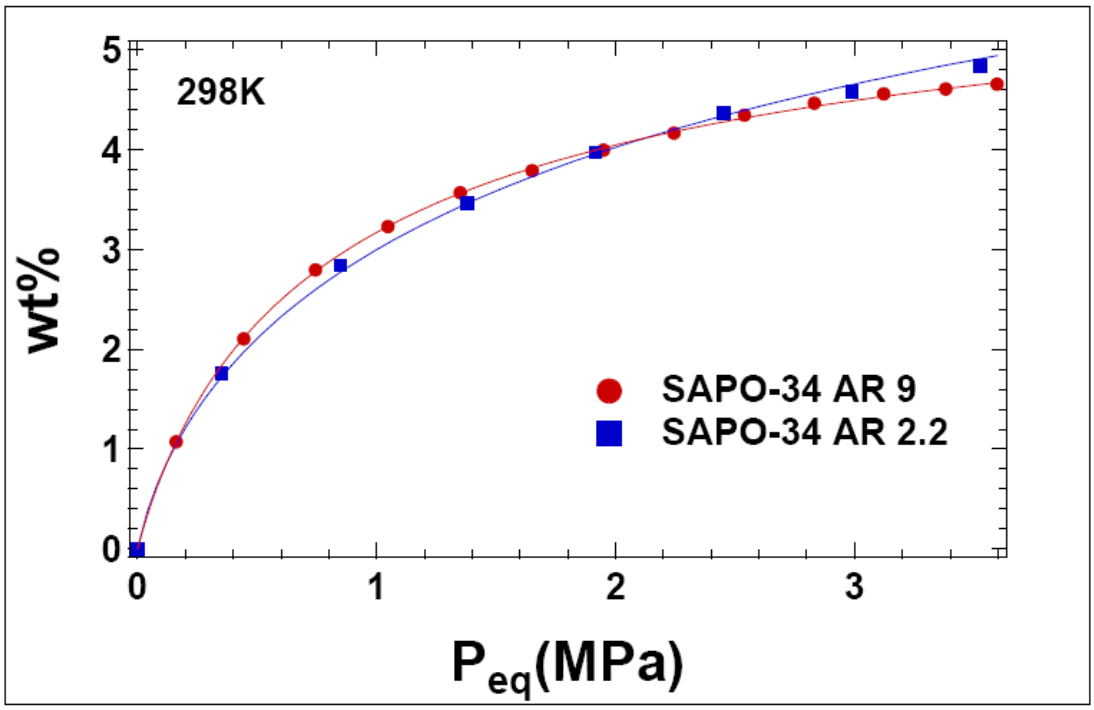

Figure 4.36(a): PcT adsorption and desorption isotherms obtained at 298K up to 3.5 MPa for SAPO 34 A.R. 9 and SAPO 34 A.R. 2.2 (markers). Lines between points represent the data fitting procedure based on the Tóth model.

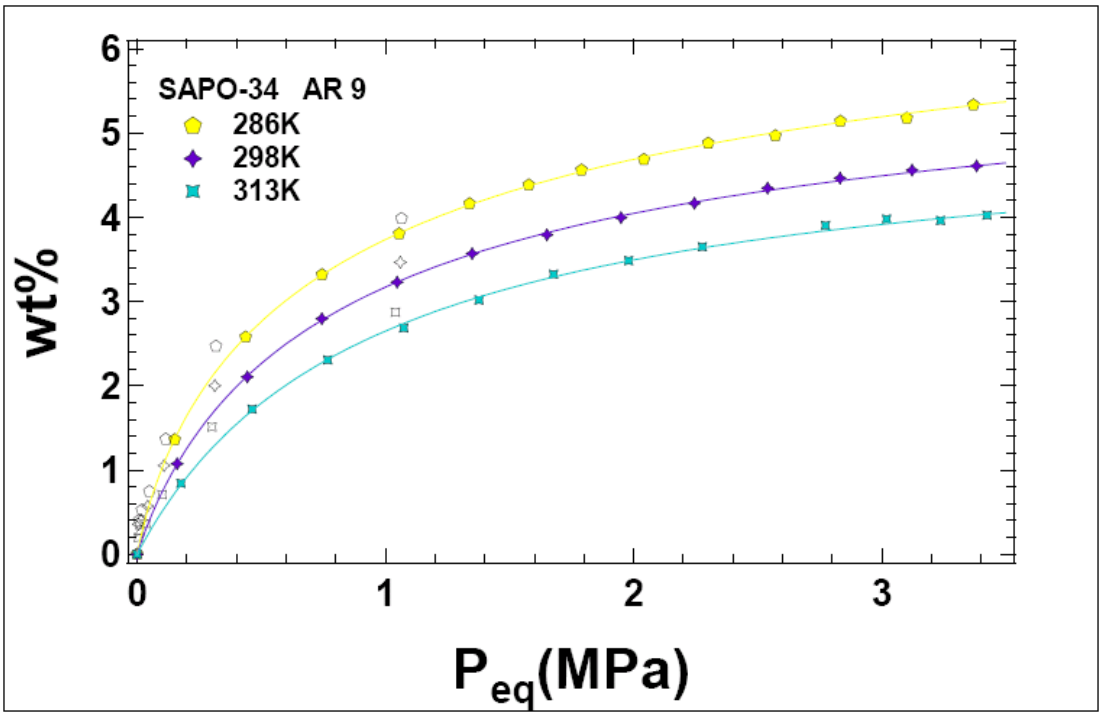

Figure 4.36(b): PcT adsorption and desorption isotherms obtained at 287K, 298K and 313K up to 3.5 MPa for the sample SAPO 34 A.R. 9 (markers). Lines between points represent the data fitting procedure based on the Tóth model.

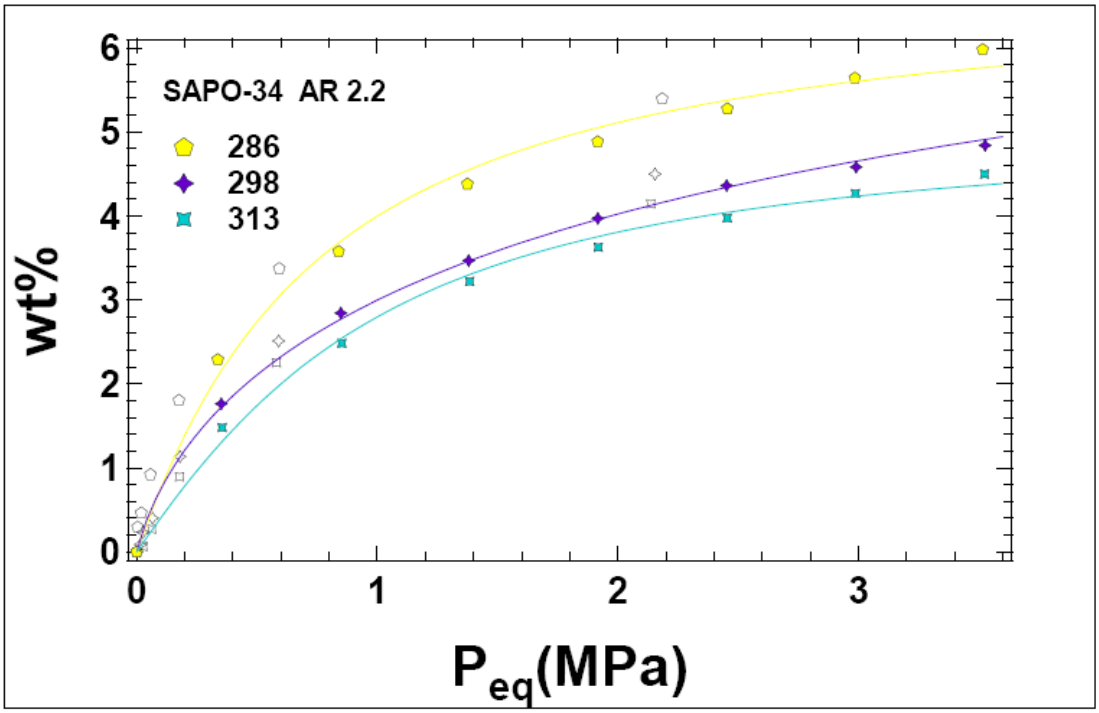

Figure 4.36(c): PcT adsorption and desorption isotherms obtained at 287K, 298K and 313K up to 3.5 MPa for the sample SAPO 34 A.R. 2.2 (markers). Lines between points represent the data fitting procedure based on the Tóth model.

In figure 4.37 are presented the curves of the adsorbed molecules per nm^2 of the two samples. It is noticed that both of the samples form one monolayer at the highest pressure but particularly the sample SAPO 34 A.R. 2.2 forms more than one monolayer (3.8 molecules/nm^2). This, as mentioned before, can explain the fact that both samples show the same capacity of adsorbing methane molecules even if they don't posses same values of SSA.

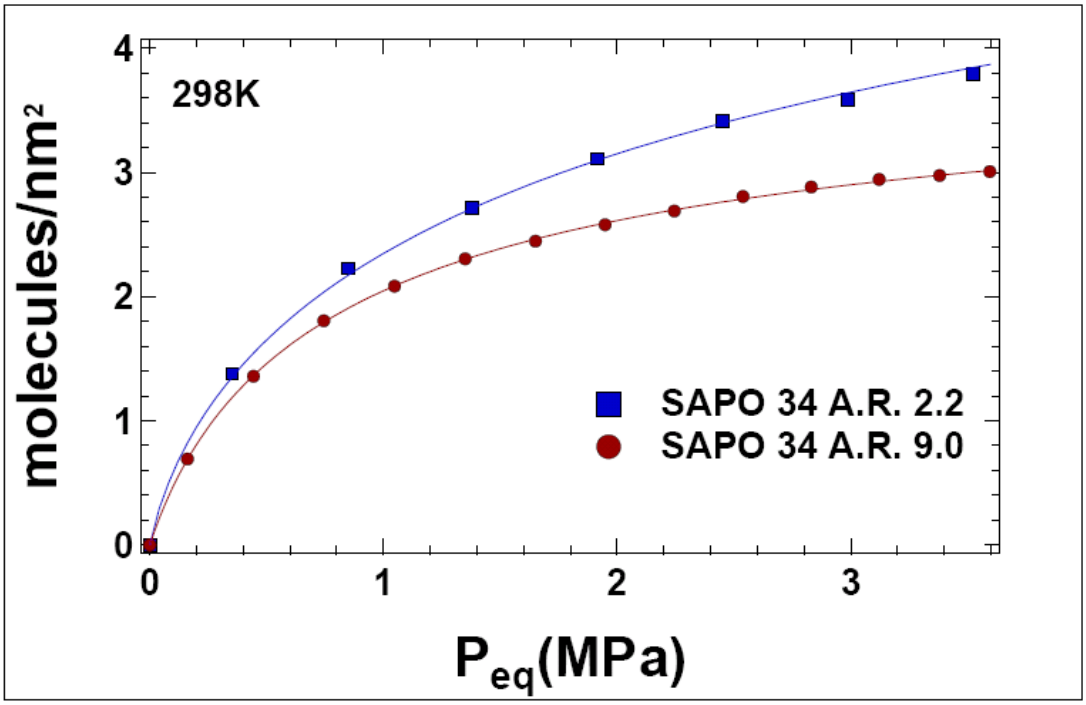

Figure 4.37: Number of molecules per surface's nm² for SAPO 34 A.R. 9 and SAPO 34 A.R. 2.2 (markers). Lines between points represent the data fitting procedure based on the Tóth model.

Fitting the adsorption isotherms with the Tóth model showed similar values of theoretical maximum storage capacity, within the error, for both samples as it was expected. Both samples possess a high K value indicating very strong interaction between the adsorbate and the surface (table 4.20). Particularly the sample SAPO 34 A.R. 9 has a higher K-value compared to the SAPO 34 A.R. 2.2, attributed to its different adsorption isotherm curvature which indicates a quicker saturation of the surface in low pressures. Finally, the t-value of both samples is similar demonstrating similar grade of surface homogeneity.

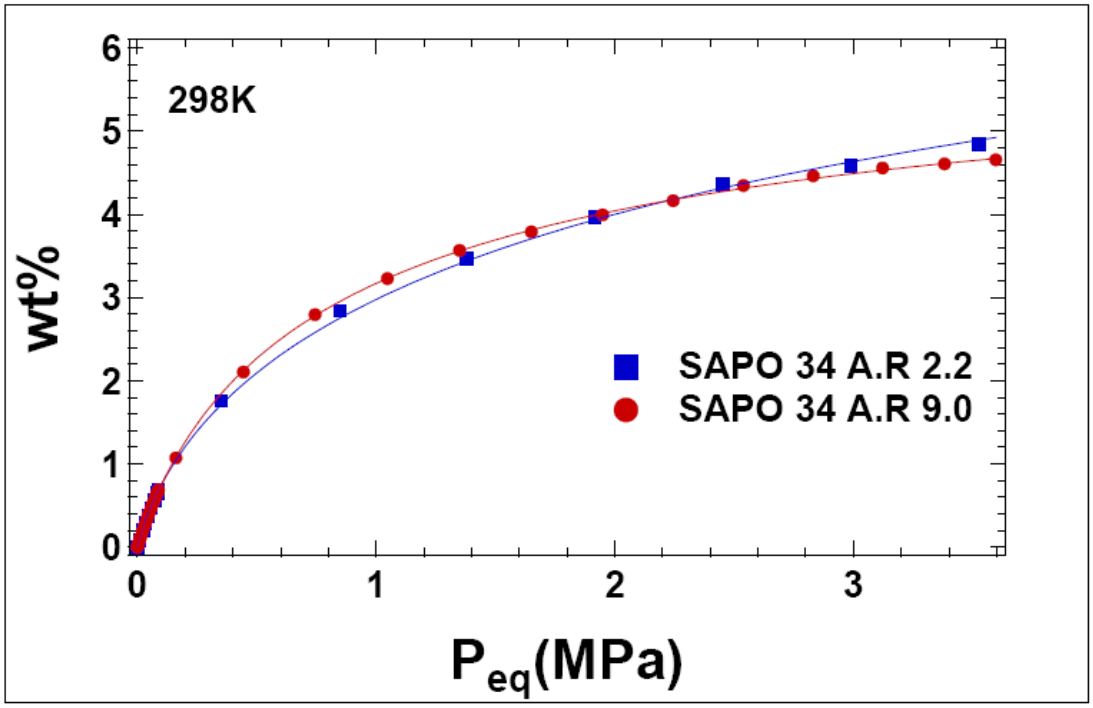

Figure 4.38: PcT adsorption isotherm obtained at 298 K up to 3.5 MPa for SAPO 34 A.R. 9 and SAPO 34 A.R. 2.2 fitted with the Tóth model according to the formula. Note that a wider data range is used to obtain a reliable evaluation of the Tóth parameters.

SAMPLE	wt% max	K ± ΔK (bar^{-1})	t ± Δt
SAPO 34 R 9.0	6.3 ± 0.07	1.50 ± 0.02	0.70 ± 0.02
SAPO 34 R 2.2	8.4 ± 0.30	1.35 ± 0.03	0.60 ± 0.02

Table 4.20: Tóth equation fitting parameters for the samples

Finally, the evaluation of enthalpy in low pressures and coverages (figure 4.39) revealed very similar values, confirming the similar affinity of the pore

surfaces towards the methane adsorption for both SAPO 34 samples (table 4.21).

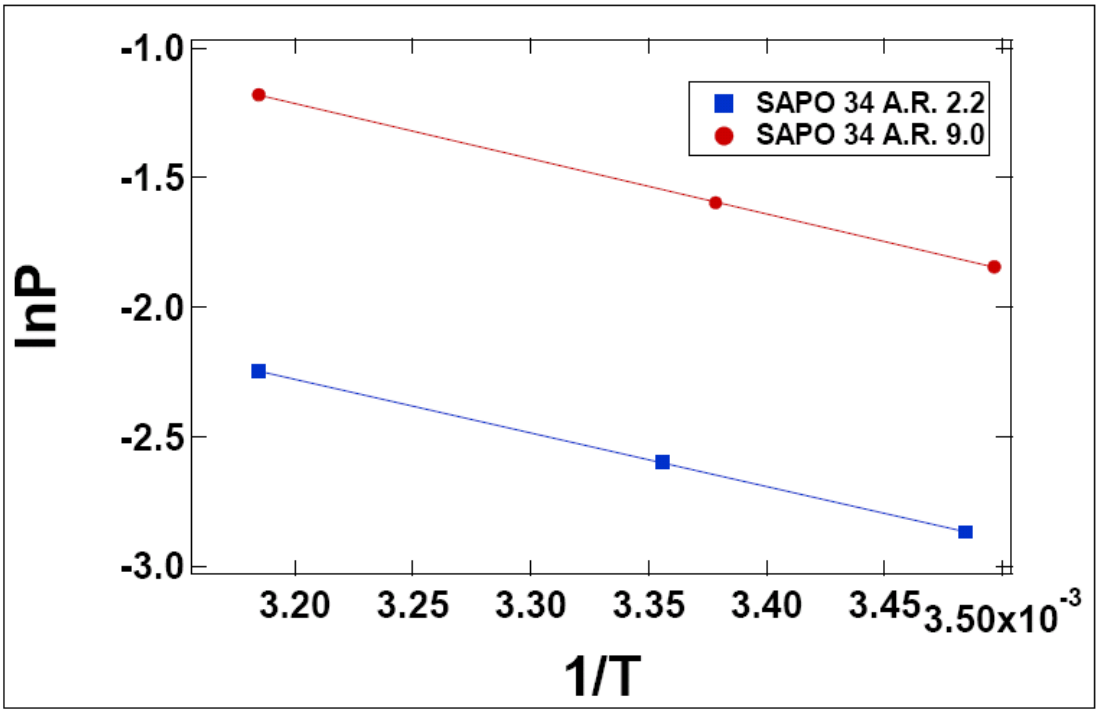

Figure 4.39: lnP vs T^{-1} graph of the sample SAPO 34 A.R. 9.0 and fitting results by using the Clausius-Clapeyron relation.

SAMPLE	ΔH (kJ/mol) low coverages	Error (kJ/mol)
SAPO 34 R 9.0	17.60	± 0.15
SAPO 34 R 2.2	17.10	± 0.20

Table 4.21: Calculated isosteric heat of adsorption and its error for all the samples.

4.3.1.2. Carbon dioxide adsorption

The carbon dioxide adsorption isotherms were obtained for the two SAPO 34 samples at 298 K and up to 0.3 MPa. On the contrary to the similar methane adsorption capacity of the samples presented above, we obtained different results for the case of carbon dioxide uptake. Specifically, as shown in figure 4.40, the sample SAPO 34 A.R. 9.0 has a higher carbon dioxide uptake which is equal to 17 wt%.

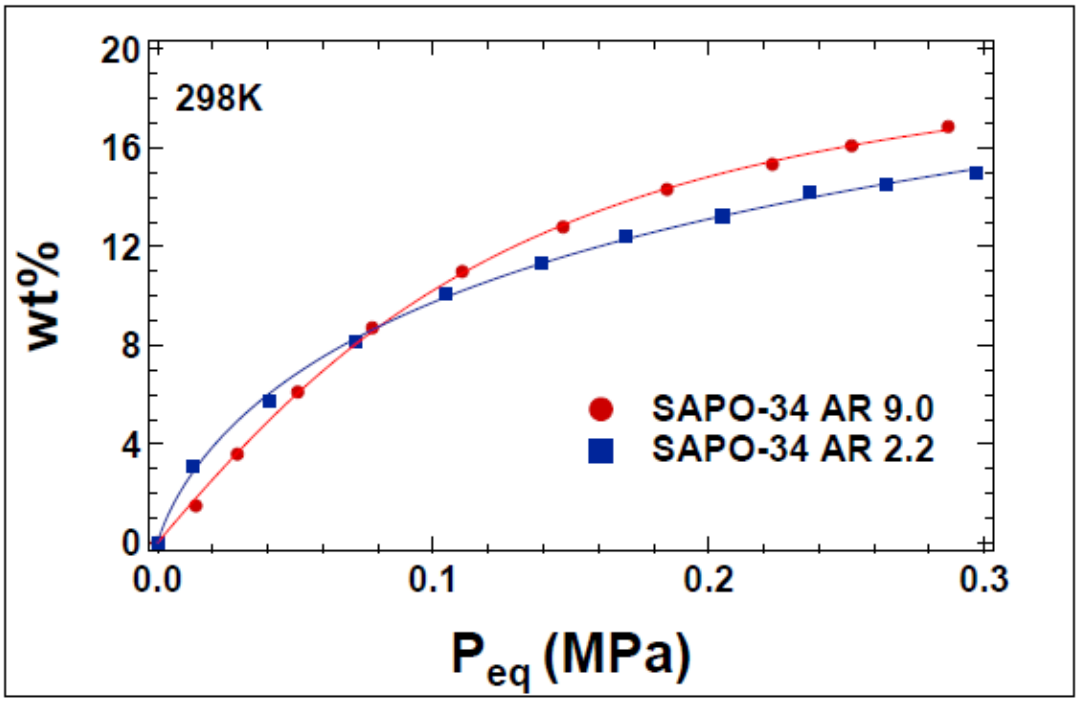

Figure 4.40: PcT CO_2 adsorption and desorption isotherms obtained at 298K up to 0.3 MPa for SAPO 34 A.R. 9 and SAPO 34 A.R. 2.2 (markers). Lines between points represent the data fitting procedure based on the Tóth model.

4.3.2 Silicalite-1

The XRD patterns of the starting and modified materials (see figure 4.41) show the typical peaks of silicalite-1, MFI topology [14].

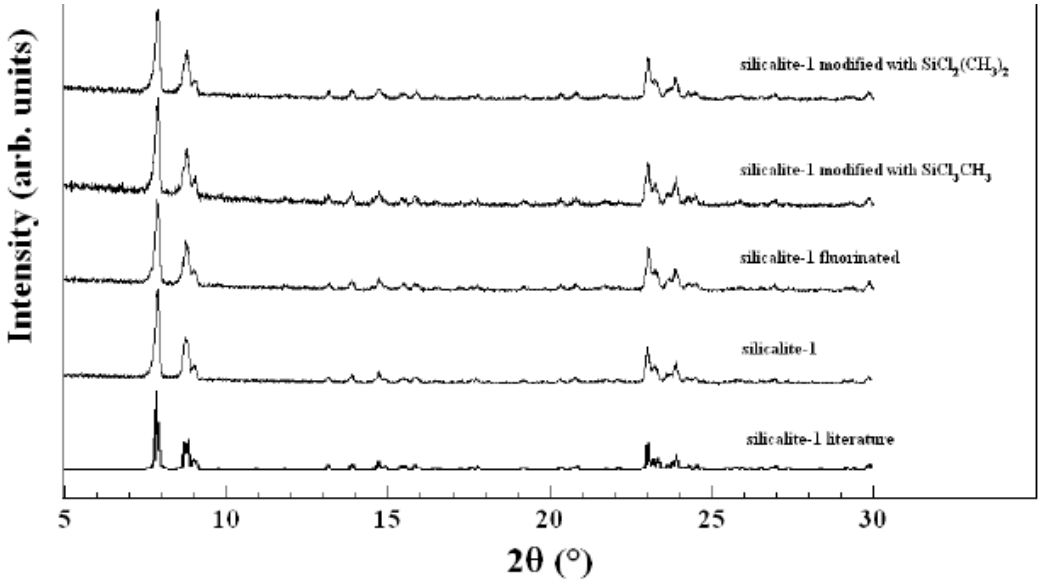

Figure 4.41 : XRD patterns of silicalite-1 before and after the modifications

The modification of silicalite-1 by organosilane molecules does not produce any structural change in the zeolite [15]. In any case, if differences are observed in the XRD pattern, they are only present in the peaks intensity and broadening of the lower order reflections due to the smaller crystallite size, or a higher degree concentration of disordering [16,17].

The SEM pictures (see figure 4.42 for Silicalite-1) show the typical morphology of Silicalite-1 with intergrowth structures of zeolites [18] indicating an average grain size of 20 μm which is unchanged after the modification.

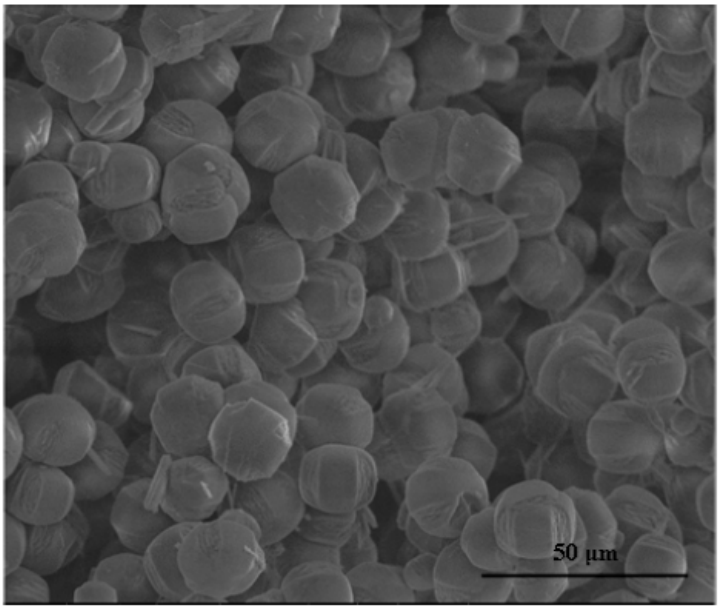

Figure 4.42: SEM image of Silicalite-1

In figure 4.43 is presented the adsorption (close symbols) and the desorption (open symbols) isotherm curves of methane on the starting Silicalite-1 and the modified samples obtained at 298K.

As presented before for the other groups of materials, the desorption isotherm curves follow exactly the adsorption isotherms, indicates that the methane gas can be easily extracted from the samples.

All samples show the same methane uptake of around 3.6 wt% at 3.5 MPa.

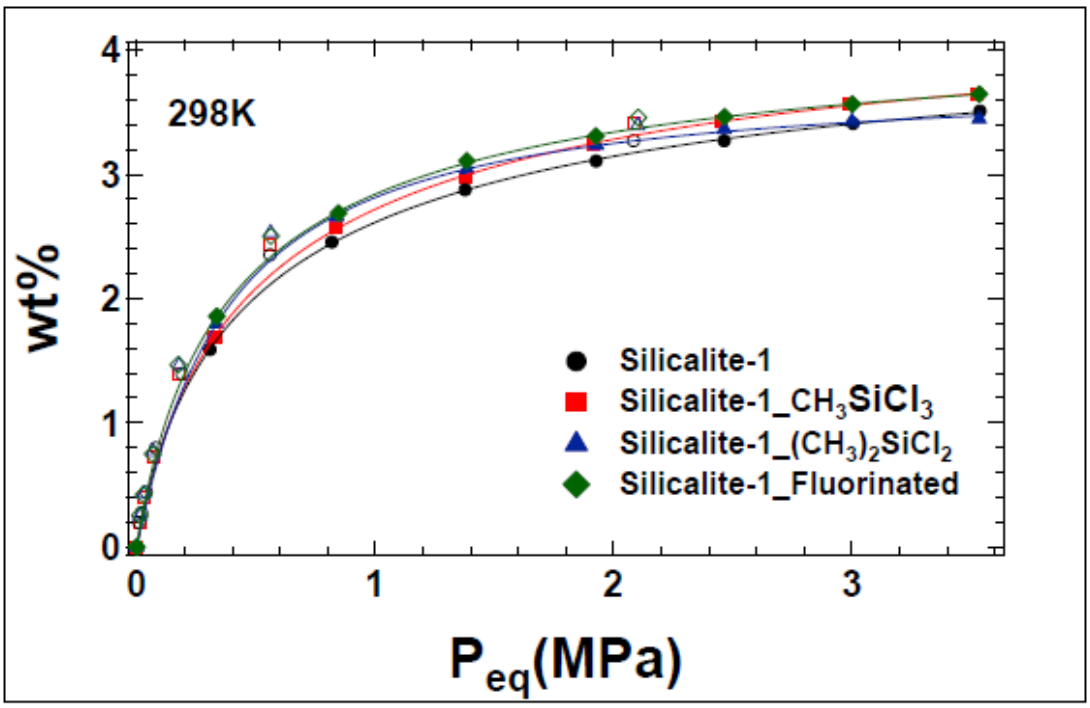

Figure 4.43: PcT adsorption and desorption isotherms obtained at 298K up to 3.5 MPa for the starting silicalite-1 sample and the modified samples (markers). Lines between points represent the data fitting procedure based on the Tóth model.

The similar methane storage capacity of the samples is significant because it means the modification does not change the Silicalite-1 adsorption properties. In view of application [19] this is extremely important because the Silicalite-1 can be bound to polymer composite by organosilane molecules with no changes in its methane adsorption properties.

As it was previously pointed out, a good estimation of the coverage in terms of molecules per nm^2 can be calculated combining the values of the wt% adsorption capacity with the surface specific area (SSA) of the samples. By assuming a SSA=425 m^2/g [20] for all the samples, it is demonstrated (figure 4.44) that the unmodified and modified silicalite-1 adsorb one monolayer of methane molecules.

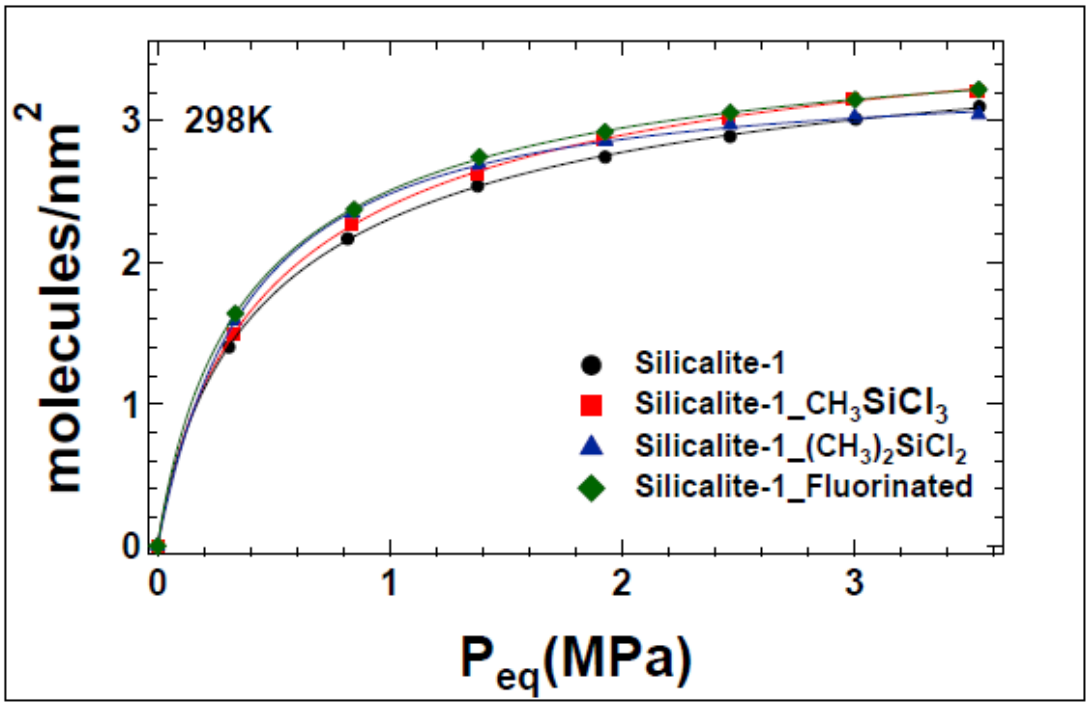

Figure 4.44: Number of molecules per surface's nm^2 for the starting silicalite-1 sample and the modified samples (markers). Lines between points represent the data fitting procedure based on the Tóth model.

All samples' adsorption isotherms were fitted with the Tóth model and the results are shown in table 4.22. As it was expected all samples show similar theoretical maximum storage capacity. Additionally, high K-values were obtained for all samples the silicalite samples indicating a very strong interaction between the methane molecules and the samples' pore walls. Furthermore, all samples show similar and high t-values fact that reveals very homogeneous surfaces.

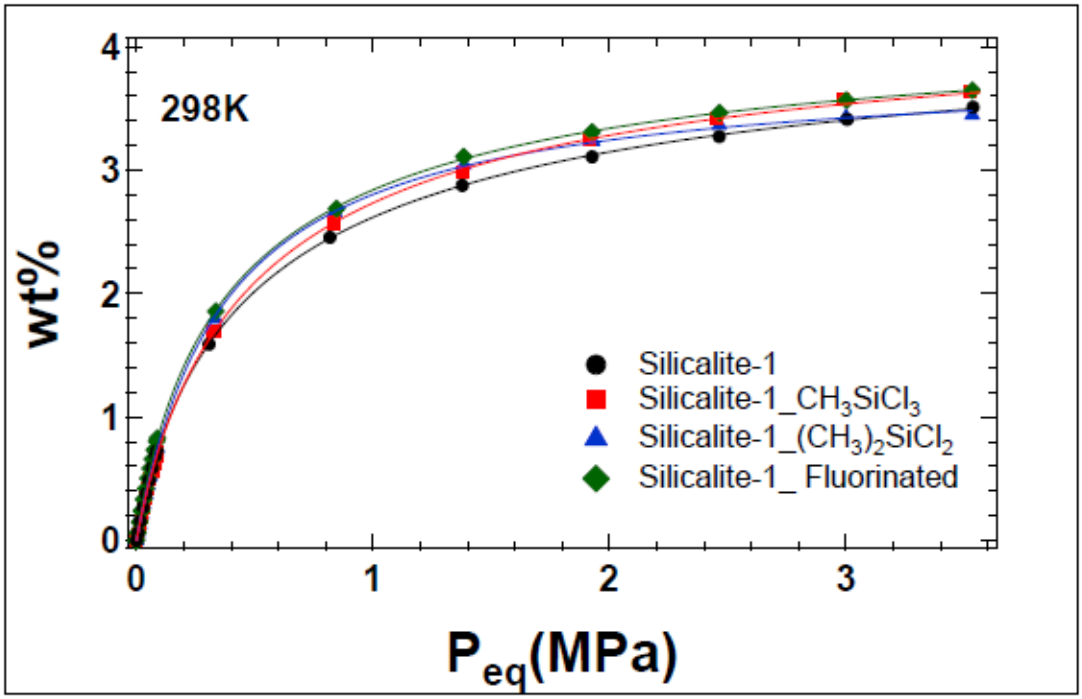

Figure 4.45: PcT adsorption isotherm obtained at 298 K up to 3.5 MPa for SAPO 34 A.R. 9 and SAPO 34 A.R. 2.2 fitted with the Tóth model according to the formula. Note that a wider data range is used to obtain a reliable evaluation of the Tóth parameters.

SAMPLE	wt% max	K ± ΔK (bar^{-1})	t ± Δt
Silicalite-1	4.4 ± 0.06	2.80 ± 0.05	0.70 ± 0.02
Silicalite-1_CH_3SiCl_3	4.5 ± 0.05	2.50 ± 0.03	0.80 ± 0.02
Silicalite-1_$(CH_3)_2SiCl_2$	3.80 ± 0.03	2.70 ± 0.03	0.90 ± 0.02
Silicalite-1_Fluorinated	4.30 ± 0.03	3.10 ± 0.03	0.80 ± 0.01

Table 4.22: Tóth equation fitting parameters for the samples

Finally, similar and high values of isosteric heat of adsorption, within the error, were found for all the four investigated samples indicating that in low pressures and coverages the bonding energy between the samples' surface and the methane molecules is strong (table 4.23).

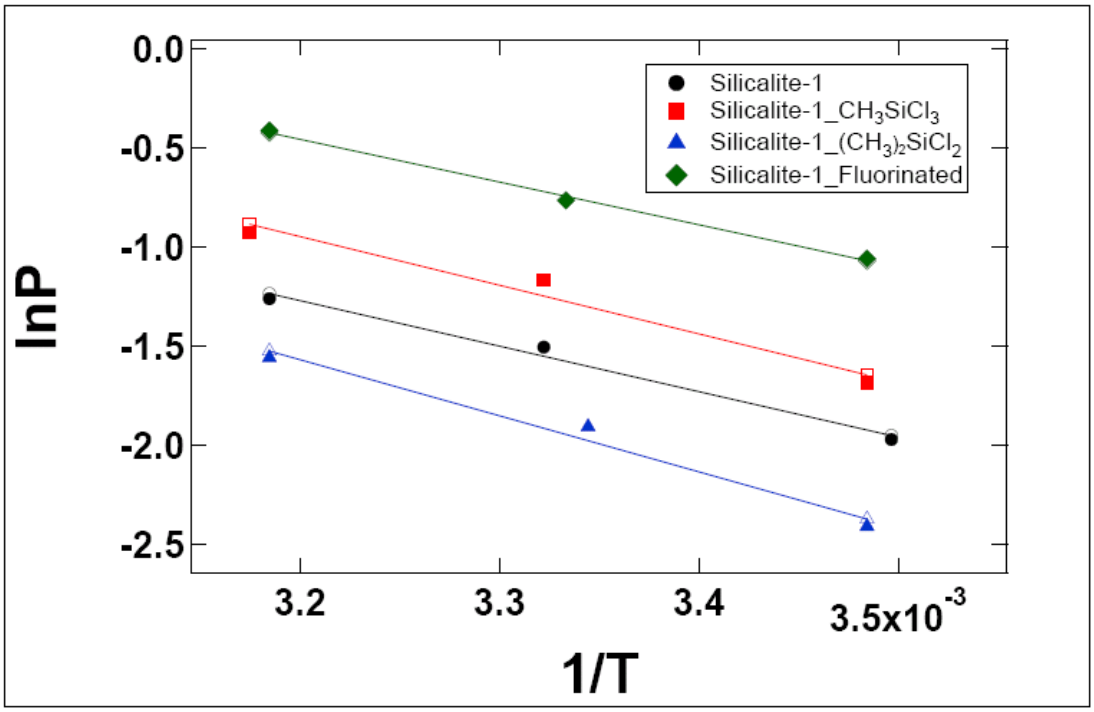

Figure 4.46: lnP vs T^{-1} graph of all the samples and fitting results by using the Clausius-Clapeyron relation.

SAMPLE	ΔH (kJ/mol) low coverages	Error (kJ/mol)
Silicalite-1	19.0	± 2.0
Silicalite-1_CH_3SiCl_3	20.0	± 3.0
Silicalite-1_$(CH_3)_2SiCl_2$	20.0	± 3.0
Silicalite-1_Fluorinated	18.0	± 1.0

Table 4.23: Calculated isosteric heat of adsorption and its error for all the samples

Bibliography Chapter 4

[1] Toth, J., Adsorption Theory Modelling and Analysis Dekker: New York, 2002.

[2] Antoniou M.K, Kalantzopoulos G.N., Enotiadis A., Maccallini E, Policicchio A., Gournis D., Agostino R.G. (In preparation)

[3] Kalantzopoulos, G. N.; Enotiadis, A.; Maccallini, E.; Policicchio, A.; Gournis, D.; Agostino, R. G. In preparation

[4] Sing, K. S. W.; Everett, D. H.; Haul, R. A. W.; Moscou, L.; Pierotti, R. A.; Rouquerol, J.; Siemieniewska, T. Pure & Appl. Chem. 1985**,** 57, (4), 603—619

[5] Bhatia, S. K.; Myers, A. L. Langmuir 2006**,** 22, 1688-1700

[6] Maccallini, E.; Agostino, R. G.; Kalantzopoulos, G.; et al. In preparation

[7] Duong D. Do, ADSORPTION ANALYSIS: EQUILIBRIA AND KINETICS. 1998; Vol. 2

[8] Myrsini K. Antoniou, Alfonso Policicchio, Konstantinos Dimos, Dimitrios Gournis, Michael A. Karakassides and Raffaele G., Agostino Micropor. Mesopor. Mater. XX(201X)XX

[9] K. Dimos, A. Meichanetzoglou, S. Lymperopoulou, M.-D. Ouzouni, I.B. Koutselas, M.K. Antoniou, D. Fokas, D. Gournis, M.A. Karakassides, R.G. Agostino, Micropor. Mesopor. Mater. XX(201X)XX

[10] K. Dimos, I.B. Koutselas, M.A. Karakassides, J. Phys. Chem. B 110 (2006) 22339

[11] Antoniou M.K., Diamanti E. K., Enotiadis A., Policicchio A., Ciuchi F., Maccallini E. , Gournis D., Agostino R.G., Langmuir XX(201X)XX

[12] Yang Z., Xia Y., Mokaya R. J. AM. CHEM. SOC. 2007; 129, 1673-1679

[13] M.G. Buonomenna, G. Golemme, A. Policicchio, M.K Antoniou, R.G. Agostino et al. (In preparation)

[14] van Koningsveld, H.; Jansen, J.C.; van Bekkum, H. Zeolite, 1990, 10, 235-242

[15] Cheng, C. H., Bae, T. H., McCool, B. A. et al. Journal of Physical Chemistry C, 2008, 112, 3543-3551

[16] Han, A. J., Guo, J. G., Yu, H. et al. Chemphyschem, 2006, 7, 607-613

[17] Shin, Y., Zemanian, T. S., Fryxell, G. E. et al. Microporous and Mesoporous Materials, 2000, 37, 49-56

[18] Kox, M. H. F., Stavifski, E., Groen, J. C. et al. Chemistry-A European Journal, 2008, 14, 1718-1725

[19] Moore, T. T., Mahajan, R., Vu, D. Q. et al. Aiche Journal, 2004, 50, 311-321

[20] Jhung, S. H., Yoon, J. W., Lee, S. et al. Chemistry-A European Journal, 2007, 13, 6502- 6507

5. Conclusions

In the present work, Periodic Nanoporous Organolicas (PNOs), Carbon nanostructuerd materials and Zeolites were studied for methane storage. Samples were structurally and morphologically characterized by XRD, SEM and He pycnometry and by the BET method in order to well characterize the samples' porosity. Methane storage properties at different temperatures (286 K, 298 K and 313 K) have been investigated by Sievert-type apparatus up to 3.5 Mpa. The PcT apparatus allowed the determination of the adsorption/desorption properties by isotherm curves analysis. The obtained isotherm curves have been analysed by the Toth equation. While the acquisition of the isotherm curves at different temperatures allowed to extract the isosteric heat of adsorption of the samples. Finally, an analysis which takes into consideration the number of adsorbed methane molecules per nm^2 has been demonstrated. In fact, this analysis considers the adsorption of methane molecules per surface unit in order to verify if the methane storage capacity, obtained by PcT isotherm curves, is mainly due to either the SSA value or the physical interaction between the adsorbent and the adsorbate.

The phenylene bridged PNO samples were obtained by the sol-gel method, changing the synthesis parameters in order to tune their chemical and physical properties. The varied synthesis parameters were:

1) surfactant used (BTB or DBTB) and its chain length (from 10 to 18 carbon atoms), in order to change the pores size distribution and the specific pore volumes;

2) the sample's aromaticity (substitution of the BTB precursor with the TEOS precursor) , in order to change the physical interaction between the adsorbent and the adsorbate;
3) insertion of cations (e.g. Li+) in order to attract more methane molecules

Starting with the effect on the methane adsorption properties due to the variation of the surfactant chain length it was shown that the adsorption properties and the number of methane molecules adsorbed per nm^2 increase reversely to the chain length. Particularly, in the case that BTB was used as precursor, the sample with the smaller chain length (C10) presented the higher methane uptake and the higher isosteric heat of adsorption. A concurrent role can be played by the long range ordering induced by the chain length: the PNO sample obtained by using C10 molecules is amorphous while a certain degree of ordering is kept in all the other samples with higher chain lenght. The fit results of Tóth equation showed the same grade of surface homogeneity for all the samples (BH_C10_100, BH_C12_100, BH_C16_100, BH_C18_100), irrespective of the chain length. Consequently, the higher methane uptake of the sample BH_C10_100 can be a result of the most favorable binding energy between the CH_4 molecules and the pore walls of this sample determined by its optimum pore size distribution and its open structure.

The same results were obtained also in the case were DBTB was used as precursor. The sample with the smaller chain length DH_C10_100 presented the higher methane uptake and the higher isosteric heat of adsorption compared to the other samples (DH_C12_100, DH_C16_100, DH_C18_100). Here we have to note, as for the case of the BH_C10_100 sample, that the DH_C10_100 sample was the only amorphous while a certain degree of

ordering was observed in all the other samples. Finally, the fit results of Tóth equation show the same high grade of surface homogeneity for all samples.

In the case of BTB substitution with TEOS, it was noticed that the methane storage capacity improves at a peculiar concentration of the two precursors. Specifically, PNOs samples were prepared with mixtures of BTB over TEOS in ratios of 0%, 25%, 50%, 75% and 100% BTB : TEOS. The absence of BTB (BH_C16_0) had as a result a high value of SSA (953 m^2/g) but a small mean pore size (1.50 nm) that caused a low adsorption capacity and low number of adsorbed molecules/nm^2. While the sample BH_C16_75 (75% BTB and 25% TEOS) owns the highest SSA (1220 m^2/g) and highest adsorption capacity compared to the other samples of this group. All of the samples that contain TEOS precursor show similar but not high grade of surface homogeneity. Finally, similar values of isosteric heat of adsorption within the error were found for all the five investigated samples indicating that in low pressures and coverages the different ratio between BTB and TEOS precursors didn't play an important role in the adsorption capacity of the samples unlike to the extracted results for higher pressures presented above.

Furthermore, a difficult modification by Li+ doping has also been attempted on the sample DH_C10_100. The sample doped with Li+ (DH_C10_100_Li) showed a high ability to attract the methane molecules but did not present any methane storage capacity improvement because of the non successful insertion of the Li+. In other words we could suppose that if the insertion of the Li+ has done successfully, we could expect a material with high adsorption capacity thanks to its high binding energy between the methane molecules and the surface of the sample.

To conclude, the morphological, structural and methane adsorption characterizations indicate that the key parameters influencing the adsorption properties of PNOs are the pore size (by changing the main chain length of the surfactants), the SSA extension and the utilization of a mixed composition of the precursor materials for the samples synthesis. Besides, the insertion of Li+ is an additional strategy that can be used in order to enhance the physical interaction between the pore walls and the methane molecules. However, in the future, the introduction of lithium atoms into the porous samples has to be improved. Furthermore, PNO samples prepared with a partial substitution of BTB or DBTB precursors with Al^{3+} cations will be tested for methane adsorption expecting an increased uptake.

Novel naphthalene containing periodic nanoporous organosilicates were synthesized by direct co-condensation of tetraethylorthosilicate and the prior composed chemical substance triethoxy(naphthalen-1-yl)silane. After chemical, structural and morphological characterization was shown that the final materials, Naph-PNO-H^+ and Naph-PNO-350, exhibit high crystallinity, high naphthalene content up to 17 wt%, surface areas above 1000 m^2/g and pore size distributions in the microporous/mesoporous boundary. Methane adsorption measurements were performed on both samples obtaining a methane uptake value of 4.2 wt% and 5.2 wt% for Naph-PNO-H^+ and Naph-PNO-350 samples respectively at 298K. The analysis of the adsorption isotherms with the Tóth model, show for both samples high and equal (within the error) t-values indicating very homogeneous surfaces. The porosity of the samples appears to have played an important role in terms of adsorption. In fact, the observed differences of the methane uptake properties of the samples could be attributed to the higher SSA and pore volume values of the Naph-PNO-350 sample.

Zeolite-like carbon materials were developed that exhibit very high surface area via a CVD route using zeolite beta as solid template. CVD was performed at three different temperatures (1023K, 1073K, and 1123K) using acetylene as carbon precursor. Acetylene was chosen as a carbon source since it can lead to carbon materials of better quality and the final materials are nitrogen-free zeolite-like carbons. The sample obtained at 1073 K showed the highest SSA (980 m^2/g) and an appropriate pore size (0.6 nm) that can store more efficiently the methane molecules, with measured uptake of 8 wt % at 298K and 3.5 MPa. All three samples (CZ1023, CZ1073, CZ1123), within the error, show a high grade of surface homogeneity and a similar binding energy between the carbon surface and the gas molecules. The morphology of the sample play the key role in terms of accessible surface: the smaller pore size and the absence of pore ordering in sample CZ1023 determine a limitation on the accessible surface for CH_4 adsorption.

In the future, zeolite-like carbon samples could be prepared using different types of zeolites as hard templates and different carbon precursors during the CVD method in order to obtain more effective methane adsorption.

SAPO 34 samples were prepared with different N/Si ratios: SAPO 34 A.R. 9.0 with N/Si: 0.50 and SAPO 34 A.R. 2.2 with N/Si: 0.27. The methane adsorption capacity of both samples is similar which indicates that the different N/Si ratios did not affect their storage uptake. On the other hand, this effect is clear in the case of carbon dioxide adsorption, where the sample SAPO 34 A.R. 9.0, with the higher N/Si ratio, attracts more efficiently the carbon dioxide molecules.

The external surface of silicalite-1 (MFI) crystals has been modified with three different chlorosilanes. The surface modifications do not change the methane adsorption capacity at 3.5 MPa and 298 K since the specific surface area values

and the number of adsorbed molecules per nm^2 are very similar. Therefore, the silicalite-1 can be bound to polymer composite by organosilane molecules with no changes in its methane adsorption properties. Besides, all four samples, within the error, show a high and similar grade of surface homogeneity. Finally, similar affinity of the pore surfaces towards the methane adsorption in low coverages was found for all samples.

6. Acknowledgements

I would like to acknowledge many people that helped me and supported me during the three years of my Ph.D.

First of all, I deeply thank my supervisor Prof. Rafaelle Giuseppe Agostino for his continuous support and guidance. I greatly thank him for believing in me and giving me the opportunity to work with him and his group.

I very thank Dr. Enrico Maccallini for his important contribution all these years. His knowledge and advices were and will always be valuable to me. He made me realize what a researcher should be.

Many thanks to Dr. Alfonso Policicchio and Dr. Georgios Kalantzopoulos for their unlimited assistance and support.

I am thankful to Prof. Elio Colavita for providing me the opportunity to work in the SPES group of the Department of Physics in the University of Calabria.

I very thank all the members of my group: Prof. Gennaro Chiarello, Prof. Vincenzo Formoso, Dr. Tommaso Caruso, Dr. Antonio Marino and the undergraduate student Francesco Demetrio Minuto.

I also acknowledge Giovanni Desiderio and Salvatore Abate for their continuous technical and friendly support all these years.

I particularly thank Prof. Dimitrios Gournis from the Department of Materials Science & Engineering (University of Ioannina, Greece) for his excellent collaboration, continuous encouragement and precious advices.

My special thanks to Dr. Apostolos Enotiadis, Dr. Evmorfia Diamanti and Dr. Konstantinos Dimos from the Department of Materials Science & Engineering (University of Ioannina, Greece) for their significant assistance, support and

friendship. I wish I will always have the fortune to work with researchers, but mostly personalities, like them.

I very want to thank Prof. Gianni Golemme and Dr. Maria Giovanna Buonomenna from the Department of Chemical Engineering (University of Calabria, Italy) for their beautiful collaboration.

I want to thank Dr. Federica Ciuchi and Dr. Alfredo Aloise for their important assistance.

I am grateful to International Doctoral School of Science and Technology "Bernadino Telesio"for the financial support during these three years.

I deeply thank my friends Simone, Kristina, Katerina, Massimiliano, Costanza and Francesca that have been a wonderful company these years. My life in Cosenza wouldn't be the same without them.

Many thanks to all my best friends in Greece, Angeliki, Alexia, Natasa, Ntina, for being always there for me and cheering up my life.

Last but not least, I want to sincerely thank my parents, Nikos and Moshanthi, and my sister, Georgia, for standing always next to me. Our endless discussions made me feel close to them, despite the distance. Their advices and encourage helped me to overcome every difficulty during these years.

This thesis is dedicated to my beloved grandmother Georgia.